

# **Characterization of a mouse model of Börjeson- Forssman-Lehmann Syndrome**

Raies Ahmed

Thesis submitted to the Faculty of Graduate and Postdoctoral Studies  
in partial fulfillment of the requirements for the degree of

Master's  
in Biochemistry  
with specialization in Human and Molecular Genetics

Department of Biochemistry, Microbiology, and Immunology  
Faculty of Medicine  
University of Ottawa, Ontario, Canada

© Raies Ahmed, Ottawa, Canada, 2019

## Abstract

Plant homeodomain finger protein 6 (PHF6) is a chromatin adaptor protein structurally defined by its two zinc-knuckle-atypical PHD (ZaP) domains. This structural configuration mediates its interaction with dsDNA, miRNA, the nucleosome remodeling and deacetylase (NuRD) complex and regulators of rDNA transcription (Upstream binding factor (UBF) and RNA polymerase-associated factor 1 complex (Paf1C)), ultimately facilitating its role as a chromatin adaptor protein and regulator of gene expression. Mutations in the gene are implicated in Börjeson–Forssman–Lehmann syndrome (BFLS), a rare X-linked intellectual disability disorder characterized by large ears, truncal obesity, and long tapering fingers. BFLS is primarily caused by missense and nonsense mutations while deletions, frameshifts and mutations disrupting the structural integrity of the ZaP domains have been described in T-cell acute lymphoblastic leukemia (T-ALL) and acute myeloid leukemia (AML) patients. To provide more insight into PHF6 and BFLS, we have generated a *Phf6* transgenic mouse line with a patient-related nonsense mutation (R342X). We show that the mutation drastically reduced *Phf6* transcript levels and produced a truncated protein at very low levels in the developing brain. Mice were born at normal Mendelian ratios but mutant mice were significantly smaller than control littermates. Volumetric analysis of the brain via high resolution MRI revealed increased sizes of the amygdala, periaqueductal gray, and hypothalamus, and decreased volumes within the striatum, hippocampus and cerebellum. Studies of the pituitary gland revealed a postnatal defect in the growth of the anterior pituitary but not the posterior or intermediate regions. This change was reflected in altered expression levels of several hormones in the hypothalamic-pituitary-adrenal axis. Preliminary behavioral tests highlighted deficits in the anxiety and depression response of the mutant mice. Additional studies to fully characterize these mice are ongoing.

## **Acknowledgements**

I would like to thank Dr. David Picketts for being a great supervisor during the last two years, providing invaluable advice with regards to my project and personal development. I would also like to thank my thesis advisory committee for the feedback. Furthermore, I would like to acknowledge the members of the Picketts lab, past and present, for their guidance. I would also like to appreciate the collaborators on this project. Last, I would like to thank my family for supporting me, my friends for tolerating me, and my dog and cats for being the amusing creatures that they are.

## Contents

1.0 Introduction.....	1
1.1 Epigenetic regulation of chromatin.....	1
1.2 Epigenetic regulation in neural development.....	4
1.3 Intellectual disability and its link to epigenetics.....	6
1.4 Clinical description of BFLS.....	7
1.5 The identification of the PHF6 gene and the mutations causing BFLS.....	9
1.6 Genomic location and structural features of the PHF6 gene and protein.....	11
1.7 The identification of PHF6 interacting partners and its inferred role.....	13
1.8 Identification of PHF6 as a tumor suppressor gene and its role in lymphoid cancers.....	15
1.9 The role of PHF6 in neuronal migration within the developing cortex.....	19
1.10 Hypothesis and Specific Objectives.....	28
2.0 Methods.....	30
2.1 Maintenance of PHF6 R342X mice.....	30
2.1A Animal husbandry.....	30
2.1B Tracking the survival rate of R342X pups and examining Mendelian ratios.....	30
2.1C Timed mating of mice.....	31
2.1D Genotyping for the R342X mutation.....	31
2.2 Preparation of mouse tissue for downstream experiments.....	33
2.2A Fixing mouse tissue.....	33
2.2B EdU injections to label embryos.....	33
2.2C Brain preparation for MRI and volumetric analysis.....	33
2.2D Blood collection to isolate plasma used in ELISA experiments.....	34

2.3 Staining of frozen tissue sections.....	34
2.3A Frozen section preparation.....	34
2.3B Histochemical staining of frozen sections.....	35
2.3C Immunofluorescent staining of frozen sections.....	35
2.3D Imaging of slides.....	36
2.4 Immunoblotting of mouse brain tissue.....	36
2.5 Nucleic acid extraction and analyses.....	37
2.5A RNA preparation for downstream applications.....	37
2.5B cDNA preparation from total RNA.....	38
2.5C RNA-seq analysis.....	38
2.5D qRT-PCR analysis.....	39
2.5E DNA sequencing analysis.....	40
2.6 Statistics.....	41
3.0 Results.....	42
3.1 Characterization of the gross phenotype of the R342X mice.....	42
3.2. Weight analysis of the R342X mice.....	44
3.3. Analysis of PHF6 protein expression in the R342X mice.....	48
3.4. Analysis of anterior pituitary gland development in the R342X mice.....	54
3.5. Structural analysis of brain development in the R342X mice.....	62
3.6 Characterization of neuronal migration in the R342X mice.....	69
3.7 Behavioural assessment of the R342X mice.....	76
4.0 Discussion.....	78
4.1 Assessing the R342X mice as a model of BFLS.....	78
4.2 Elucidating the pituitary gland postnatal growth defect in the R342X mice...	82
4.3 Characterizing the brain development phenotype in the R342X mice.....	84

4.4 Exploring the PHF6 R342X protein as a functional hypomorphic protein....	87
5.0 Collaborations.....	90
6.0 Appendix.....	91
6.1 Supplementary Figures.....	91
6.2 Supplementary Tables.....	93
6.3 Antibodies and Primers.....	96
7.0 References.....	98
8.0 Copyright permissions.....	113

## List of Figures

Figure 1-1. Chromosome organization and the epigenetic regulation of chromosomes....	4
Figure 1-2. Physical features of BFLS patients as presented in the study by Mangelsdorf et al. in 2009.....	8
Figure 1-3. Schematic representation of the PHF6 protein.....	11
Figure 1-4. Schematic representation of the ZaP domain of the PHF6 protein .....	13
Figure 1-5. Development of T-cells in the thymus .....	17
Figure 1-6. The formation of the neural tube during embryogenesis which gives rise to the cerebral cortex .....	20
Figure 1-7. Cortical development .....	21
Figure 1-8. Temporally regulated cortical layer formation.....	22
Figure 1-9. Feedback loop determining the fate of migrating neurons in the developing cortex as described in Srinivasan et al. 2012.....	25
Figure 3-1. Mendelian ratios and tracking of R342X pups.....	43
Figure 3-2. Body weight comparisons of the R342X mice.....	46
Figure 3-3. Organ weight/body weight ratios of R342X/Y mice.....	47
Figure 3-4. PHF6 expression profile in R342X mice.....	51
Figure 3-5. Investigation into the presence of <i>PHF6a</i> and <i>PHF6b</i> transcripts in R342X mice.....	52
Figure 3-6. Increased separation of the R342X PHF6 band during western blot.....	53
Figure 3-7. Morphology and PHF6 expression within the pituitary glands of WT and R342X mice.....	57
Figure 3-8. RNA expression analysis of targets involved in hormonal .....	58
Figure 3-9. ELISA of hormonal markers from P21 plasma samples. ....	59
Figure 3-10. Immunofluorescent stains of hormone produce cells in the pituitary gland...	61
Figure 3-11. Nissl stains comparing WT and R342X brain regions.....	65
Figure 3-12. MRI images comparing WT and R342X mouse brain structures.....	66

Figure 3-13. Volumetric analysis of the MRI data comparing WT and R342X mice brains.....	67
Figure 3-14. RNA-seq differentially expressed genes and qRT-PCR validation.....	68
Figure 3-15. PHF6 expression in E13.5 R342X cerebral cortex.....	71
Figure 3-16. Investigation of the process of cortical development in the E13.5 R342X cerebral cortex.....	72
Figure 3-17. Investigation of the process of cortical development in the E15.5 R342X cerebral cortex.....	73
Figure 3-18. Investigation of the process of cortical development in the E18.5 R342X cerebral cortex.....	74
Figure 3-19. Investigation of the process of cortical development in the P5 R342X cerebral cortex.....	75
Supplementary Figure 6-1. PCA plot comparing the variation in the data between samples.....	91
Supplementary Figure 6-2. Behavioral tests measuring anxiety in the R342X mice.....	91
Supplementary Figure 6-3. Behavioural test measuring behavioral despair.....	92
Supplementary Figure 6-4. Behavioral tests measuring learning and memory.....	92
Supplementary Figure 6-5. Behavioral test measuring strength.....	92

## List of Tables

Table 1-1. List of <i>PHF6</i> mutations in male and female BFLS patients.....	10
Supplementary Table 6-1. RNA-seq analysis results for genes of interest selected for qRT-PCR.....	93
Supplementary Table 6-2. RNA-seq analysis results for protocadherins and <i>Smarca5</i> .....	95
Supplementary Table 6-3. Percentage of hydrocephalic brains at P21 when comparing WT and R342X mice.....	95



## Abbreviations

5mC- 5-methylcytosine  
Ascl1 - Achaete-Scute family BHLH transcription factor 1  
ACTH - Adrenocorticotrophic hormone  
ADP - Adenosine diphosphate  
AML - Acute myeloid leukemia  
AP - Anterior pituitary  
AQP1 - Aquaporin 1  
Atbf1 - AT Motif-Binding Factor 1  
ATP - Adenosine triphosphate  
ATRX - Alpha Thalassemia/Mental Retardation Syndrome X-Linked  
BAF - BRG-/BRM-associated factor  
BFLS - Börjeson-Forsman-Lehman Syndrome  
BMP - Bone morphogenetic protein  
BPTF - Bromodomain PHD finger transcription factor  
bRG - Basal radial glia  
BSA - Bovine serum albumin  
CBP - CREB-binding protein  
CD - Cluster of differentiation  
cDNA - Complementary deoxyribonucleic acid  
CpG - 5'-C-phosphate-G-3'  
CHD 4 - Chromodomain helicase DNA binding protein 4  
CML - Chronic myelogenous leukemia  
CMP - Common myeloid progenitor  
CLP - Common lymphoid progenitor  
CP - Cortical plate  
CSF - Cerebral spinal fluid  
CSPG5 - Chondroitin sulfate proteoglycan 5  
CT - Computed tomography  
CTIP2 - Chicken ovalbumin upstream promoter transcription factor-interacting proteins 1  
CUX1 - Cut like homeobox 1  
DNA - Deoxyribonucleic acid  
DN - Double negative  
DP - Double positive  
dsDNA - double stranded deoxyribonucleic acid  
DNMT1 - DNA (cytosine-5)-methyltransferase 1  
DNMT3 - DNA (cytosine-5)-methyltransferase 3  
Fezf2 - Fez family zinc finger 2  
FOXP1 - Forkhead box P1  
ECL - Enhanced chemiluminescence  
EDTA - Ethylenediaminetetraacetic acid  
EdU - 5-ethynyl-2'-deoxyuridine

EMSA - Electrophoretic mobility shift assay  
Emx2 - Empty spiracles homeobox 2  
ESE - Exon splicing enhancer  
ESS - Exon splicing silencer  
FGF - Fibroblast growth factor  
Folr1 - Folate receptor 1  
Foxg1 - Forkhead box G1  
Foxp1 - Forkhead box protein P1  
FSH - Follicle stimulating hormone  
GH - Growth hormone  
GHRH - Growth hormone-releasing hormone  
HCC - Hepatocellular carcinoma  
His - Histidine  
HAT - Histone acetyltransferase  
HDAC - Histone deacetylase  
HDMT - Histone demethyltransferase  
Hes1 - Hairy and enhancer of split-1  
HMT - Histone methyltransferase  
Hmga1b - High mobility group AT-hook 1b  
HL - Hodgkin lymphoma  
HPA - Hypothalamic pituitary adrenal  
HPLC - High pressure liquid chromatography  
HSC - Hematopoietic stem cell  
ID - Intellectual disability  
ING2 - Inhibitor of growth 2  
IZ - Intermediate zone  
IP - Intermediate progenitor  
IP - Intermediate pituitary  
IGF-1 - Insulin-like growth factor 1  
JAK1 - Janus kinase 1  
JmjC - Jumonji C  
JMJD3 - Jumonji C (JmjC) domain-containing protein 3  
LDS - Lithium dodecyl sulfate  
LH - Luteinizing hormone  
Lhx2 - LIM/homeobox protein 2  
Lis1 - Lissencephaly-1  
mESC - Mouse embryonic stem cell  
MHC - Major histocompatibility complex  
MBD - Methyl-CpG-binding domain  
MECP2 - Methyl CpG binding protein 2  
miRNA - MicroRNA  
MPP - Multipotent progenitors  
MRI - Magnetic resonance imaging

MZ - Marginal zone  
NEC - Neuroepithelial cell  
Neurod4 - Neuronal differentiation 4  
Neurog1 - Neurogenin 1  
Neurog2 - Neurogenin 2  
NLS - Nuclear localization signal  
NMD - Nonsense-mediated decay  
NoLS - Nucleolar localization signal  
NOTCH1 - Notch homolog 1 translocation-associated  
NP-40 - Nonyl phenoxypolyethoxylethanol-40  
NSC - Neural stem cell  
NuRD - Nucleosome remodeling and deacetylase  
NURF - Nucleosome remodeling factor  
OCT - Optimal cutting temperature  
OHRI - Ottawa Hospital Research Institute  
Paf1C - Polymerase II associated factor complex  
PAX6 - Paired box protein 6  
PBS - Phosphate buffered saline  
PFA - Paraformaldehyde  
PHD - Plant homeodomain  
PHF6 - Plant homeodomain finer protein 6  
PP - Posterior pituitary  
PIT1 - POU class 1 homeobox 1  
Pol - Polymerase  
Pomc - Pro-opiomelanocortin  
PTM - Post translational modification  
Prl - Prolactin  
qRT-PCR - Quantitative reverse transcriptase-polymerase chain reaction  
RBBP4 - Retinoblastoma-binding protein 4  
rDNA - Ribosomal DNA  
REST - RE1-silencing transcription factor  
RGC - Radial glial cell  
RIPA - Radioimmunoprecipitation assay  
RNA - Ribonucleic acid  
rRNA - Ribosomal RNA  
RT - Room temperature  
Satb2 - AT-rich sequence-binding protein 2  
SDS - Sodium dodecyl sulphate  
Shh - Sonic hedgehog  
shRNA - Short hairpin RNA  
SKRTT - Skip exon 10 Resulting in Triple Three amino acids  
SOX2 - SRY-Box 2  
Sox5 - SRY-Box 5

SP - Single positive

SP - Subplate

Smarca5 - SWI/SNF Related, Matrix Associated, Actin Dependent Regulator Of Chromatin, Subfamily A, Member 5

SET-NUP214 - Su(var)3-9 enhancer-of-zeste and trithorax nucleoporin 214

SWI/SNF - SWItch/Sucrose Non-Fermentable

SVZ - Subventricular zone

T3 - Triiodothyronine

T4 - Thyroxine

T-ALL - T-cell Acute Lymphoblastic Leukaemia

TBST - Tris-buffered saline tween 20

TBR1 - T-box brain protein 1

TBR2 - T-box brain protein 2

TET1 - Ten-eleven translocation methylcytosine dioxygenase 1

Tle1 - Transducin like enhancer of split 1

TLX - T Cell Leukemia Homeobox

TRH - Thyrotropin-releasing hormone

XLID - X-linked intellectual disability

UBF - Upstream binding factor

UTR - Untranslated region

VZ - Ventricular zone

WAT - White adipose tissue

## **1.0 Introduction**

### **1.1 Epigenetic regulation of chromatin**

The epigenetic landscape in eukaryotes involves careful and synchronized input from all the components of the system to bring about change at the most minute level of biological systems, the effect of which reverberates throughout the whole organism. DNA at the most basic level is organized into coding and non-coding regions, comprising the genome, and is tightly wound around proteins known as histones, forming nucleosomes. Other proteins interact with histones and the chromosome, to either condense or unwind the DNA, allowing transcription, replication and repair. Errors in the processes involved can lead to lethal consequences. Therefore, epigenetic regulation at the chromatin level can be thought of as players of an orchestra working together to play out an exceptionally complex musical piece.

Nucleosomes consists of the histone core and the DNA wrapped around it as described by Luger et al. in 1997. The histone core consists of two copies of each of the proteins that comprise the core (H2A, H2B, H3 and H4) and the 145-147 base pairs of DNA that are wrapped around the core. The nucleosome is further compacted by the histone H1 that binds the linker DNA. This arrangement allows the DNA to be either present in a closed/compact conformation which is known as heterochromatin or an open/accessible conformation which is known as euchromatin (Campos and Reinberg 2009). Modifications of the epigenetic landscape can affect the configuration state of the chromosome.

One modification which affects the open/closed state of chromatin is DNA methylation. DNA methylation occurs on the cytosine nucleotide of DNA within a CpG dinucleotide, and often on the palindromic repeats of 5'-C-phosphate-G-3' (CpG) islands (Ooi et al. 2009). The methylation of the cytosine nucleotide exists in the form of a 5-methylcytosine (5mC) mark (Ooi

et al. 2009). The mark can be deposited by the DNA (cytosine-5)-methyltransferase 1 (DNMT1) protein and the DNA (cytosine-5)-methyltransferase 3 (DNMT3) family of proteins (DNMT3A, DNMT3B) (Ooi et al. 2009). Since these enzymes induce an epigenetic modification, they are categorized as “writers.” Meanwhile, the ten-eleven translocation (TET) family of proteins oxidize the 5mC mark, leading to the formation of the 5-hydroxymethylcytosine (5hmC) mark, which eventually leads to the loss of the methylation modification following DNA replication (Rasmussen and Helin 2016). 5mC marks mediate repression of DNA transcription by preventing binding of proteins which drive transcription at that location or by recruiting methyl-CpG-binding domain (MBD) containing proteins which serve a similar function (Klose and Bird 2006). Enzymes which recognize epigenetic modifications to mediate further epigenetic regulation are categorized as “readers.”

The N-terminal and C-terminal tails of histone proteins contain residues which can be modified forcing adjustment of DNA compaction around the respective histone core (Campos and Reinberg 2009). There are many different types of modifications that have been described with acetylation, methylation, and phosphorylation the best studied, and briefly reviewed here.

Histone acetyltransferases (HATs), a class of writer proteins, acetylates lysine residues on histones, decreasing the interaction between the positively charged lysine residue and the negatively charged DNA backbone (Shahbazian and Grunstein 2007). This leads to a more open chromatin state as the DNA is not as tightly wound around the modified histone. The open chromatin is then relatively more accessible to other proteins which can drive transcription. Moreover, the histone-bound HAT itself can serve as a binding site for such proteins (Shahbazian and Grunstein 2007). On the other hand, histone deacetylases (HDACs) deacetylate acetylated residues, generally producing the opposite effect to HATs (Shahbazian and Grunstein

2007). Since HDACs remove histone modifications, they are a part of an enzyme class called “erasers.” Like HATs, HDACs can act as binding sites for other proteins, but in this case, it generally brings about repression (Shahbazian and Grunstein 2007).

With regards to histone methylation, basic residues of the histone can be methylated by writers called histone methyltransferases (HMTs) while the reversal of histone methylation is achieved by histone demethyltransferases (HDMTs) (Greer and Shi 2012). The methylation of a lysine residue can vary from a mono- to a tri- methylation state (Hyun et al. 2017). Tri-methylation states on specific residues (eg. H3K4, H3K36 and H3K79) force an open chromatin state, while tri-methylation of other residues (eg. H3K9, H3K27 and H4K20) lead to a closed chromatin state (Hyun et al. 2017). There are over 500 histone interacting proteins (writers, erasers, readers) involved in the methylation and acetylation modification dynamic (Xu et al. 2017). From this fact alone, one can realise how massive the operation of epigenetic regulation entails.

Moreover, histone residues can be reversibly phosphorylated, ubiquitylated and ADP (adenosine diphosphate)-ribosylated to mediate epigenetic change (Bowman and Poirier 2015). Regulation also involves ATP (adenosine triphosphate)-dependent nucleosome remodelers which can slide nucleosomes along DNA and remove or exchange nucleosomes (Hargreaves and Crabtree 2011). Overall, epigenetic regulation does not involve exclusive events but events which work in conjunction to provide a plethora of possible post translation modification (PTM) combinations and interactions across the genome, generating complex chromatin states across different tissues, individuals and timepoints (Suganuma and Workman 2008).

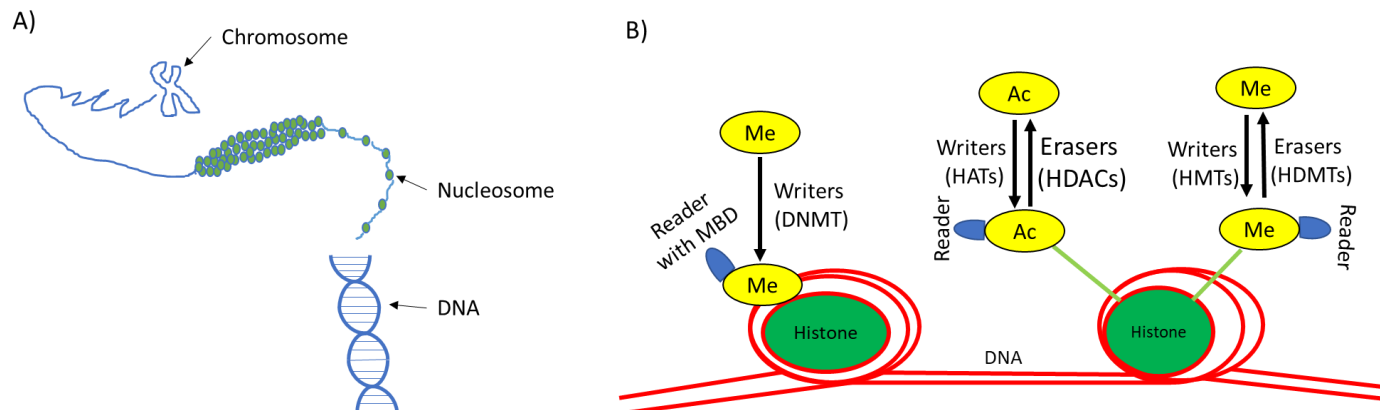


**Figure 1-1. Chromosome organization and the epigenetic regulation of chromosomes (Niederberger et al. 2017).** (A) DNA in blue is wrapped around histones in green to form nucleosomes which further compact the DNA. This compaction strategy allows for the efficient storage of a large amount of DNA and the regulation of DNA based biological processes. (B) Epigenetic regulation of the chromosome via DNA modification and histone PTMs. Me denotes methyl group, and Ac, acetyl group.

## 1.2 Epigenetic regulation in neural development

Neural development in mammals is a complex process. As described by Juliandi et al. in 2010, neural progenitors (NPCs) involved in the development of the mammalian brain have the ability to undergo symmetric division to increase the progenitor pool or produce two mature differentiated cells, and asymmetric division to produce another progenitor and a differentiated neuron, oligodendrocyte or astrocyte, which contributes to the mature cell population of the brain. The NPC proliferation and differentiation processes are carefully regulated, such that the appropriate number of mature cells are generated to migrate and contribute to developing structures in the brain. Cell cycle regulation occurs from the embryonic stage and into adulthood as neural progenitors are present in the adult brain as well (Yao and Jin 2014). Furthermore, epigenetic regulation is involved in the maintenance of mature cells in terms of neural health and function (Sultan and Day 2011).



Reviewing the literature in the context of the epigenetic processes, allows us to appreciate how important epigenetic regulation is in neural development. In 1999, Okano et al. showed that *Dnmt3b* knock-out mice were afflicted with neural tube developmental defects. In 2010, Wu et al. showed that DNMT3a plays an important role in neurogenesis in the mouse brain. Methyl CpG binding protein 1 (MBD1) has been shown to be important in neurogenesis and neural differentiation (Zhao et al. 2003 and Jobe et al. 2016). CREB-binding protein (CBP), a HAT, has been shown to be important in neuron differentiation and development (Lee et al. 2009; Wang et al. 2010). Deacetylation of H3 by HDACs was shown to be important in the myelination of the developing brain (Shen et al. 2005). Jumonji C (JmjC) domain-containing protein 3 (JMJD3), is a HDMT involved in neuronal commitment (Burgold et al. 2008). Components of the SWItch/Sucrose Non-Fermentable (SWI/SNF) complex, an ATP-dependent nucleosome remodeling complex, are involved in neurogenesis and differentiation (Sokpor et al. 2017). Interestingly, epigenetic genes have been shown to be involved in cultivating neural plasticity and consequentially, these genes have an effect on the learning behaviour of animals (Bronfman et al. 2014). For example, in one study it was shown that the acetylation of H3 and H4 is important in the recovery of impaired learning by mediating the necessary neural re-networking events (Fischer et al. 2007). Dendrites are processes of the neuron which allow neurons to exhibit their function (Smrt and Zhao 2010). Dendrite health is important in learning and memory and interestingly, methyl CpG binding protein 2 (*Mecp2*) knock-out mice, have abnormal dendritic spine morphology (Smrt et al. 2007). Mutations in *MECP2* lead to Rett syndrome, a well-known X-linked intellectual disability disease that primarily affects young girls (Kriaucionis and Bird 2003). These examples are just a glimpse into the role of epigenetic

regulation in neural development as there are numerous other genes involved (Fagiolini et al. 2009; Hu et al. 2014; Murao et al. 2016).

### **1.3 Intellectual disability and its link to epigenetics**

Intellectual disability (ID) is a debilitating characteristic of several neurodevelopmental disorders and intellectual disability syndromes. The defining characteristic of the feature is an IQ score of <70, with severity ranging from mild to severe (Vissers et al. 2015). The world-wide prevalence of intellectual disability is around 1% (Maulik et al. 2011). Intellectual disability inhibits the cognitive, linguistic and motor capabilities of the patients, placing stress on the affected families and communities (Katz and Lazcano-Ponce 2008). The recent advancements in the screening techniques for mutations in patients has paved the way for an upsurge in identification of genes involved in disorders (van Bokhoven 2011). Around 750 genes have been shown to be involved in disorders associated with ID (Kochinke et al. 2016). Of the many genes involved in ID, mutations in more than 100 genes on the X-chromosome are associated with ID (Piton et al. 2013). Diseases with ID as the primary feature, caused by mutations in genes on the X-chromosome are referred to as X-linked intellectual disability (XLID) syndromes. Around 55 epigenetic genes have been implicated in ID and 25 of these genes are located on the X-chromosome (Kleefstra et al. 2014). One such gene, plant homeodomain finger protein 6 (*PHF6*) encodes a chromatin adaptor protein implicated primarily in Börjeson–Forssman–Lehmann syndrome (BFLS), a rare XLID syndrome. The disease was first described in 1962 (Borjeson et al. 1962) and the *PHF6* gene was discovered to be causative of the disease by a positional cloning approach (Lower et al. 2002).

#### **1.4 Clinical description of BFLS**

In 1962, Börjeson et al. reported on three individuals with ID and similar facial and body dysmorphia. Upon further investigation, these individuals were found to be related to each other. More detailed description of the individuals highlighted additional characteristics like epilepsy, a hunched posture with knocked-knees, presence of fatty tissue around the mammary and trunk, inhibition of genitalia development, hypometabolism and defects in digits of the limbs. Based on the interpretation from the pedigree and the common characteristics shared between the patients, Börjeson et al. were the first to describe BFLS clinically. Since then, the *PHF6* gene was discovered to be implicated in the disease and the clinical description of BFLS has been expanded as 17 families with BFLS patients have been described (Zweier et al. 2013). The main phenotype in males is comprised of intellectual disability (ranging from mild to severe), deep set eyes, large ears, coarse facial features, gynecomastia, truncal obesity, hypogonadism, long tapering fingers, short toes and hypotonia (Turner et al. 2004; Zweier et al. 2013). These symptoms arise during childhood through adolescence (Turner et al. 2004; Zweier et al. 2013). A broad range of other symptoms are present in patients and they vary from individual to individual (Turner et al. 2004; Zweier et al. 2013). Notable conditions include microcephaly, macrocephaly, cortical defects, polyneuropathy, inhibition in the development of male genitalia, and defects in hormonal homeostasis (Lower et al. 2004; Gecz et al. 2006; Carter et al 2009; Jahani-Asl et al. 2016; Kasper et al. 2017). In females, the phenotype is similar to the male phenotype but ranges from mild to severe with a high degree of heterogeneity for the manifestation of certain features. For example, some females are affected by linear skin hyperpigmentation while others are not (Zweier et al. 2013). This could be attributed to the effect of variable X-chromosome inactivation which differs in tissues and between patients as well

(Zweier et al. 2013). Interestingly, the clinical overlap between male and female patients is inconsistent, with some females possessing facial features not present in male patients, which leads to inaccurate diagnoses in some of the females when they are children (Zweier et al. 2013).

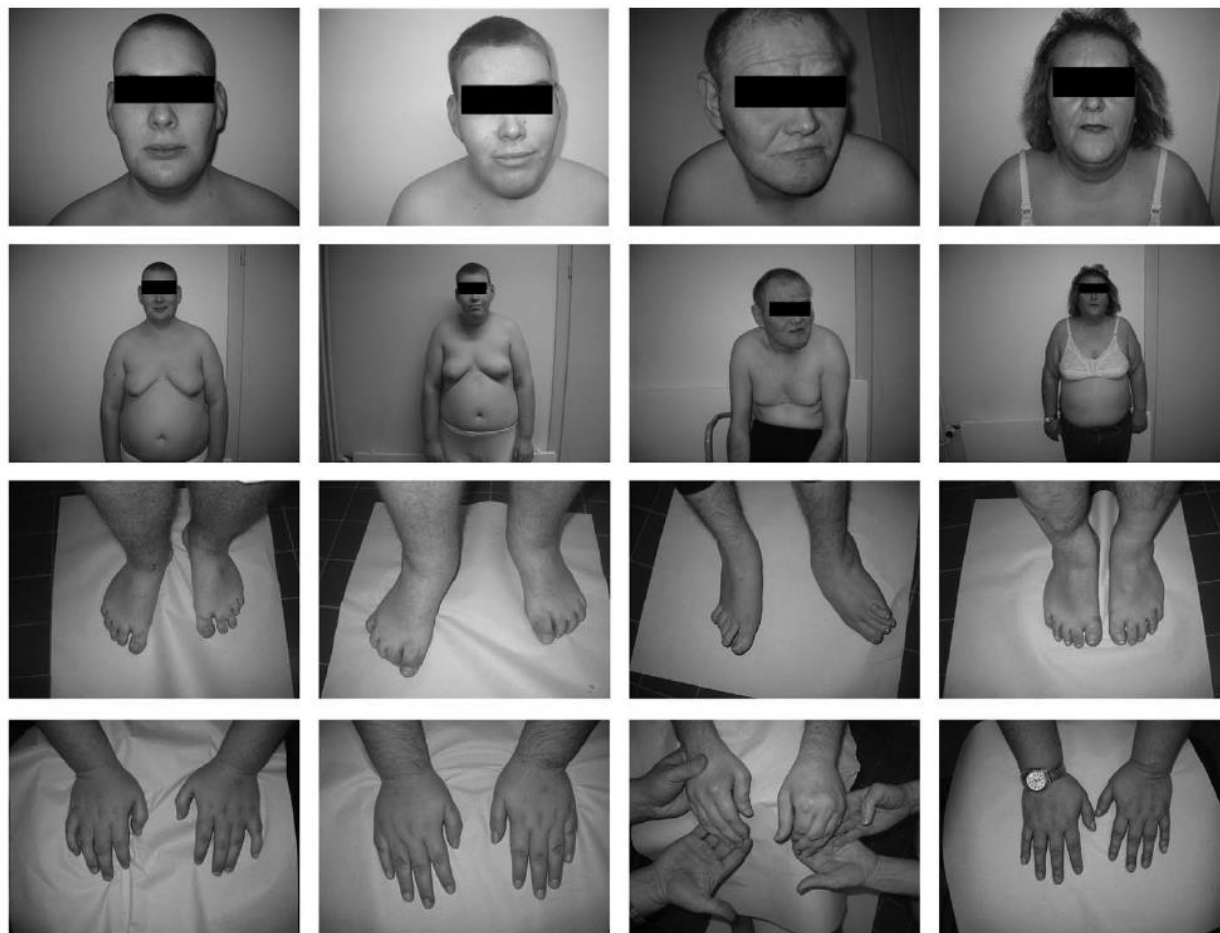


**Figure 1-2. Physical features of BFLS patients as presented in the study by Mangelsdorf et al. in 2009.** Each column corresponds to a different patient. The patients in column 1 and column 2 are siblings. Their mother is a carrier but does not present with the BFLS phenotype, perhaps because she is on the extremely mild end of the disease severity spectrum. Columns 3 and 4 are the uncle and aunt of the siblings, respectively. The uncle presented with the classical male BFLS phenotype while the aunt presented with a mild BFLS phenotype. As evident from the first row of panels, BFLS patients have coarse facial features and large ears. From the second row we can see that patients are affected by truncal obesity, gynecomastia and hypotonia. From the panels in the third row, we can see that the patients have shortening of the toes and syndactyly. The last row of panels displays the long tapering fingers shared by BFLS patients.

### **1.5 The identification of the *PHF6* gene and the mutations causing BFLS**

Initially, in 1996, Gedeon et al. determined that the gene associated with BFLS was present in a ~17 Mb region flanked by the microsatellite markers DXS425 and DXS105 on the X-chromosome. In 2002, Lower et al. narrowed this down to a ~9Mb region. Gene candidates were then selected based on their expression patterns in the brain and their relative similarity to known genes involved in X-linked mental retardation. This approach allowed them to discover *PHF6* and its mutations in BFLS patients, establishing its implication in the disease.

Since then, a significant number of *PHF6* mutations have been successfully identified in patients diagnosed with BFLS. Missense mutations and nonsense mutations are more prevalent in male BFLS patients while female BFLS carriers have been observed to possess point mutations, frameshift mutations and deletions as well (Table 1-1). Interestingly, mutations span the entire *PHF6* gene and it seems that mutations in the structural domains do not increase disease severity. Overall, no correlation has been noticed between the location, the type of *PHF6* mutation and the corresponding collection of symptoms from that mutation (Todd et al. 2015). Many patients with phenotypic features of BFLS have been reported to not possess any *PHF6* mutations (Todd et al. 2015). This has been attributed to the overlap of symptoms with other conditions like Coffin-Lowry syndrome, Klinefelter syndrome, Prader-Willi syndrome, Wilson-Turner syndrome and Cohen syndrome and is less likely to result from genetic heterogeneity (Turner et al. 2004; Todd et al. 2015). Many female patients who do not share similar features to male patients, have been misdiagnosed with Coffin-Lowry syndrome in their childhood (Zweier et al. 2013).

Gender	Type of mutation	Location of mutation	Frequency of mutation
M	p.M1T missense	Exon 2	2
M	p.C45Y missense	Exon 2	2
M	p.G89V missense	Exon 4	1
M	p.C99F missense	Exon 4	1
M, F	p.H229R missense	Exon 7	2 (1M, 1F)
M	p.K234E missense	Exon 7	1
M	p.R257G missense	Exon 8	2
M	p.I314V missense	Exon 9	1
M	p.K8X nonsense	Exon 2	1
F	p.R319X nonsense	Exon 9	1
M	p.R342X nonsense	Exon 10	5
F	p.G10fs*21 frameshift	Exon 2	1
M	M46fsΔexon3 frameshift	Exon 3	1
F	p.G226fsE*53 frameshift	Exon 7	1
F	p.C305F frameshift	Exon 9	1
F	Duplication mutation	Exons 4-5	2
F	6 kb deletion	Exons 4–5	1
F	100 kb deletion	Exons 6-10	1
F	15 kb deletion	Exons 9–11	1
M	c.999–1001 delTGA p.D333 deletion	Exon 10	2
F	PHF6 gene	Whole	2

**Table 1-1. List of *PHF6* mutations in male and female BFLS patients (Todd et al. 2015).**

### 1.6 Genomic location and structural features of the PHF6 gene and protein

The *PHF6* gene is located on the X chromosome (Xq26.2; X:134,373,311-134,428,791), contains eleven exons that are transcribed to produce a 4.5 kb mRNA product with exons 1 and 11 comprising the 5'- and 3'-untranslated regions (UTRs), respectively. The PHF6 protein consists of 365 amino acids and is encoded by exons 2-10. The PHF6 protein contains nuclear localization signals (NLSs) and nucleolar localization signal (NoLS) sequences and two atypical plant homeodomain motifs (Figure 1-3). There is 97.5% amino acid sequence similarity of the protein between humans and mice and there are no structural homologs in invertebrates (Voss et al. 2007).

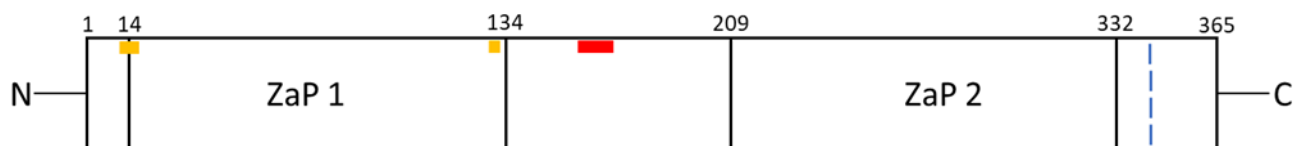


**Figure 1-3. Schematic representation of the PHF6 protein.** The N-terminus of the protein is denoted with the letter N and the C-terminus of the protein is denoted with the letter C. The position based on amino acid count is marked on the upper portion of the schematic. The two zinc knuckle atypical PHD structural domains of the PHF6 protein are abbreviated as ZaP1 and ZaP2. The two Nuclear location sequences (NLSs) are marked in yellow and the nucleolar localization sequence (NoLS) is marked in red. The R342X mutation, which is the most common human BFLS mutation is marked by the blue dotted line.

The PHF6 protein contains two zinc knuckle-atypical PHD (ZaP) domains. A typical plant homeodomain (PHD) finger domain is comprised of a Cys4-His-Cys3 sequence producing cross-brace motifs stabilized by two zinc ions (Capili et al. 2001). The PHD domain was discovered in 1993 by Schindler et al. in *Arabidopsis* and was shown to have DNA binding ability. Eventually, the PHD domain was shown to possess histone modification capability, highlighting the tendency of proteins with the domain to be associated with epigenetic

regulation, a few of them mentioned here. The PHD domain of the bromodomain PHD finger transcription factor (BPTF) subunit of the nucleosome remodeling factor (NURF) complex has been shown to recognize the H3K4me3 mark, mediating NURF function (Wysocka et al. 2006). The NURF complex is an ATP-dependent nucleosome remodeler which drives transcription (Badenhorst 2002). The inhibitor of growth 2 (ING2) protein is a PHD domain containing protein of the mSin3a–HDAC1 histone deacetylase complex which also recognizes the H3K4me3 mark, but it facilitates repression (Shi et al. 2006). The recognition of the mark is important in mediating the DNA damage repression response (Shi et al. 2006). Following these studies, PHD domain containing proteins have been shown to be able to bind to H3K4me0 and H3R2 (Sanchez 2011). Interestingly, mutations in the PHD domains of other chromatin remodeling proteins lead to intellectual disability, like in the case of ATRX mutations corresponding to the Alpha Thalassemia/Mental Retardation Syndrome X-Linked (ATR-X) syndrome (Gibbons et al. 1997).

The atypical PHD domain of PHF6 consists of a Cys3-His-Cys3-His amino acid sequence. This results in PHF6 being unique from other PHD-finger like proteins by having a greater positive charge, being able to bind double stranded deoxyribonucleic acid (dsDNA) non-specifically but being unable to bind histones (Liu et al. 2014). Interestingly, this variant of the PHD domain is unique to the PHF6 protein alone (Liu et al. 2014). The first ZaP and second ZaP domains of PHF6 share 49% amino acid sequence similarity but has been suggested to be structurally similar (Bao et al. 2015).



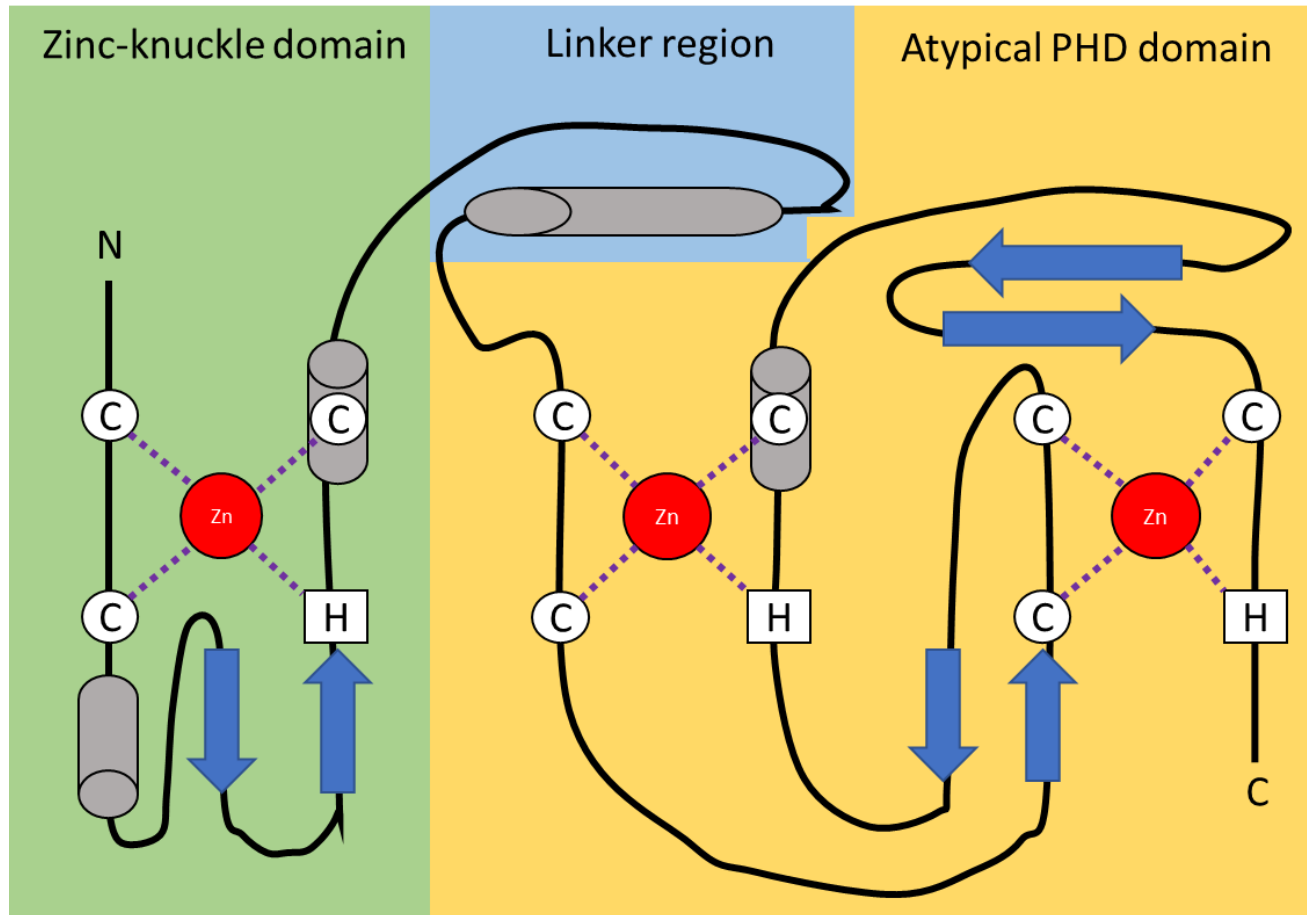


**Figure 1-4. Schematic representation of the ZaP domain of the PHF6 protein. Adapted from Liu et al. 2014.** The zinc-knuckle domain in green precedes the atypical PHD domain of the ZaP domain in orange. The region in blue is the linker regions between the two domains. In the atypical PHD domain, the second zinc ion surrounded by the Cys3-H residues instead of Cys4 residues differentiates the atypical PHD domain from a typical PHD domain. Cysteine residues are represented in circles and histidine residues are represented in squares.  $\alpha$ -helices are represented as grey cylinders and  $\beta$ -pleated sheets as blue arrows. Zinc ions are presented as red circles.

### 1.7 The identification of PHF6 interacting partners and its inferred role

Unlike other proteins with PHD domains, PHF6 is unable to bind histones but binds dsDNA non-specifically (Liu et al. 2014). This inability to bind histones obscures the functionality of PHF6 as a chromatin remodeling protein. The fact that PHF6 binds to dsDNA non-specifically points to the possibility that PHF6 acts a gene regulator. Indeed, this was proven

by Liu et al. in 2014 who have shown that PHF6 acts as a direct transcriptional repressor at the DNA level. Furthermore, PHF6 has been shown to have interactions with microRNA (miRNA), some of which are involved in important temporal processes such as neural development (Todd et al. 2015; Franzoni et al. 2015).

To identify PHF6 interacting proteins, one group expressed a FLAG-tagged version of PHF6 and immunoprecipitated interacting proteins which they identified by mass spectrometry. In this way, PHF6 was shown to interact with multiple proteins of the nucleosome remodeling and deacetylation (NuRD) complex (Todd and Picketts 2012). These interactions were later confirmed by another group in several experiments. In one experiment, they used GST-tagged PHF6 to pull down the purified recombinant retinoblastoma-binding protein 4 (RBBP4) subunit of the NuRD complex which was then detected by immunoblotting (Liu et al. 2014). In other experiments, they produced the co-crystal structure of RBBP4 with the portion of the PHF6 protein shown to interact with the subunit (Liu et al. 2015). An RBBP4 interaction was also shown in co-immunoprecipitation experiments where FLAG-tagged versions of PHF6 were used to detect RBBP4 interactions by immunoblotting (Liu et al. 2015). The NuRD complex is a chromosome remodeling protein complex which can interact with histones (Basta and Rauchman 2015) and is involved in oncogenesis (Lai and Wade 2011), embryonic development (Hu and Wade 2012), neurogenesis (Nitarska et al. 2016) and hematopoiesis (Ramírez and Hagman 2009). This points to the fact that the NuRD complex is a master regulator involved in development via epigenetic change. Liu et al. showed in 2015 that the transcriptional repression activity of PHF6 was dependent on its interaction with the RBBP4 subunit of the NuRD complex. Thus, one could postulate that PHF6 interacts with the NuRD complex, recognizes a DNA sequence whilst bound, bringing the NuRD complex to its targets, and allowing it to

achieve its functions. In one study, cell lines expressing SBF-tagged PHF6 were subjected to tandem affinity purification and then subjected to mass spectrometry analysis (Wang et al. 2013). The upstream binding factor (UBF) was found to be an interacting partner of PHF6 (Wang et al. 2013). Co-immunoprecipitation experiments confirmed the interaction between PHF6 and UBF (Wang et al. 2013). The authors then went on to discern that PHF6 negatively regulates the upstream binding factor (UBF) to repress ribosomal RNA (rRNA) transcription (Wang et al. 2013). In the absence of PHF6, UBF interacts with RNA polymerase (Pol) I complex to drive transcription of ribosomal DNA (rDNA) (Goodfellow and Zomerdijk 2012). Moreover, in another study, it was shown that PHF6 interacts with the RNA polymerase II associated factor complex (Paf1C) (Zhang et al. 2013). The authors employed immunoprecipitation followed by mass spectrometry to find that all the subunits of the Paf1C interacted with PHF6, confirming the interactions in co-immunoprecipitation experiments. The Paf1C is involved in the functioning of the Pol I enzyme as well as the Pol II enzyme, driving transcriptional elongation, again suggesting that PHF6 is involved in rDNA transcription (Zhang et al. 2010). Therefore, it is possible that PHF6 might be regulating gene expression levels by controlling the level of ribosome expression by controlling UBF and Paf1C function. Interestingly, it has also been shown that the Paf1C has the ability to mediate histone modifications, suggesting another way PHF6 might achieve chromatin regulation indirectly (Krogan et al. 2003; Tomson and Arndt 2013).

### **1.8 Identification of PHF6 as a tumor suppressor gene and its role in lymphoid cancers**

PHF6 has also been shown to be implicated in various cancers. *PHF6* was present as a secondary mutation along with other oncogenes like T cell leukemia homeobox 1 (*TLX1*) and T cell leukemia homeobox 3 (*TLX3*) in T-ALL patients as reported by Vlierberghe et al. in 2010. In

a cohort of T-cell acute lymphoblastic leukaemia (T-ALL) patients, *PHF6* mutations were present in 16% of pediatric patients and 38% of adult patients (Vlierberghe et al. 2010). In another study, *PHF6* was present as a secondary mutation in T-ALL patients with notch homolog 1 translocation-associated (*NOTCH1*), *su(var)3-9* enhancer-of-zeste and trithorax nucleoporin 214 (*SET-NUP214*) and janus kinase 1 (*JAK1*) mutations (Wang et al. 2011).

Development of T-cells occurs from the myeloid lineage (Katsura 2002; Radtke et al. 2013). As described by Katsura in 2002, and Radtke et al. in 2013, the earliest progenitors in the lymphoid development pathway are the hematopoietic stem cells (HSCs) in the bone marrow which gives rise to multipotent progenitors (MPPs). The MPPs then differentiate either into common lymphoid progenitors (CLPs) or common myeloid progenitors (CMPs). CMPs eventually lead to the production of members of the innate immune response and to the production of the red blood cell components. Meanwhile, the CLPs give rise to the adaptive immune response components. CLPs travel from the bone marrow to the thymus where differentiation into T cells occurs. CLPs are first present in the form of double negative (DN) cells. These cells are cluster of differentiation (CD)4-CD8- and are further categorized into DN1, CD44+CD25-; DN2, CD44+CD25+; DN3, CD44-CD25+; and DN4, CD44-CD25-. Rearrangement of the T-cell receptor  $\alpha$  chain leads to maturation into CD4, CD8 double positive (DP) cells. Further selection via major histocompatibility complex (MHC) class I and MHC class II self-peptides leads to CD4+ single positive (SP) cells or CD8+ SP cells.

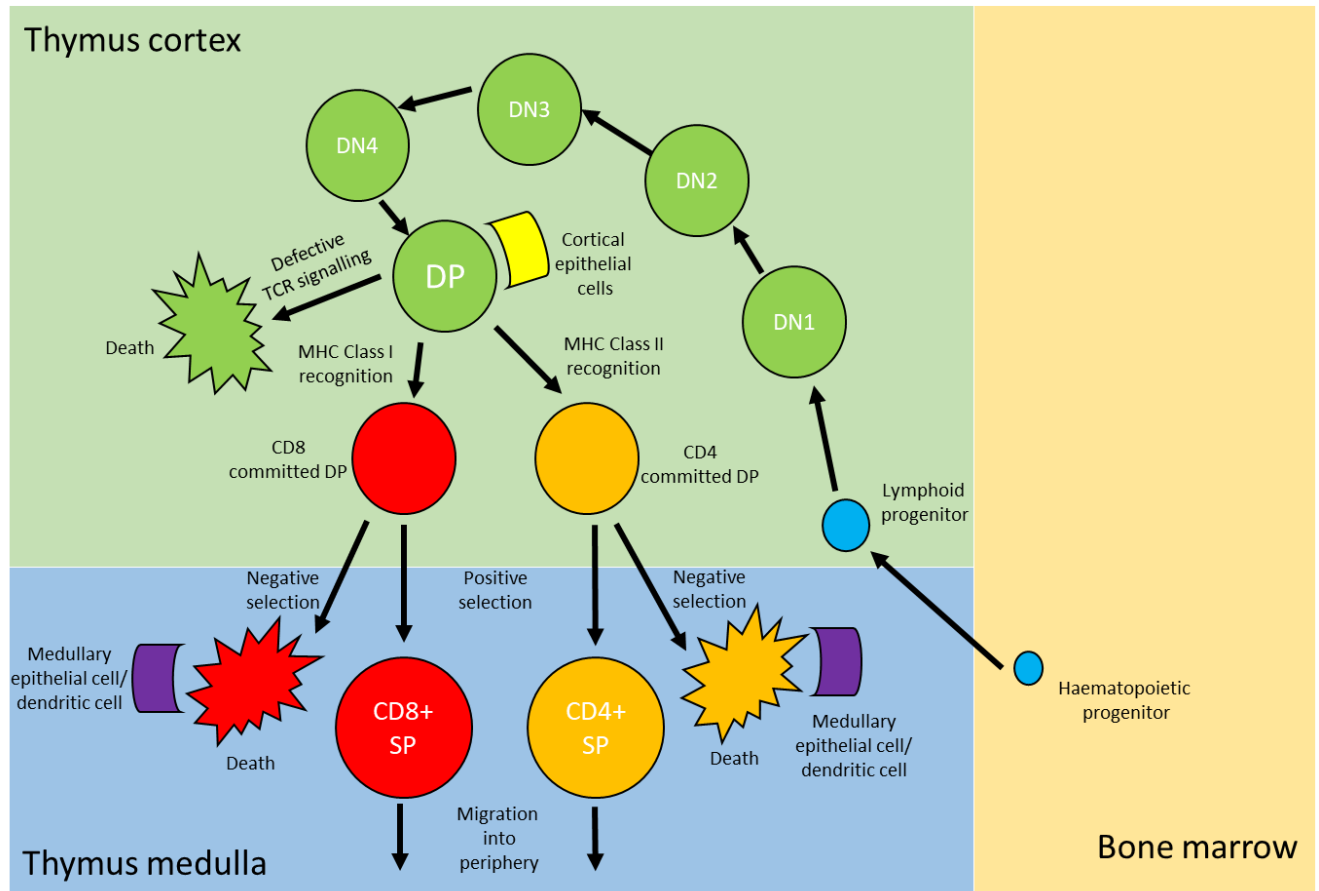


**Figure 1-5. Development of T-cells in the thymus. Adapted from Radtke et al. 2013.** The lymphoid progenitor arrives at the thymus from the bone marrow, undergoing the first round of selection in the cortex. Differentiated cells then pass into another stage of selection/differentiation in the medulla of the cortex, finally giving rise to CD4+ SP cells or CD8+ SP cells.

T-ALL arises when translocation events and mutations in oncogenes leads to arrest in the developmental pathway of T-cells (Peirs et al. 2014). Interestingly, high PHF6 expression was seen in human thymus tissue and human lymphoid cells which were CD4+CD8+, suggesting a possible role of PHF6 mediated regulation at this stage of the developmental trajectory (Vlierberghe et al. 2010).

The Vlierberghe et al. study in 2010 showed that the T-ALL patient *PHF6* mutations were frameshift mutations, deletion mutations and missense mutations unique to T-ALL patients

and never observed before in BFLS patients. The *PHF6* mutations in the Wang et al. study in 2011 were frameshift mutations or missense and nonsense mutations thought to interfere with the function of the second ZaP domain. Furthermore, the Vlierberghe et al. study in 2010 used immunohistochemistry to investigate PHF6 expression in lymphoblast cells from the T-ALL patients of the cohort they were investigating. Cells with some mutations led to unaffected PHF6 expression, while others led to a decrease in PHF6 expression. This variable expression pattern of PHF6 in T-ALL patients points to the possibility that the *PHF6* mutations considerably affect either the function or the abundance of the protein and that PHF6 functions as a tumour suppressor. Interestingly, in another study, a BFLS patient was diagnosed with T-ALL at the age of seven (Chao et al. 2010). However, this is the only reported case of a cancer diagnosis in a BFLS patient. Therefore, we cannot assume that BFLS mutations are oncogenic from this single event.

Acute myeloid leukemia (AML) arises from translocation events and mutations in oncogenes which leads to the abnormal proliferation and differentiation ability of the progenitors in the myeloid lineage (Steffen et al. 2005). In one cohort of AML patients, 3% had *PHF6* mutations including frameshift, missense and nonsense mutations (Vlierberghe et al. 2011). In the same study, they investigated the levels of PHF6 in mouse myeloid cells by qRT-PCR and found it to be relatively lower than the lymphoid cells. Another study investigating a larger cohort, found *PHF6* mutations in 2% of AML patients (de Rooij et al. 2015). Both studies showed that the *PHF6* mutation was present as a secondary mutation. Therefore, overall it seems that *PHF6* plays less of an impact in AML in comparison to T-ALL, given the frequency of AML patients with a *PHF6* mutation and the expression pattern of the protein in myeloid cells.

*PHF6* mutations have also been present as a secondary mutation in a few cases of chronic myelogenous leukemia (CML), hodgkin's lymphoma (HL), hepatocellular carcinoma (HCC) and several other cancers (Yoo et al. 2011; Li et al. 2012; Hajjari et al. 2015; Todd et al. 2015).

### **1.9 The role of PHF6 in neuronal migration within the developing cortex**

The high expression of PHF6 within the developing cortex has suggested an important role for this protein during corticogenesis. Here, I summarize the development of the cerebral cortex in mouse and the studies indicating an important role for PHF6. The developmental trajectory for the cortex begins with the formation of the neural tube (Darnell and Gilbert 2016). The neural tube forms as the neural plate folds to form the neural tube (Darnell and Gilbert 2016). The shape of the neural tube allows bone morphogenetic protein (BMP) and sonic hedgehog (Shh) signalling to regulate the formation of the forebrain in a spatial and temporal manner (Tabata 2001; Rowitch and Kriegstein 2010). The rostral end of the neural tube gives rise to the forebrain and the dorsal region of the respective cross section gives rise to the dorsal telencephalon (Lupo et al. 2006). As shown in figure 1-6, the neural tube houses the ventricular zone (VZ) which contains the progenitors responsible for producing the cerebral cortex. The proliferation and differentiation trajectory of these progenitors give rise to the cortex in a manner which maintains a progenitor pool while at the same time generating mature neurons to migrate and occupy regions of the developing brain (Paridaen and Huttner 2014). There are two classes of neurons which form the cortex, projection neurons/glutamatergic neurons and interneurons/GABAergic neurons (Molyneaux et al. 2007). Projection neurons migrate radially while interneurons migrate tangentially from the ganglionic eminence (Wilkinson et al. 2013). Hereafter, I will focus on the development of the cortex with respect to projection neurons. As described by Paridaen and Huttner in 2014, development of the cerebral cortex occurs in an

inside out manner, whereby the lower layers are formed first, followed by the intermediate layers and finally the upper layers.

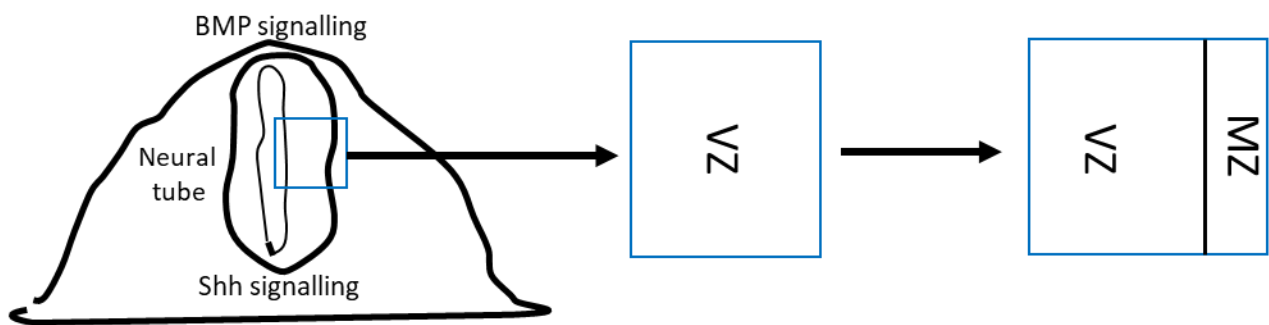


**Figure 1-6. The formation of the neural tube during embryogenesis which gives rise to the cerebral cortex. Adapted from Rowitch 2004.** The spatial organization of the developing brain occurs in relation to the shape of the neural tube. Therefore, formation of the cerebral cortex from the VZ in the neural tube occurs perpendicular to the canal of the neural tube.



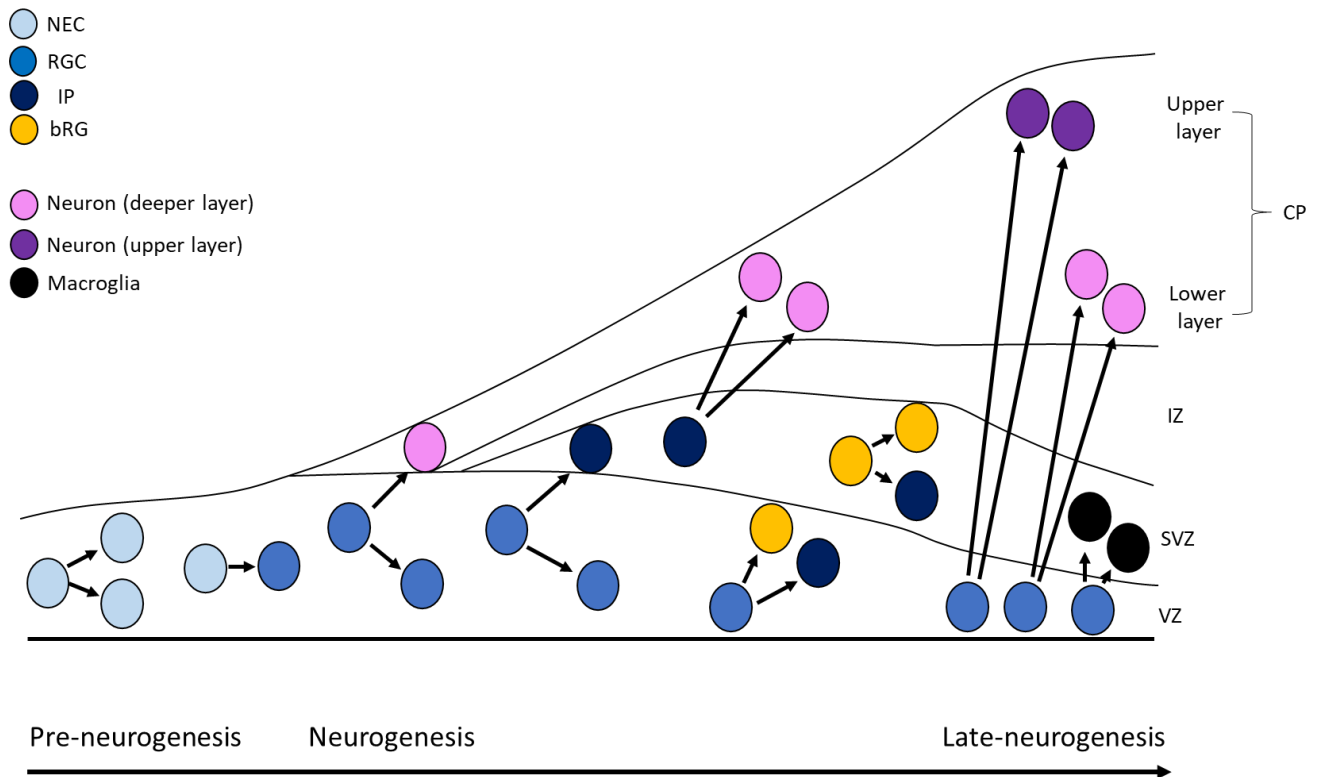


**Figure 1-7. Cortical development.** Adapted from Paridaen and Huttner 2014. Neural progenitors consist of neuroepithelial cells (NECs) and radial glial cells (RGCs). NECs go through symmetric and asymmetric division, giving rise to RGCs in the latter event. NECs also undergo transition phases to RGCs. RGCs go through symmetric and asymmetric division as well. In doing so, they give rise to either a neuron or intermediate progenitor (IP) through asymmetric division. IPs go through symmetric division producing two neurons.

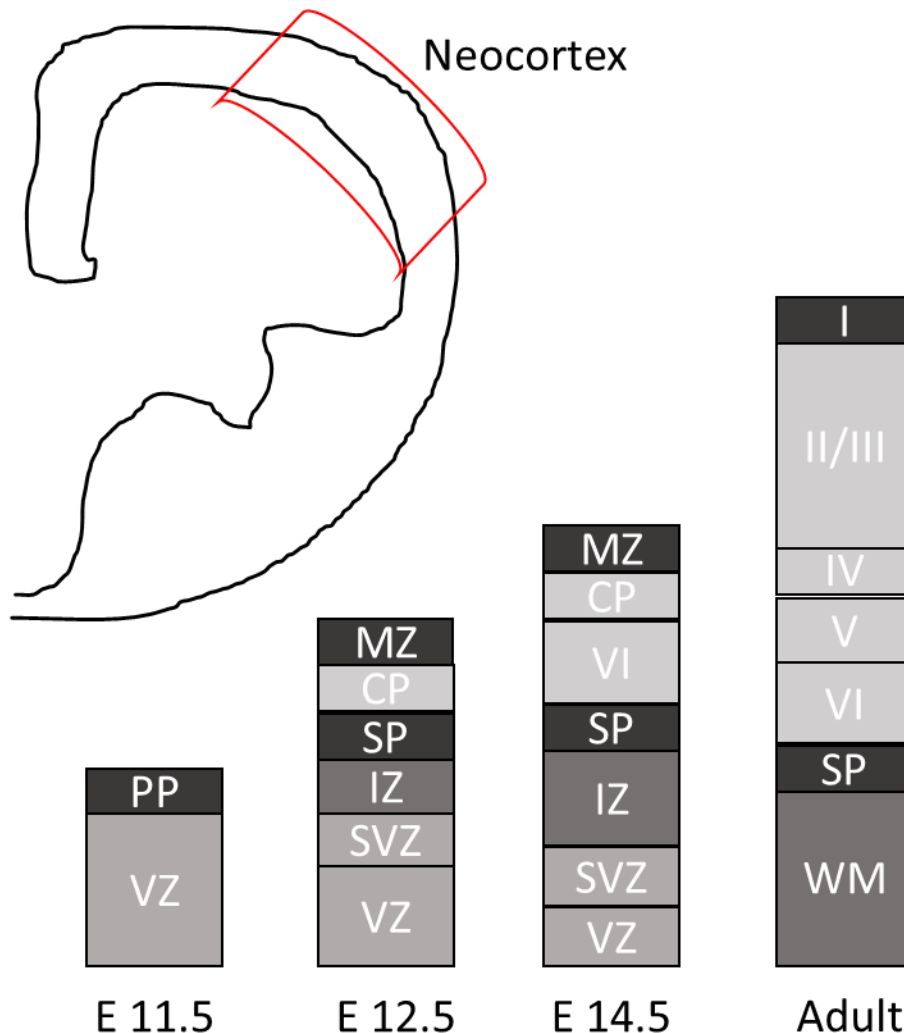


**Figure 1-8. Temporally regulated cortical layer formation. Adapted from Rodriguez et al. 2012 and Sakayori et al. 2013.** The ventricular zone (VZ) houses the progenitors which at E10.5 begin producing the first round of differentiated cells which migrate and form the preplate (PP). At E12.5, differentiated cells from the subventricular zone (SVZ) and VZ, begin to migrate past the intermediate zone to partition the PP into the marginal zone (MZ) and the subplate (SP), with the cortical plate (CP) constituting the region in between. Shortly after, the formation of the six-layer cortex begins as differentiated cells from the VZs migrate pass the IZ and SP to form the lower layers first. As cortical development progresses, new born neurons migrate past the layers which have already been formed to contribute to the newer superficial layers underneath the MZ. Layer VI formation begins at E 12.5 and is complete by E13.5. Layer V formation begins at E13.5 and is complete by E14.5. Layer IV formation begins at E14.5 and is complete by E15.5. Layers II/II formation begins at E15.5 and is complete by birth. Postnatally, the MZ is then referred to as layer I. In the context of figure 1-7, we can see how the progenitor population undergoes symmetric and asymmetric division to maintain the progenitor pool present in the VZs and contributes to mature neurons which form the six-layer cortex.

What drives the switch in cell fate during corticogenesis? As shown in figure 1-7, one of the changes in cell fate is the switch from symmetric to asymmetric division. Paridaen and Huttner in 2014, described the switch, which occurs with the onset of neurogenesis. The type of division is determined by the regulation of spindle orientation. Symmetric division occurs when the cleavage plane is perpendicular to the apical surface while an oblique orientation results in asymmetric division. Given that the spindle organization is important for driving the type of division in the progenitor pool, it is interesting that lissencephaly-1 (*Lis1*), a gene involved in microtubule organization, when downregulated leads to a loss of the progenitor pool required for cortical formation (Gupta et al. 2002). *Lis1* mutations causes lissencephaly in humans, a disease imposing a severe cortical defect (Dobyns et al. 1993). The planar pressure during asymmetric division affects the distribution of factors in the mother and daughter cells, consequentially determining cell fate (Paridaen and Huttner 2014). These factors include proteins involved in signalling, polarity maintenance, cell-cycle regulation and mitosis (Bultje et al. 2009; Schwamborn et al. 2009; Vessey et al. 2012; Dong et al. 2012; Kusek et al. 2012; Kawaguchi et al. 2013). Temporal determination also plays a factor as the older centriole is adopted by the mother cell (Wang et al. 2009; Paridaen et al. 2013).

Furthermore, given that the junction at the apical surface of RGCs is important in maintaining their proliferative capacity, genes expressed in the daughter cell downregulate cadherins, allowing cells to detach from the membrane, migrate and differentiate (Rousso et al. 2012; Itoh et al. 2013; Paridaen and Huttner 2014). The basal processes attached to the basal surface also grant RGCs and basal radial glial (bRG) cells their proliferative capacity (Paridaen and Huttner 2014). The primary difference between bRGs and RGCs is the lack of apical surface attachment in bRGs (Hevner and Haydar 2012). Meanwhile, fate determined cells do not

have a direct attachment to the basal surface (Paridaen and Huttner 2014). Other external factors like blood vessels and the presence of microglia affect the dynamic aspect of proliferative states in NECs (Stubbs et al. 2009; Antony et al. 2011; Cunningham et al. 2013).

In 2013, Wilkinson et al. described the cortical development regulation mechanism involving neurogenin 1 (*Neurog1*), neurogenin 2 (*Neurog2*) and Achaete-Scute family BHLH transcription factor 1 (*Ascl1*). *Neurog1* and *Neurog2* drive the cell fate of progenitors to projection neurons while *Ascl1* drives the fate of progenitors to inhibitory neurons. The authors describe an out of phase oscillation dynamic involving *Neurog2* and *Ascl1* as both genes initiate Notch signalling to promote hairy and enhancer of split-1 (*Hes1*) expression which leads to downregulation of *Neurog2* or *Ascl1*. *Hes1* eventually inhibits itself, allowing *Neurog2* or *Ascl1* expression. Maintained expression of either *Neurog2* or *Ascl1* leads to differentiation into projection or inhibitory neuron fates respectively. The swaying of the oscillation pattern is achieved by epigenetic and transcriptional regulation. Interestingly, the Wnt signalling pathway maintains *Neurog2* levels while fibroblast growth factor (FGF) signalling maintains *Ascl1* expression.

Cell fate is also determined by the configuration of transcription factor levels, birth date of neurons and spatial identity in the cortex (Srinivasan et al. 2012). In 2012, Srinivasan et al. investigated the feedback loop involving fez family zinc finger 2 (*Fezf2*), T-box brain 1 (*Tbr1*), chicken ovalbumin upstream promoter transcription factor-interacting protein 2 (*Ctip2*) and special AT-rich sequence-binding protein 2 (*Satb2*) (Figure 1-9). Immunohistochemistry of the developing cortex in transgenic mice models were used to elucidate the feedback loop involving the four genes. Using the described feedback loop, the authors were able to describe the regulation pattern in the developing cortex. Initially, SRY-Box 5 (*Sox5*) is expressed in the

subplate and layer VI, which upregulates *Tbr1*. TBR1 binds to the *Fezf2* locus, inhibiting *Fezf2* expression. *Tbr1* drives differentiated neurons to migrate and form layer VI. *Sox5* is then downregulated, restoring *Fezf2* expression, which downregulates *Satb2*, allowing *Ctip2* to be expressed which drives migration of neurons to layer V. Lastly *Fezf2* expression is reduced, allowing *Satb2* to suppress *Ctip2*, by binding the *Ctip2* locus, and upregulating *Tbr1*, leading to the migration of post-mitotic neurons to the layers II-V. The described feedback mechanism provides a glimpse into the tightly regulated methods used to assemble the cortical layers.

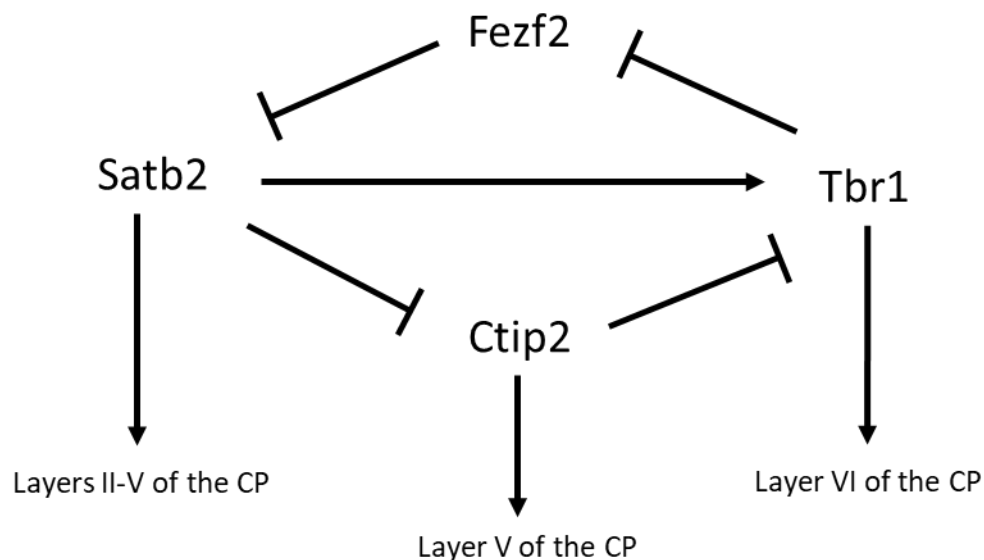


**Figure 1-9. Feedback loop determining the fate of migrating neurons in the developing cortex as described in Srinivasan et al. 2012.**

Furthermore, transcription factors like paired box protein 6 (*Pax6*), forkhead box G1 (*Foxg1*), empty spiracles homeobox 2 (*Emx2*) and LIM/homeobox protein 2 (*Lhx2*) are important during the early cortical development process (Stoykova et al. 2000; Muzio and Mallamaci 2005; Asami et al. 2011). Interestingly, in one study, it was shown that the BRG-/BRM-associated factor (BAF)170 or BAF155 subunits of the mouse SWI/SNF complex

interacts with PAX6 and the RE1-silencing transcription factor (REST)-corepressor complex to inhibit *Pax6* downstream targets T-box brain protein 2 (*Tbr2*), cut like homeobox 1 (*Cux1*), and transducin like enhancer of split 1 (*Tle1*) affecting IP and neuron production (Tuoc et al. 2013).

Interestingly, studies have shown PHF6 to be involved in neuronal migration. In 2013, Zhang et al. investigated PHF6 in the context of cortical development. They electroporated mice with *Phf6* short hairpin RNA (shRNA) at E14 and studied the development of the cortex in these mice at E19. Transfected cells seemed to have difficulty migrating to the upper layers and were stranded in the intermediate and lower layers, even forming white matter heterotopias. The authors found the Paf1C to be an interacting partner of PHF6. Interestingly, *in utero* electroporation using shRNA against *Paf1* produced a similar migration defect observed from PHF6 knockdown. They hypothesized that PHF6 interacted with the Paf1C complex, to regulate a downstream target involved in neuronal migration. Indeed, they did find such a target in the gene chondroitin sulfate proteoglycan 5 (*Cspg5*), which was regulated by *Phf6* and Paf1C. *In utero* electroporation of shRNA against *Cspg5* at E14 led to the expected neuronal migration defect which was observed in the previous experiments. Interestingly, the defect from *Phf6* and *Paf1* knockdown could be rescued using exogenous *Cspg5* expressing vectors. Lastly, CUX1+ transfected cells at the age of P6 seemed to be unable to reach their destined layer, further confirming a neuronal migration defect.

In another study, the authors investigated the role of miR-128, a miRNA, in neuronal migration (Franzoni et al. 2015). They performed *in utero* electroporation at E15 and investigated the corresponding effects at postnatal timepoints. Overexpression of miR-128 led to inhibition of neuronal migration in transfected cells destined for the upper layers, as they were found stranded in the intermediate layers, lower layers and as white matter heterotopias.

Blocking of free miR-128 led to over migration of neurons to the upper layers. miR-128 was then shown to be an interacting partner for *Phf6*. Furthermore, they were able to show that PHF6 exogenous expression was able to rescue the defect in neuronal migration from miR-128 overexpression.

While these studies showed direct involvement of PHF6 in neuronal migration, another study, looked at the effect of the NuRD complex, an interacting partner of the PHF6 protein, on neuronal migration (Nitarska et al. 2016). As mentioned by Basta and Rauchman in 2015, the NuRD complex is comprised of several units. It contains the HDAC1 and HDAC2 subunits which provide histone deacetylation activity. It contains the chromodomain helicase DNA-binding (CHD)3, CHD4 and CHD5 subunits which provide ATP dependent chromatin remodeling activity, helicase activity and histone binding activity. MBD 2 and MBD 3 are two other subunits which provide DNA and protein binding domains. RBBP4 and RBBP7 act as scaffold proteins and also provide histone binding activity. Last, GATA binding protein (GATA2)A and GATA2B provide DNA and protein binding domains. The study by Nitarska et al. in 2016 showed that knockout of *Chd4* led to decrease in the proliferative capacity of IPs during neocortical development, decreasing the output of neurons which comprise the intermediate and upper layers. Moreover, knockdown of *Chd5* or *Chd3* via *in utero* electroporation led to inhibition of neuronal migration to the upper layers, leading to the accumulation of upper layer destined neurons in the intermediate layers and lower layers. Furthermore, the authors mention that the CHD subunits work with the HDAC components of the complex to activate their temporal function in cortical development. Deletion of the MBD3 subunit has also been shown to have negative effects on neuronal migration (Knock et al. 2015). Defects in the NuRD complex and the corresponding neuronal migration abnormalities speak to

the importance of chromatin remodeling as a carefully regulated mechanism during embryonic development.

Interestingly, in one study, magnetic resonance imaging (MRI) was performed on two female BFLS patients (Kasper et al. 2017). The results indicated that they shared similar cortical defects suggesting faults in cortical development. The authors argue that these defects are responsible for the epilepsy symptom shared by the patients. Of note, the patients shared the same mutation.

### **1.10 Hypothesis and Specific Objectives**

To better understand BFLS and the function of the PHF6 protein, we generated a mouse embryonic stem cell (mESC) line with a patient-related nonsense mutation (R342X) in the *Phf6* gene using CRISPR-Cas9 technology. In theory, this should produce a truncated protein. Interestingly, the R342X mutation is the most frequent *PHF6* mutation in BFLS patients (Todd et al. 2015). My goal was to characterize the mice in the context of determining the role of PHF6 within BFLS pathogenesis. Therefore, my **hypothesis** was that the  $Phf6^{R342X/Y}$  mice, here on referred to as the R342X mice, would recapitulate the human BFLS phenotype at a molecular level, physiological level and behavioural level. To investigate this hypothesis, I set out several objectives. One, as part of the gross characterization of the transgenic mice, we would investigate the most obvious morphological phenotypes of the mice. Two, we would need to determine the PHF6 expression pattern in the R342X mice. Three, the development of the brain in the R342X mice would be examined. As part of this objective, and given the literature highlighting the role of PHF6 in neuronal migration, we planned to study neuronal migration in the R342X mice. This would provide novel insights into the role of PHF6 in corticogenesis given that in our model PHF6 was hypothesized to be nonfunctional or absent prior to the initiation of



corticogenesis, while in the studies by Zhang et al. 2013 and Franzoni et al. 2015, acute knock-down of *Phf6* was performed during the cortical development process. Lastly, any observed defects would be further investigated in the context of PHF6's biological functions.

## 2.0 Methods

### 2.1 Maintenance of PHF6 R342X mice

#### *2.1A Animal husbandry*

Dr. Picketts' lab had previously generated transgenic chimeric mice with the *Phf6* R342X mutation following injection of 129/SV mouse embryonic stem cells (mESCs) carrying the R342X mutation into C57BL/6J blastocysts. The C57BL/6J;129/SV chimeric male mice harbouring the *Phf6* R342X mutation were bred with C57BL/6J WT female mice from the Jackson laboratory. Next, R342X heterozygous agouti female progeny were identified and bred with C57BL/6J WT males from the Jackson laboratory. Finally, mixed background R342X heterozygous female progeny were backcrossed to WT C57BL/6J male mice to generate litters used for most experiments. To generate homozygous R342X female mice, R342X heterozygotes were bred to R342X males. All experiments were performed according to the guidelines set by the University of Ottawa's Animal Care ethics committee adhering to the guidelines of the Canadian Council on Animal Care.

#### *2.1B Tracking the survival rate of R342X pups and examining Mendelian ratios*

Pups from R342X heterozygous females ( $\geq 6^{\text{th}}$  generation) and WT C57BL/6J males were tracked from the day the pups were born. The day pregnant mothers gave birth, tail clippings were obtained from live pups and dead pups. Cages were then monitored for dead pups every day, and if a dead pup was present, tail clippings were obtained from the dead pup. Finally, at 21 days of age, ear clippings were obtained from the remaining mice in the litter. Tissue obtained from the mice were used to perform genotyping for the R342X *Phf6* gene mutation. In this way,

we were able to track the survival rate of all the pups in a litter until they reached weaning age and the data was used to examine Mendelian ratios.

### ***2.1C Timed mating of mice***

To obtain embryos at a specific embryonic timepoint, timed matings were set up. R342X heterozygous females were placed in cages with WT C57BL/6J males. Females and males were separated 12 hours after they were introduced. The time point of the separation was referred to as E0. If the mouse did not seem pregnant by E13, females and males were re-introduced.

### ***2.1D Genotyping for the R342X mutation***

Mouse tissue (tail or ear clipping) was lysed in lysis buffer (0.95 N NaOH, 0.0076 M EDTA) and then placed in an Eppendorf Master Cycler Ep Gradient Thermocycler (90 °C for 60 minutes). The samples were then neutralized using an equal volume of neutralization buffer (0.97 M Tris-HCl pH 8.0). Next, the PCR reaction mixture was set up as follows:

DNA	1.4 $\mu$ l	
10X PCR	2.5 $\mu$ l	(1X) Final concentration
2.5 mM dNTPs	2.5 $\mu$ l	(0.25 mM) Final concentration
50 mM MgCl <sub>2</sub>	0.75 $\mu$ l	(1.5 mM) Final concentration
10 $\mu$ M Forward Primer	0.5 $\mu$ l	(0.2 $\mu$ M) Final concentration
10 $\mu$ M Reverse Primer	0.5 $\mu$ l	(0.2 $\mu$ M) Final concentration
Taq Polymerase	0.25 $\mu$ l	
H <sub>2</sub> O	16.6 $\mu$ l	
Total	25 $\mu$ l	

and the genotyping sample was PCR amplified in an Eppendorf Master Cycler Ep Gradient Thermocycler using the following program:

95 °C – 3 min	
95 °C – 30 sec	10 cycles
70 °C*(-1 °C temperature increase) – 45 sec	
72 °C – 30 sec	
95 °C – 30 sec	35 cycles
60 °C – 45 sec	
72 °C – 30 sec	
72 °C – 5 min	
4 °C - hold	

The PCR products were then digested for 1 hour at 37 °C using FastDigest HindIII (Thermo Fisher Scientific) as follows:

PCR product	15 µl
FastDigest Buffer	4 µl
FastDigest HindIII	2 µl
H <sub>2</sub> O	9 µl
Total	30 µl

and digested products were run on a 2% agarose gel at 95 V for 20 minutes.

## **2.2 Preparation of mouse tissue for downstream experiments**

### **2.2A Fixing mouse tissue**

Above the age of 10 days, mice were perfused via cardiac perfusion using 4% PFA (Sigma). Perfused tissue was then placed in 4% PFA overnight at 4 °C. If tissue from younger mice had to be fixed, mice were euthanized, and tissues were extracted and placed into 4% PFA overnight at 4 °C.

### **2.2B EdU injections to label embryos**

To label embryonic tissues with EdU, pregnant mothers were injected subcutaneously around the abdomen with 10 µl/g of pregnant mother's weight, of 10 mg/ml EdU (Santa Cruz) for 1 hour. The mothers were then euthanized, and embryonic tissues extracted for fixation as described in 2.2A.

### **2.2C Brain preparation for MRI and volumetric analysis**

For high resolution MRI, brains were prepared as per the protocol (MICE Contrast-Enhanced Brain Perfusion Protocol version 10, April 2017) sent by Dr. Jason Lerch (SickKids Toronto). Briefly, mice were euthanized with 200 µl of pentobarbital (ACVS uOttawa) injected subcutaneously around the abdomen and perfused using a perfusion pump (Ismatec REGLO ICC) running at 3 ml/min. Perfused brains were dissected and placed in 4% PFA with 2 mM Prohance overnight at 4 °C. The following day, the 4% PFA with 2 mM Prohance was replaced with autoclaved 1X PBS containing 0.02% sodium azide and 2 mM Prohance. 10X PBS with a final pH of 7.4 was prepared using 1.37 M NaCl, 0.027 M KCl, 0.1 M Na<sub>2</sub>HPO<sub>4</sub>, 0.019 M KH<sub>2</sub>PO<sub>4</sub>. Brains were inserted to Scintillation vials (Sigma), submerged in the solution and stored at 4 °C until they were shipped to Dr. Lerch for MRI imaging.

## ***2.2D Blood collection to isolate plasma used in ELISA experiments***

Mice to be used for ELISA experiments were fasted for 6 hours prior to blood collection. For blood collection, mice were euthanized and then decapitated. EDTA coated microvettes (Sarstedt) were used to collect trunk blood. Halt Protease Inhibitor (Thermo Fisher Scientific) and DPPIV (1:100) (Millipore) were added to the blood and then samples were centrifuged at 1000xg for 10 minutes at 4 °C. The clear supernatant was retrieved, diluted (1:50) in 1X PBS and sent to Eve Technologies to be run on ELISA plates (“STTHD-Serum/Plasma” and “MIGF1-01-101”).

## **2.3 Staining of frozen tissue sections**

### ***2.3A Frozen section preparation***

Following fixation (described in 2.2A), tissue was placed in 30% sucrose solution (prepared with autoclaved 1X PBS containing 0.03% sodium azide) at 4 °C, until the tissue sunk to the bottom of the vial. The tissue was then placed in a 1:1 solution of 30% sucrose solution and OCT (VWR) overnight at 4 °C. The following day, the tissue was submerged in an embedding mold (VWR) containing 1:1 solution of 30% sucrose solution and OCT, and then frozen by placing the mold on a petri dish floating on liquid nitrogen. Frozen tissue was stored at -80 °C. The frozen tissue was then sectioned using the Leica CM1850 cryostat and sections picked up using SuperFrost slides (Thermo Fisher Scientific). Brains were cut at 12 µm thickness while pituitary glands were cut at 8 µm thickness. Slides with sections were dried at RT and then stored at -80 °C.

### ***2.3B Histochemical staining of frozen sections***

For Nissl staining, slides containing dried sections were rehydrated by sequentially submerging them in 95% ethanol (10 minutes), 70% ethanol (1 minute), 50% ethanol (1 minute), and ddH<sub>2</sub>O (5 minutes x 2). Rehydrated slides were stained using a 0.25% cresyl violet (Thermo Fisher Scientific) solution (15 minutes) and then washed in ddH<sub>2</sub>O (4 minutes x 2). The slides were then dehydrated in 50% ethanol (2 minutes), 70% ethanol with 0.5% acetic acid (10 seconds), 95% ethanol (2 minutes), and xylene X3 (5 minutes). The slides were then allowed to dry for 5 minutes after which coverslips (Thermo Fisher Scientific) were mounted onto the slides using Permount (Thermo Fisher Scientific). Mounted slides were allowed to dry in the fume hood overnight.

For H&E stained sections, slides were prepared as described 2.3A and sent to the uOttawa Histology Core Facility for staining.

### ***2.3C Immunofluorescent staining of frozen sections***

Slides with dried sections were first washed with 1X PBS, and depending on the antibody used, some slides were subjected to antigen retrieval next, while others were not. For antigen retrieval, sodium citrate solution (pH 6) was heated for 10 minutes at medium power in the microwave. Slides were placed in the solution and reheated for another 10 minutes at low power. After antigen retrieval, all slides were washed with 1X PBS, blocked with 10% horse serum prepared in 1X PBS with 0.4% Triton X-100 for 30 minutes at RT, and incubated with primary antibody prepared in 1X PBS with 0.4% Triton X-100 and 3 mg/ml BSA overnight at 4 °C. The next day slides were washed with 1X PBS and incubated with secondary antibody prepared in 1X PBS with 0.4% Triton X-100 for 1 hour. If slides were to be stained for EdU, following 1X

PBS wash, slides were incubated with an EdU staining solution (2 mM CuSO<sub>4</sub>, 10 μM fluorescent azide, 50 mM ascorbic acid) for 1 hour. After EdU staining, all slides were washed with 1X PBS, and then incubated with Hoechst dye for 15 minutes. Finally, the slides were washed with 1X PBS and then coverslips mounted using Dako fluorescent mounting medium and nail polish.

### ***2.3D Imaging of slides***

The cresyl violet or H&E stained slides were imaged using a microscope (Carl Zeiss Axio Imager M2) and Zen software (2.3 Blue edition). Slides stained with an immunofluorescent stain were imaged using a microscope (Carl Zeiss Axio Imager M1) and processed using AxioVision SE64 Rel. 4.9.1.

### **2.4 Immunoblotting of mouse brain tissue**

Tissues were flash frozen in liquid nitrogen following dissections. Frozen tissues were homogenized and lysed using RIPA lysis buffer (150 mM NaCl, 1% NP-40, 0.1% SDS, 50 mM Tris pH 8.0, 5 mM EDTA, 0.5% Na-deoxycholate), to which Halt Protease Inhibitor (Thermo Fisher Scientific) was added. Protein concentration was measured using Bio-Rad Protein Assay Dye Reagent Concentrate (Bio-Rad) and absorbance measured using Ultrospec 3100 Pro. Protein samples were prepared with NuPAGE LDS Sample Buffer as per the instruction of the manufacturer and the SDS polyacrylamide gel was run at 90 V-150 V using the Bio-Rad Mini-PROTEAN Tetra Cell and the Bio-Rad Power Pac 200. 10X running buffer was prepared using 0.25 M Tris, 1.92 M glycine, 0.035 M SDS. Protein from the gel was then transferred onto PVDF membranes (Bio-Rad) using the Bio-Rad Mini Trans-Blot cell and the Bio-Rad Power Pac 200 at 0.35 A for 90 mins. 10X transfer buffer was prepared using 0.25 M Tris and 1.92 M



glycine. 10X transfer buffer was diluted using water and 20% methanol. For larger gels and membranes, the PROTEAN II xi Cell (Bio-Rad) at 200 V, Trans-Blot Cell (Bio-Rad) at 1.50 A for 2 hours, and the Power Pac 1000 (Bio-Rad) were used. Membranes were blocked using 5% skim milk for 1 hour, incubated with primary antibody overnight (at a minimum), and incubated for 1 hour minimum with secondary HRP antibody the following day. The Clarity Western ECL substrate (Bio-Rad) was used for film-based imaging of the membranes. 1X TBST was used for washing membranes (3x at RT for 5-10 min with shaking) in between incubation steps. 10X TBST was prepared using 15 M NaCl, 1 M Tris-HCl pH 8.0, and 5% Tween 20.

## **2.5 Nucleic acid extraction and analyses**

### ***2.5A RNA preparation for downstream applications***

Tissue was flash frozen in liquid nitrogen following dissections. The Trizol reagent (Thermo Fisher Scientific) was used to prepare RNA in solution following the manufacturer's instructions. The PureLink RNA Mini Kit (Thermo Fisher Scientific) was used for RNA purification following the manufacturer's instructions. To overcome the very low yield of RNA from pituitary gland samples, the GeneJET RNA Purification Kit (Thermo Fisher Scientific) was used to purify and concentrate RNA as per the manufacturer's instructions. DNA digestion via DNase I was achieved using the DNA-free DNA Removal Kit (Thermo Fisher Scientific) according to the manufacturer's instructions. However, DNA digestion was not performed on pituitary gland RNA to further improve yield. RNA quality was checked by running a small amount of RNA on a 1% agarose gel run at 150 V for 10 minutes and the gel was imaged using the ChemiDoc-It Imager. The quality of 28S and 18S ribosome was evaluated by examining the clarity of both bands on the gel. RNA quality was further validated using the Nanodrop 1000 (Thermo Fisher Scientific) to measure the 280/260 nm and 260/230 nm ratio.

### ***2.5B cDNA preparation from total RNA***

cDNA was generated using RevertAid Reverse Transcriptase (Thermo Fisher Scientific) and random hexamers (Thermo Fisher Scientific #SO142) as per the published RevertAid Reverse Transcriptase protocol for first strand cDNA synthesis. 1 µg of RNA was used as input RNA. However, when pituitary gland RNA was used to generate cDNA, 250 ng of input RNA was used. Incubation of the reaction mixture was performed on an Eppendorf Master Cycler Ep Gradient Thermocycler.

### ***2.5C RNA-seq analysis***

RNA was prepared as described in section 2.5A and each sample was sent to the StemCore Laboratory (OHRI). 100 ng of each sample was prepared in 40 µl of HPLC water. A separate aliquot of 5 µl with 50 ng of RNA was sent for quality control. RNA quantification was done using the Qubit HS RNA assay (Thermo Fisher Scientific) and fragments analyzed using the Fragment Analyzer HS RNA assay (AATI). Library construction was performed using the Truseq RNA v2 Library prep kit (Illumina), barcodes prepared so as to be usable in the Illumina NextSeq 500 platform, quantification of the libraries performed with the Qubit HS DNA assay (Thermo Fisher Scientific) and library fragment size evaluated with the Fragment Analyzer HG NGS assay (AATI). Libraries were prepared at the same concentration, then samples were pooled, and the pool was diluted and run on one High Output Flow Cell on the NextSeq 500 undergoing 2 x 75 cycles of paired-end sequencing. PhiX was used as a control in the run. Data was analyzed by Laura Goodwin and Dr. Farshad Niri from Dr. Picketts Lab at OHRI. As part of the analysis of the data from the sequencing experiment, reads were trimmed using Cutadapt v1.18, read quality was measured using FastQC v0.11.7 and read mapping was performed using HISAT2 v2.1.0. Next, aligned and sorted reads were converted to BAM files using Samtools

v1.3.1. Reads were then counted using HTSeq-count v 0.9.1 under the following parameters: --order pos --mode intersection-strict --stranded=no --minqual 1 --type exon --idattr gene\_id. Finally, differential gene expression was calculated using DESeq2 and cBioconductor v in R v3.3.3.

### 2.5D qRT-PCR analysis

RNA and cDNA were prepared as outlined in sections 2.5A and 2.5B respectively. Next, PCR reactions were set up on plates as follows:

cDNA	2 $\mu$ l	
The SensiFAST SYBR Lo-ROX Kit (Bioline)	10 $\mu$ l	
10 $\mu$ M Forward Primer	0.8 $\mu$ l	(2.5 $\mu$ M) Final concentration
10 $\mu$ M Reverse Primer	0.8 $\mu$ l	(2.5 $\mu$ M) Final concentration
H <sub>2</sub> O	6.4 $\mu$ l	
Total	20 $\mu$ l	

Plates were run on an Agilent Stratagene Mx3000P as follows:

95 °C – 2 min	
95 °C – 5 sec	40 cycles
Annealing temperature for primer sets are specified in the appendix – 10 sec	
72 °C – 20 sec	
95 °C – 1 min	
55 °C – 30 sec	
95 °C – 30 sec	

After the reaction, amplification plots and dissociation curves were examined on the MxPro software (Mx3000P v3.20 Build 340, Schema 74). 15  $\mu$ l of the product was run on a 2% agarose gel at 95V for 20 minutes to confirm the absence of non-specific bands. Imaging of the gel was performed using the ChemiDoc-It Imager.

### ***2.5E DNA sequencing analysis***

RNA and cDNA were prepared as outlined in sections 2.5A and 2.5B respectively. Next, PCR reactions were set up using the Platinum Taq DNA polymerase (Thermo Fisher Scientific) as per the manufacturer's instruction and then run on an Eppendorf Master Cycler Ep Gradient Thermocycler. The program used in the thermocycler was as follows:

94 °C – 3 min	
94 °C – 45 sec	30 cycles
Annealing temperature for primer sets is specified in the appendix – 30 sec	
72 °C – 50 sec	
72 °C – 10 min	
40 °C – hold	

PCR products were separated on a 1% agarose gel and imaged on a ChemiDoc-It Imager. Bands were visualized using a UV Transilluminator (VWR M-20E) and excised from the gel with a razor blade. DNA from excised bands was extracted using the QIAquick Gel Extraction Kit (Qiagen) following the manufacturer's instructions and sent to the StemCore Laboratory (OHRI) for Sanger sequencing on the Applied Biosystems 3730 DNA Analyzer after amplification with the Big Dye Terminator (BDT) v3.1 kit. MEGA 7.0.26 was used to read the chromatogram files.

## 2.6 Statistics

A Chi-Square test was used to determine if pups were born in normal Mendelian ratios. A Student's t-test was used to determine significant differences for experiments involving animal and organ weights, qRT-PCR, ELISA, cell counts, and behavioural assessments of mice. “\*”, “\*\*”, “\*\*\*”, and “\*\*\*\*” represent p-values of <0.05, <0.01, <0.001, and <0.0001, respectively. The t-tests were unpaired, parametric and SD was assumed to be the same. If the SD was not equal from the f-test, the t-test was performed with Welch's correction. When evaluating the MRI data and the RNA-seq data, an FDR approach was used to generate an adjusted p-value (q-value). For the volumetric analysis, an adjusted p-value cutoff of <0.01 was used, and for the RNA-seq analysis, an adjusted p-value cutoff of <0.1 was used. A Two-way ANOVA was used to analyze the fear conditioning behaviour data.

## 3.0 Results

### 3.1 Characterization of the gross phenotype of the R342X mice

After breeding the chimeric animals with the R342X mutation to C57BL/6J mice we identified heterozygous female animals that were backcrossed to male C57BL/6J mice to obtain hemizygous male mice with the R342X mutation. On the mixed background we observed that the mice were born at normal Mendelian ratios and were fertile when they reached sexual maturity. As the mixed background strain was backcrossed onto the C57BL/6J background, it appeared that the R342X mice had some degree of postnatal lethality on the C57BL/6J background. We tracked the genotypes of 100 pups ( $\geq$  6th generation) to assess whether we were obtaining mutants at Mendelian ratios and to examine their survival. We observed that R342X mice were born in normal Mendelian ratios but the survival rate for R342X male pups after 1 day was around 39% and the survival rate for R342X male pups after day 11 was 19% (Figure 3-1A). Dead R342X male mice were noticeably smaller than WT male mice (Figure 3-1B). Weaning was postponed by 1-2 weeks for R342X male mice on the C57BL/6J background since the animals were too small and weak to survive on their own. Upon weaning, gel food was provided for another 2 weeks to further facilitate healthy development. Following this protocol, R342X male mice eventually reached normal survival rates after weaning.

A)

Breeding pair	+/R342X Female (Heterozygous) x +/Y Male (WT C57BL/6J)				
Progeny genotype (6 <sup>th</sup> and 7 <sup>th</sup> generation)	+/+ Female	+/R342X Female	+/Y Male	R342X/Y Male	
Expected	25 (25%)				
Observed	28 (27%)	19 (19%)	27 (27%)	26 (26%)	100
					Total

↓

Survival rate (1 day)

Progeny genotype (6 <sup>th</sup> and 7 <sup>th</sup> generation)	+/+ Female	+/R342X Female	+/Y Male	R342X/Y Male
	25 (89.3%)	18 (94.7%)	22 (81.5%)	10 (38.5%)

Survival rate (11 days)

Progeny genotype (6 <sup>th</sup> and 7 <sup>th</sup> generation)	+/+ Female	+/R342X Female	+/Y Male	R342X/Y Male
	24 (85.8%)	17 (89.5%)	21 (77.76%)	5 (19.2%)

B)

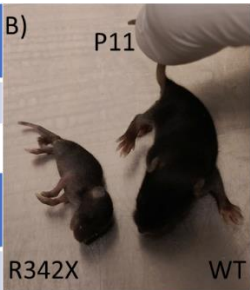


**Figure 3-1. Mendelian ratios and tracking of R342X pups.** (A) 100  $\geq$ 6<sup>th</sup> generation progeny born from the +/R342X females and +/Y males were tracked until weaning age. Mice were born in normal Mendelian ratios but the survival rate after 1 day for R342X/Y pups was 38.5% in comparison to >80% survival rates for +/+ females, +/R342X females and +/Y males. Survival rate after 11 days for R342X/Y pups was 19% in comparison to >77% for +/+ females, +/R342X females and +/Y males. (B) R342X pups which died were noticeably smaller and appeared to have poor development. On the left is an 11-day old dead R342X/Y pup and on the right is a live 11 day old +/Y male.

### 3.2. Weight analysis of the R342X mice

The first noticeable morphological difference in the R342X mice compared to control littermates was that they appeared smaller in size. This reduced weight phenotype was observed in both the mixed strain and remained present after numerous backcrosses onto a pure C57BL/6J background. To quantify these differences, R342X male mice were weighed at regular daily intervals (between 2-5 days) for 60 days, starting at 8 days old, and then for comparison we also measured their weight after one year. The R342X male mice weighed significantly less than WT mice at every interval examined (Figure 3-2A and 3-2B). Similarly, we compared the weights of R342X homozygote females and R342X heterozygote females at similar intervals (2-5 days) for 45 days, starting at 5 days old (Figure 3-2C). R342X homozygote females were not statistically different from R342X heterozygote females but they did show a trend towards being smaller than the R342X heterozygote females. Unfortunately, we did not compare the R342X mutant females to WT females in our weight analysis experiment.

In mice, PHF6 is expressed in the liver during embryogenesis, and in the brain, spleen, thymus, kidney, and testes from embryogenesis and into adulthood (Voss et al. 2007). Furthermore, human PHF6 expression was relatively high in the thymus and moderate in the spleen and testes (Vlierberghe et al. 2010). Given the expression pattern of PHF6, we measured organ/body weight ratios of the brain, spleen, thymus, liver, kidneys and testes at 2 months of age in an effort to determine whether there were any defects in the development of these organs. Investigation of the testes was also important since hypogonadism is a recurrent phenotype in male BFLS patients and low testosterone levels was observed in one male BFLS patient (Turner et al. 2004; Carter et al. 2009). However, no difference was observed in the organ/body weight ratios indicating that these organs in the R342X male mice were proportional in size to their WT



counterparts (Figure 3-3). We extended measurements to other organs including the lungs and heart due to ease of extraction, but no difference was observed in the comparison between R342X male mice and WT male mice indicating that these organs were also proportional in size (Figure 3-3A).

Given that male BFLS patients are affected by truncal obesity, R342X mice are affected by a decrease in weight, and PHF6 is moderately expressed in human adipose tissue, we wanted to investigate if there was a fat accumulation defect in the R342X mice (Turner et al. 2004; Vlierberghe et al. 2010). Therefore, we measured organ/body weight ratios of specific white adipose tissues (WATs) (epididymal fat, retroperitoneal fat, inguinal subcutaneous fat). These specific fat tissues were chosen for extraction based on the fact that they are major components of the WAT arrangement and they are easy to dissect with precision. However, we did not observe any significant difference (Student's t test,  $p < 0.05$ ) in the organ/body weight ratio comparisons of these specific WATs in R342X male mice and WT male mice (Figure 3-3B).

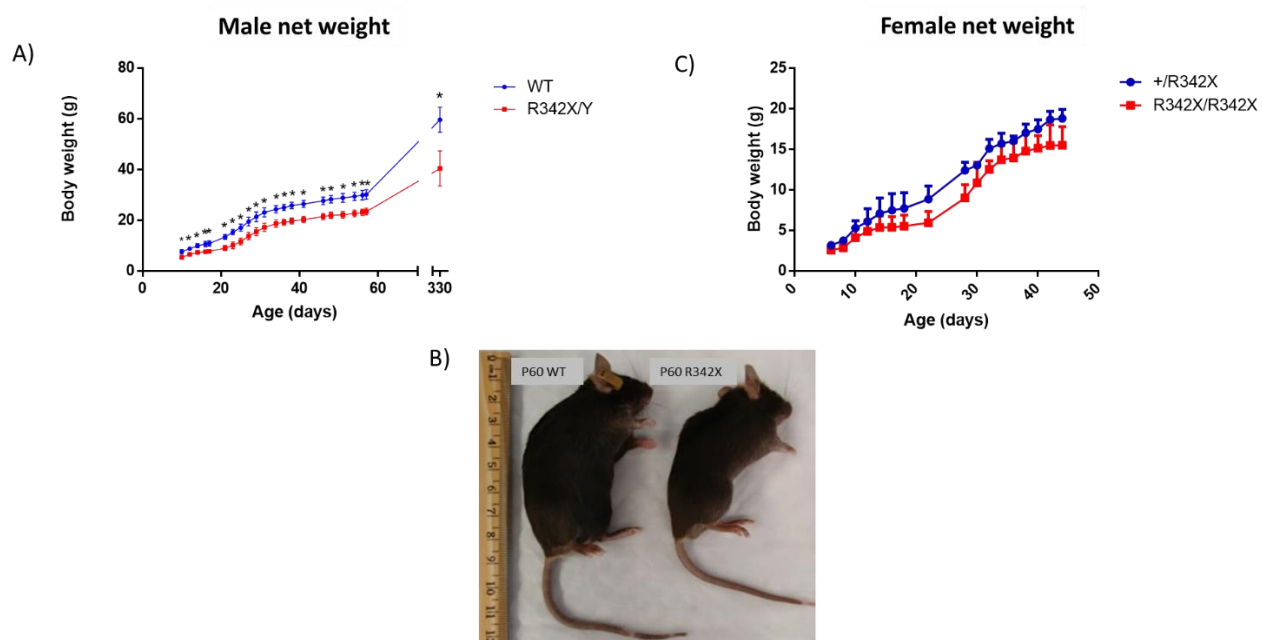


**Figure 3-2. Body weight comparisons of the R342X mice.** (A) R342X/Y mice were significantly smaller than male WT mice at every interval measured over the 60 days.  $n=12$ ,  $p<0.05$ . (B) A 60-day old R342X/Y mouse on the right is significantly smaller than a 60-day old WT male on the left. (C) R342X/R342X females show a trend of being smaller than +/R342X females when weights were compared at intervals over 45 days.  $n=4$ .

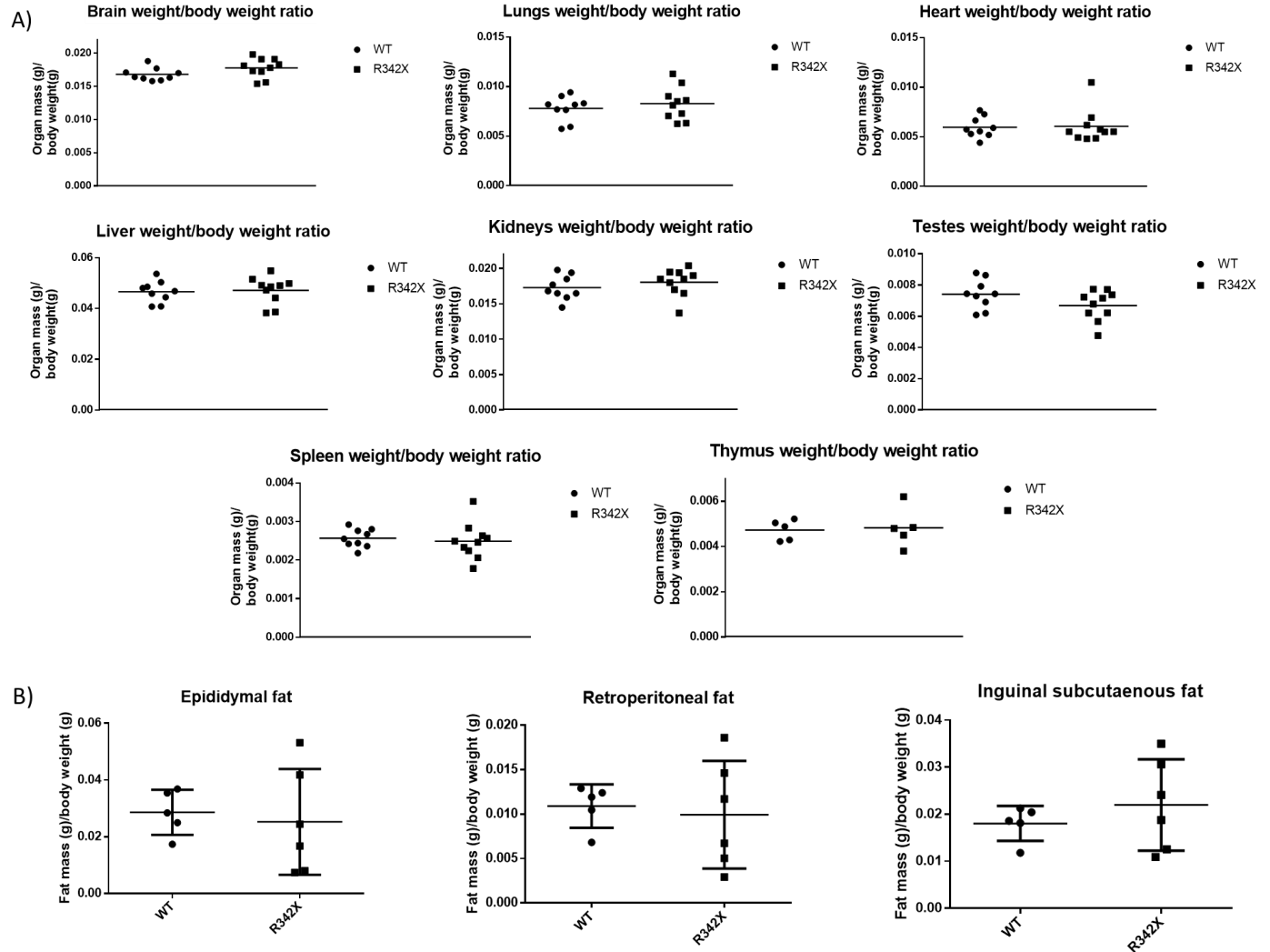


**Figure 3-3. Organ weight/body weight ratios of R342X/Y mice.** The mice were weighed before dissections, euthanized, and then individual organs extracted and weighed. (A) For the liver, heart, testes, brain, lungs, spleen and kidneys experiments, WT n=9 and R342X n=10, and the age of the mice was 2 months old. For the thymus experiment, n=5 and mice were 20 days old. (B) For the fat experiments, WT n=5 and R342X n= 6, and mice were 90 days old.

### **3.3. Analysis of PHF6 protein expression in the R342X mice**

To investigate PHF6 expression in the R342X mice, we performed immunoblots from cortical samples isolated from postnatal day 1 (P1) mice. Since PHF6 is highly expressed in the mouse brain during embryogenesis, we believed investigation of PHF6 from P1 mouse cortices would provide an adequate description of the PHF6 expression state in the comparison of R342X mice and WT mice (Voss et al. 2007). We observed PHF6 protein expression in the WT male mice samples, lower but variable expression in the R342X heterozygote female samples, which we expected occurred due to X-inactivation, and we did not detect any PHF6 expression in the R342X males or the R342X homozygote females (Figure 3-4A). The R342X mutation results in a truncated protein lacking the last 24 amino acids. Theoretically, the truncation could affect PHF6 in two ways: either severely affecting stability of the RNA or protein leading to no detectable protein or partially affecting stability of the RNA or protein leading to reduced levels of protein. To determine if the R342X protein was produced at all, we repeated the immunoblot experiment but increased the amount of protein that was loaded (8-9 times more for R342X samples, relative to WT samples). Under these conditions, we were able to notice a faster migrating PHF6 band in low abundance in the R342X samples, suggesting that a truncated PHF6 protein was being produced with a ~40-fold decrease relative to WT samples (Figure 3-4B). Through the examination of *Phf6* RNA levels via qRT-PCR, we detected a 2-fold reduction in the amount of *Phf6* transcript present in the R342X mice cerebral cortices at P0 (Figure 3-4C). This suggests that R342X *Phf6* transcripts in the mice are unstable, which contributes to significantly reduced levels of truncated PHF6 protein.

Previous studies by an Australian group (Mark Corbett & Josef Gecz, Adelaide, Australia) showed that a second human transcript (*PHF6b*) was produced, and that this was the

prevalent transcript in R342X patients. This transcript includes the intron between exon 10 and exon 11 (Figure 3-5A). Normally, this transcript is less abundant than the main transcript, *PHF6a*, suggesting that *PHF6a* transcripts are degraded by nonsense-mediated-decay (NMD). Indeed, they confirmed that *PHF6a* transcripts were degraded by NMD in human BFLS patient lymphoblast cell lines. They were also able to detect a very low amount of the truncated protein in R342X human BFLS patient lymphoblast cell lines. Furthermore, they were able to show that in R342X patients, it is only the *PHF6a* transcript which undergoes NMD while the *PHF6b* transcript is stable. To determine if a similar *PHF6b* transcript was produced in the R342X mice, we designed primers to detect this transcript variant using RT-PCR in P0 cerebral cortex samples. Again, since PHF6 expression is high in this tissue at this timepoint, we expected no difficulty in detecting comparable *Phf6* transcripts. The *Phf6a* transcript was expected to produce a 500 bp band with the primers used and we did observe this band (Figure 3-5B). However, we did not observe the expected 800 bp band from the *Phf6b* transcript. Instead, we found that the R342X cells produced a novel isoform corresponding to a 370 bp band (Figure 3-5B). Sequencing of this isoform revealed it to be lacking exon 10 which encompassed the mutation. The novel isoform named “Skip exon 10 Resulting in Triple Three amino acids” (SKRTT), has its reading frame maintained with the potential to produce a protein of 333 amino acids. The R342X protein is 38.5 kDa while the novel isoform produced would be 37.4 kDa, thus making it difficult to determine which of the transcripts correspond to the truncated protein band we previously observed in the R342X samples by western blot. Since the SKRTT protein includes novel amino acids and disrupts the second ZaP domain, this protein, if produced, could possibly result in a gain of function phenotype (Figure 3-5C). Given that this transcript has not been identified in humans, any production of SKRTT would complicate the applicability of the

R342X mice as a model for human BFLS. To resolve this conundrum, we ran a large SDS polyacrylamide gel to increase the separation and resolution of the bands (Figure 3-6A). We loaded a larger amount of protein from R342X lysates in comparison to WT samples. The migration distance of the known molecular markers from a reference point were plotted on a log graph and the size of the PHF6 WT and R342X truncated protein bands were determined by extrapolation based on their relative distance travelled (Figure 3-6B). Using the results from this experiment, we concluded that only one transcript was translated since we only observed a single band in the R342X samples after increased separation. Moreover, we conclude that the novel isoform is not translated since the smaller band from the R342X samples was ~39 kDa which is closer to the predicted size of the R342X protein than the hypothetical SKRTT protein.

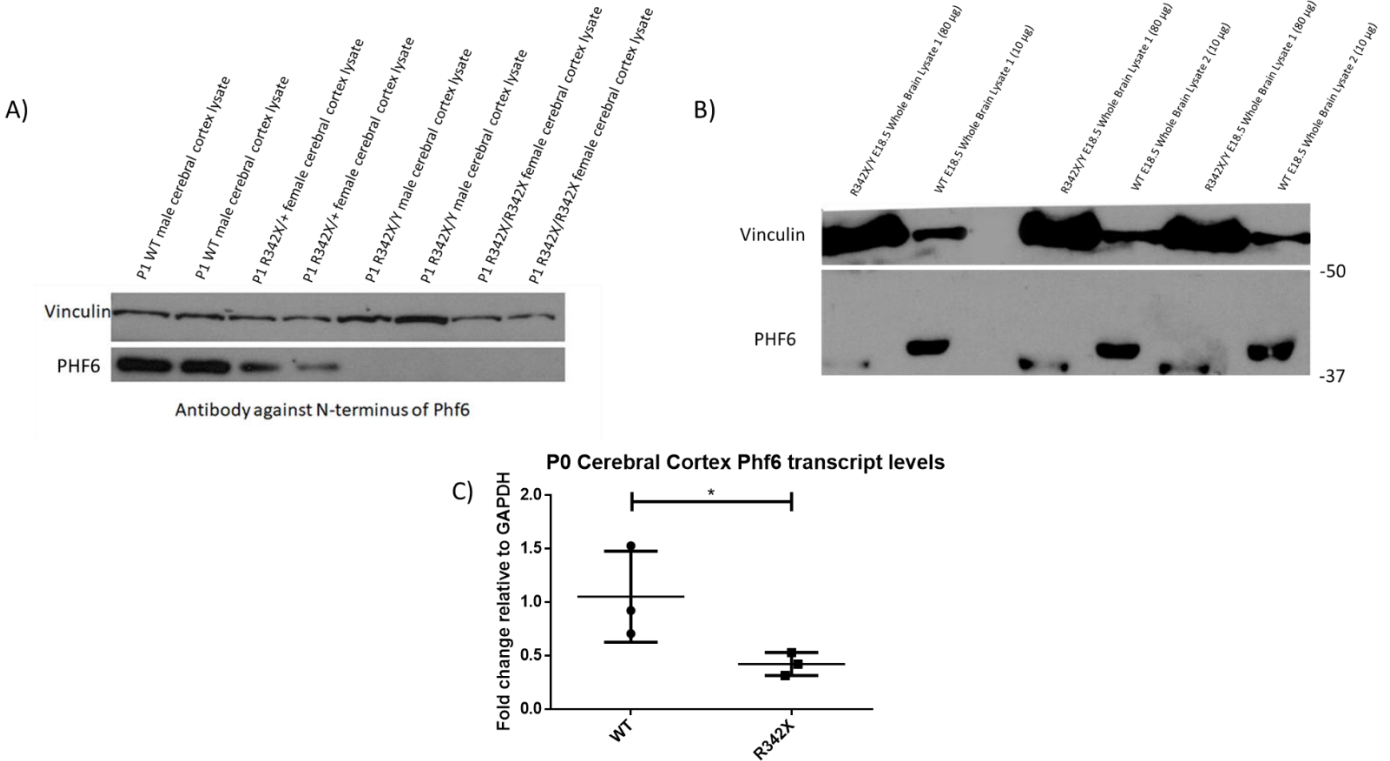


**Figure 3-4. PHF6 expression profile in R342X mice.** (A) A 10% SDS polyacrylamide gel was used to separate protein lysate from the cortices of 1-day old WT males, R342X males, R342X/+ female and R342X/R342X females. Vinculin was used as a loading control and PHF6 detected at ~41 kDa. (B) A 10% SDS polyacrylamide gel was used to separate protein lysate from the brains of E18.5 WT males and R342X males. 8-9 times more R342X sample protein lysate was loaded in comparison to WT protein samples. Vinculin was used as a loading control and PHF6 detected at ~41 kDa. A smaller PHF6 protein expressed at lower levels was observed for R342X samples. (C) qRT-PCR of newborn cerebral cortex amplifying *Phf6* RNA. As expected, R342X *Phf6* RNA levels were lower than WT levels indicating nonsense mediated decay. n=3, p<0.05.

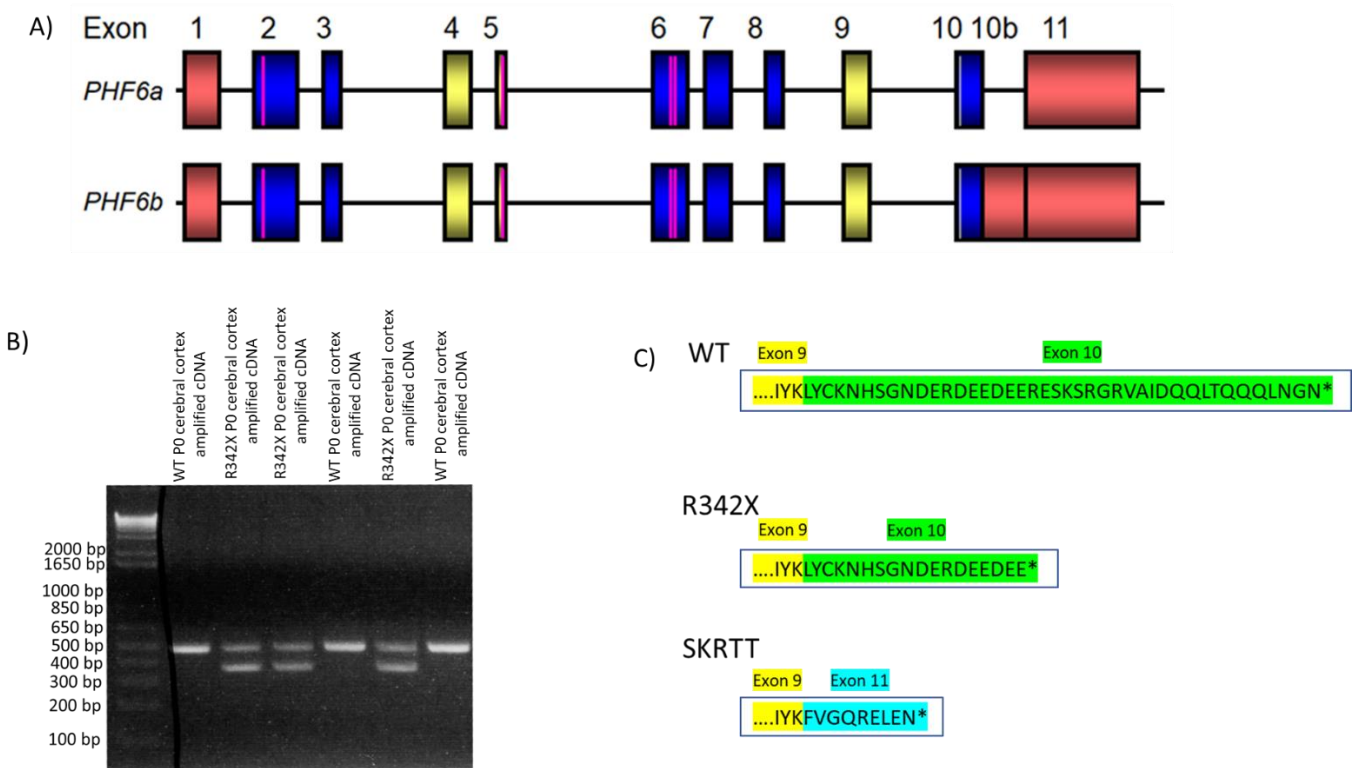


**Figure 3-5. Investigation into the presence of *PHF6a* and *PHF6b* transcripts in R342X mice.** (A) Schematic for the two *PHF6* transcripts produced in humans. *PHF6b* includes the intron 10b between exon 10 and exon 11. (B) An agarose gel ran with WT and R342X *Phf6* cDNA obtained from newborn mouse cerebral cortex RNA. Primers were used to amplify the cDNA from the end of *Phf6* exon 9 till the beginning of *Phf6* exon 11. The mutant samples showed an unexpected band at ~370 bp which when sequenced showed to be missing exon 10. (C) Schematic showing the new amino acids (teal) which are included in the SKRTT protein if it were to be translated.



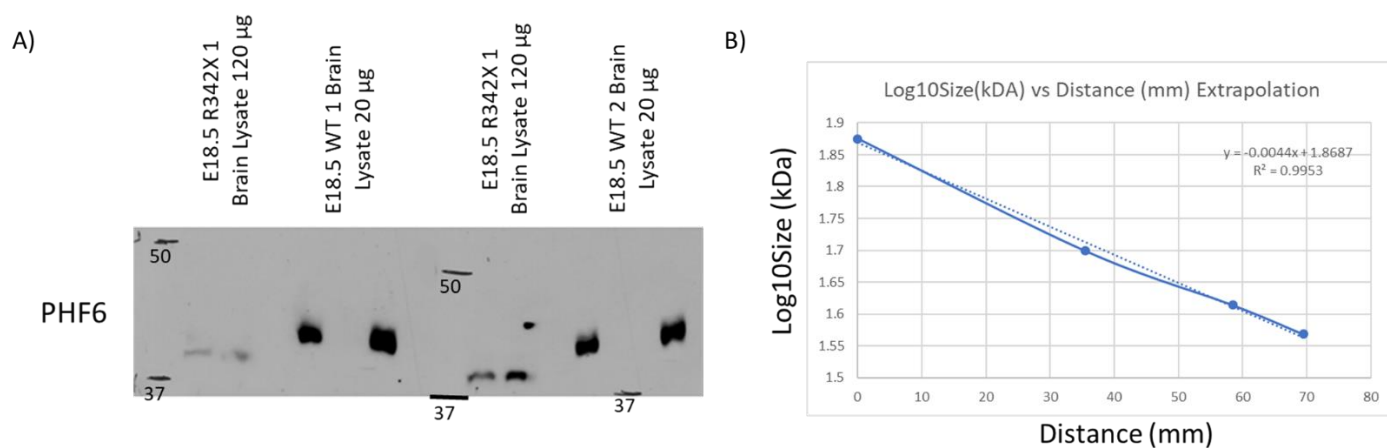


**Figure 3-6. Increased separation of the R342X PHF6 band during western blot.** (A) A large 12.5% SDS polyacrylamide gel was used to separate protein lysate from the brains of E18.5 WT males and R342X males. 6 times more R342X protein was loaded in comparison to WT samples. (B) The imaged gel was used to estimate the approximate size of the R342X band using a LogSize vs Distance graph.

### **3.4. Analysis of anterior pituitary gland development in the R342X mice**

Some BFLS patients have presented with dysregulated homeostasis of the hormones of the hypothalamic-pituitary-adrenal (HPA) axis. BFLS patients have been reported to be affected by hypoglycemia, hypothyroidism, low growth hormone (GH), low cortisone, low follicle-stimulating hormone (FSH), low luteinizing hormone (LH) and even atrophy of the pituitary gland (Birrell et al. 2003; Turner et al. 2004; Crawford et al. 2006; Zweier et al. 2013). Furthermore, PHF6 expression was high in adult human thyroid tissue (Vlierberghe et al. 2011). Therefore, it appears that PHF6 is involved in hormonal regulation and/or the development and maintenance of organs which are involved in hormonal regulation. We decided to investigate whether the weight defect observed in the R342X mice was the result of a pituitary gland abnormality. In mice, PHF6 is moderately expressed in the anterior pituitary gland early during development (Voss et al. 2007).

To begin with, we looked at the structure of the whole pituitary gland at several time points in an effort to investigate the pituitary gland development timeline in the R342X mice. At E18.5, the R342X pituitary gland and the WT pituitary gland were similar in size (Figure 3-7A). At P25 and P35, the R342X anterior pituitary was significantly smaller than the WT animals while the size of the posterior and intermediate pituitary were unchanged (Figure 3-7A). The murine anterior pituitary gland is structurally fully developed by birth and all the endocrine cell populations which produce the specific hormones are present (Rizzoti 2015). These cell populations undergo expansion phases postnatally in a spatially and temporally regulated manner (Rizzoti 2015). Therefore, it seems that the postnatal anterior pituitary gland development of the R342X mice is affected. Next, we looked at the expression of PHF6 in the pituitary gland to determine if the PHF6 expression levels were similar to what was observed previously by other

investigators (Voss et al. 2007). The R342X mice showed no expression of PHF6 in the pituitary gland at E18.5 while the WT gland showed significant PHF6 expression in the anterior pituitary (Figure 3-7C). Despite knowing that PHF6 expression is low in the R342X mice, the antibody cannot detect the extremely low amounts of protein via immunofluorescence. Consistent with this result, we showed that the *Phf6* RNA expression level was reduced to a similar level to what was observed in the cortex (Figure 3-7B).

Given that we discovered a developmental defect in the anterior pituitary gland of the R342X mice, we set out to investigate whether hormonal homeostasis is altered. Pituitary homeostasis was analyzed at three levels. First, we investigated RNA levels of the hormones produced by the pituitary gland by performing qRT-PCR of the respective hormones from pituitary gland tissue. Second, we performed immunofluorescent counts using antibodies to different hormones which allowed us to investigate cell population dynamics in the anterior pituitary gland. Last, we performed hormone ELISAs from plasma isolated from the R342X mice which provided a perspective on the downstream regulation of hormonal homeostasis. We postulated that analysis at these three levels would allow us to form a general interpretation of the state of regulation of hormonal homeostasis mediated by the anterior pituitary gland in the mice. From the qRT-PCR experiment, we found growth hormone (*Gh*) and prolactin (*Prl*) to be downregulated in the R342X pituitary gland (Figure 3-8A). From the immunofluorescent staining we found there were fewer PRL producing cells in the R342X anterior pituitary gland compared to controls (Figure 3-10D and 3-10E). From the ELISA experiment, we found thyroxine (T4) to be lower in the R342X plasma (Figure 3-9). Interestingly, transthyretin (Ttr), a transporter for thyroxine, was shown to be twelve-fold upregulated in the R342X P0 cerebral cortex by RNA-seq analysis (Dr. Farshad Niri and Laura Goodwin assisted in data analysis)

(Supplementary Table 1). Indeed, qRT-PCR for Ttr validated the twelve-fold increase suggesting that there could be a defect with T4 regulation (Figure 3-8B). In conclusion, from the qRT-PCR, ELISA and immunofluorescent stain experiments, it does seem that there is a hormone defect in the smaller anterior pituitary gland of the R342X mice. This defect seems to be in pathways which involve GH, PRL, and TSH.

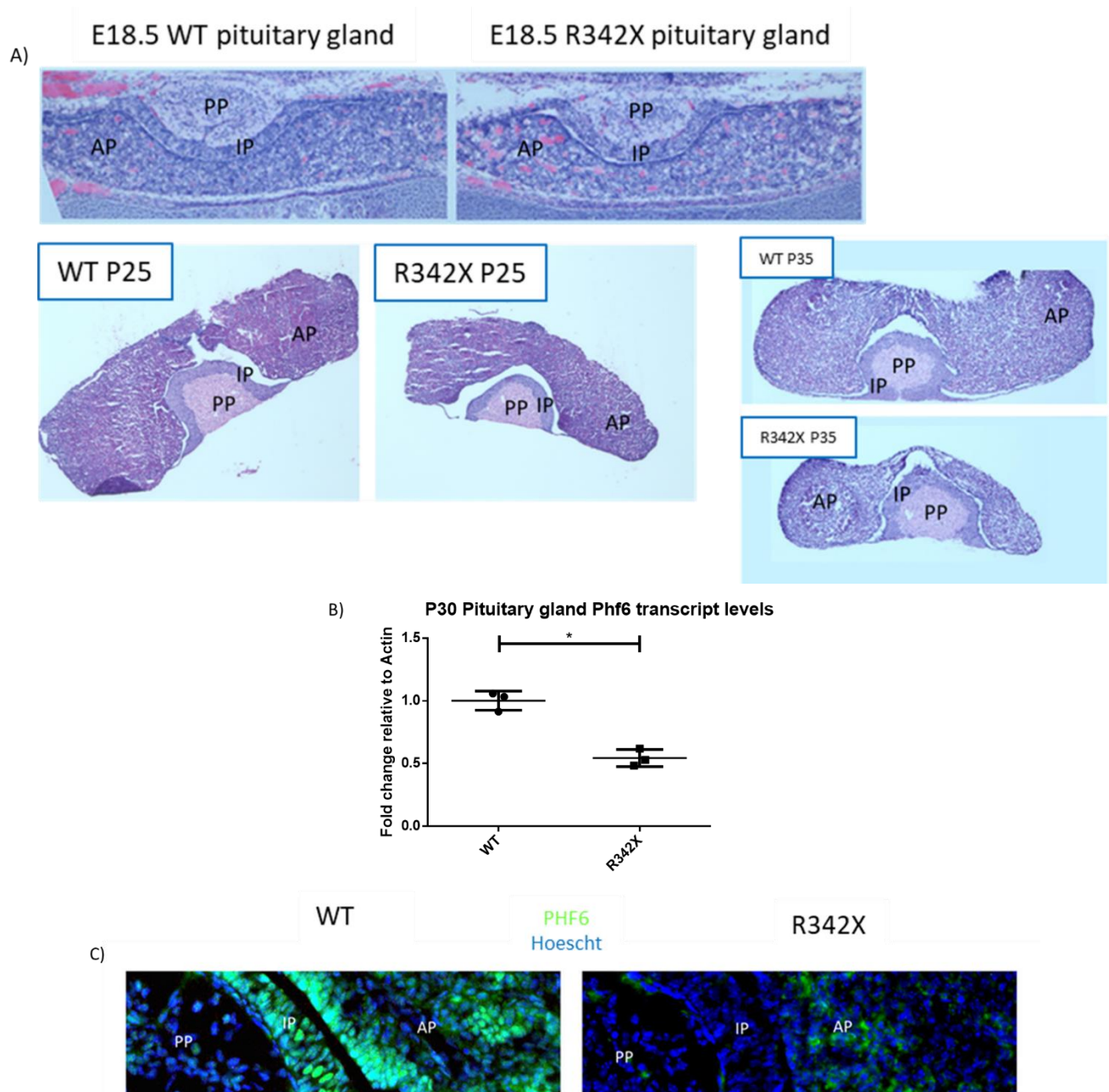


**Figure 3-7. Morphology and PHF6 expression within the pituitary glands of WT and R342X mice.** (A) H&E stained sections of the pituitary gland isolated at different ages. The E18.5 pituitary gland of WT and R342X mice are similar in size. However, at P25 and P35 the AP for mutant mice is smaller. The magnification is 10X for the E18.5 pituitary glands and 5X for the 25-day old and 35-day old pituitary glands. AP denotes the anterior pituitary, IP the intermediate pituitary and PP the posterior pituitary gland. (B) qRT-PCR analysis of *Phf6* RNA levels in the pituitary gland of 30-day old mice.  $n=3$ ,  $p<0.05$ . (C) Immunofluorescently stained images of E18.5 pituitary gland showing PHF6 expression present in WT mice but not R342X mice. PHF6 labeling (green) and Hoechst nuclear stain (blue) are shown. The magnification is at 20X.

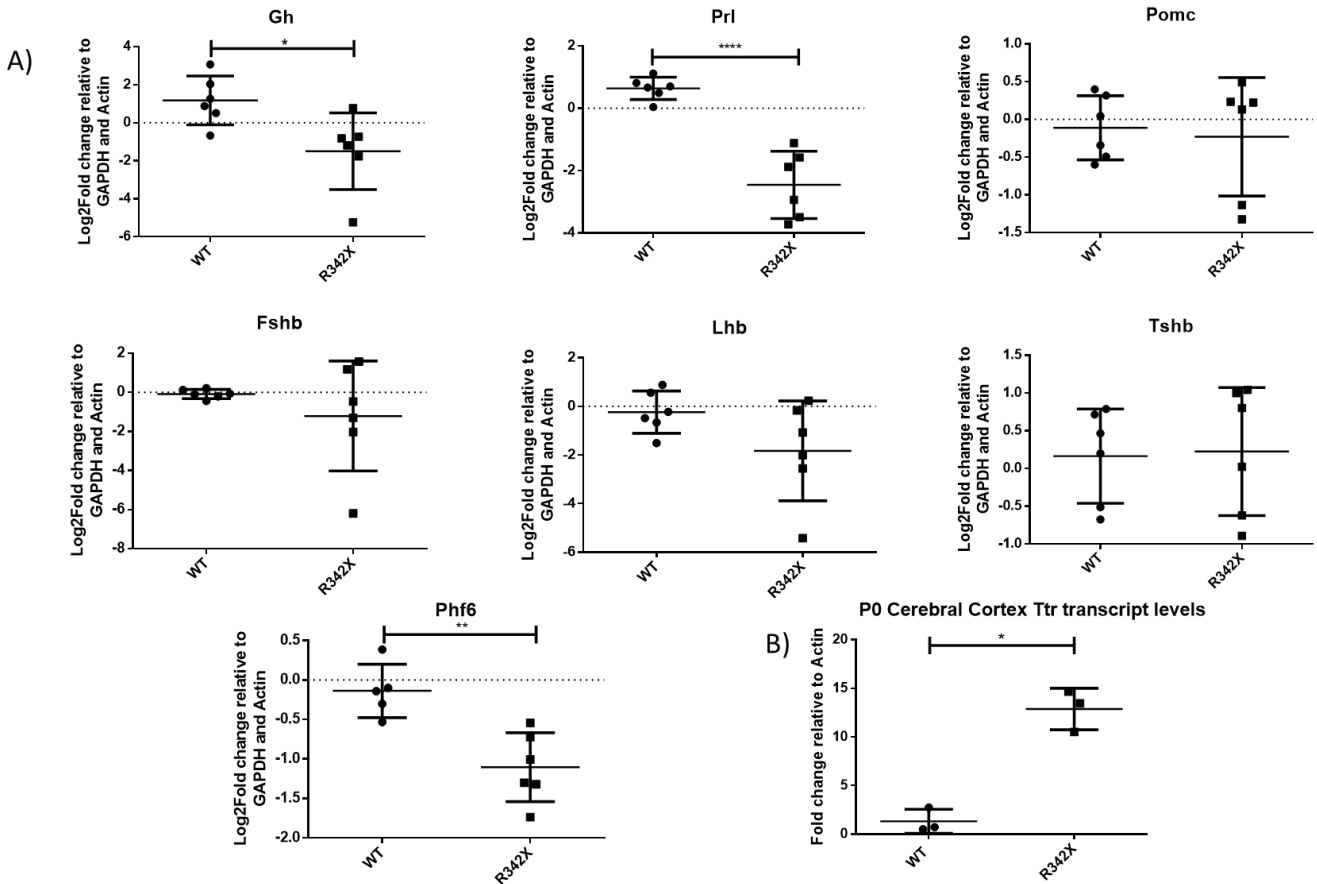


**Figure 3-8. RNA expression analysis of targets involved in hormonal regulation.** (A) qRT-PCR analysis of hormone RNA levels in the pituitary gland of 21-day old mice. Growth hormone (*Gh*) and prolactin (*Prl*) RNA were downregulated while expression of luteinizing hormone beta (*Lhb*), proopiomelanocortin (*Pomc*), the precursor involved in forming adrenocorticotrophic hormone (ACTH), follicle-stimulating hormone beta (*Fshb*), and thyroid-stimulating hormone beta (*Tshb*) RNA did not change. *Phf6* RNA expression showed a reduced level, similar to our observations of the pituitary gland at P30 (Figure 3-7B). n=6, \* = p<0.05, \*\* = p< 0.01, \*\*\*\* = p<0001. (B) qRT-PCR analysis of *Ttr* RNA expression in P21 pituitary glands. *Ttr* was chosen as a potential candidate for misregulation since it was highly upregulated in 1-day old cerebral cortex samples analyzed by RNA-seq (Supplementary Table 6-1). n=3, p<0.05.

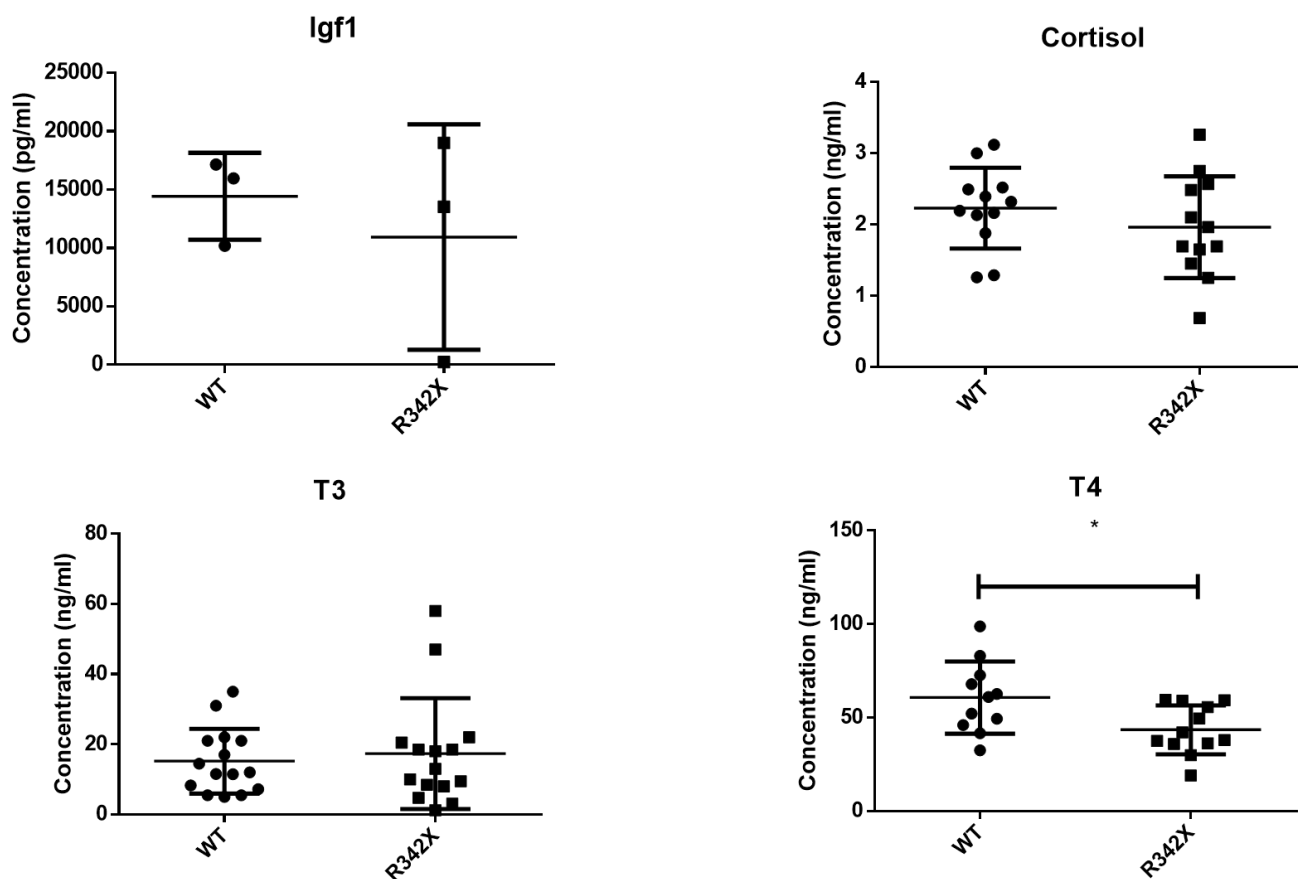


**Figure 3-9. ELISA of hormonal markers from P21 plasma samples.** Separate graphs corresponding to each hormone analyzed by ELISA from 21-day old mouse plasma are shown. Each dot represents a single plasma sample. Tests for insulin-like growth factor 1 (IGF-1) (WT n=3 and R342X n=3), cortisol (WT n=12 and R342X n=12) and triiodothyronine (T3) (WT n=15 and R342X n=15) showed no differences between WT and R342X mice while ELISA for T4 (WT n=11 and R342X n=12) showed a lower level in the R342X mice.  $p < 0.05$ .

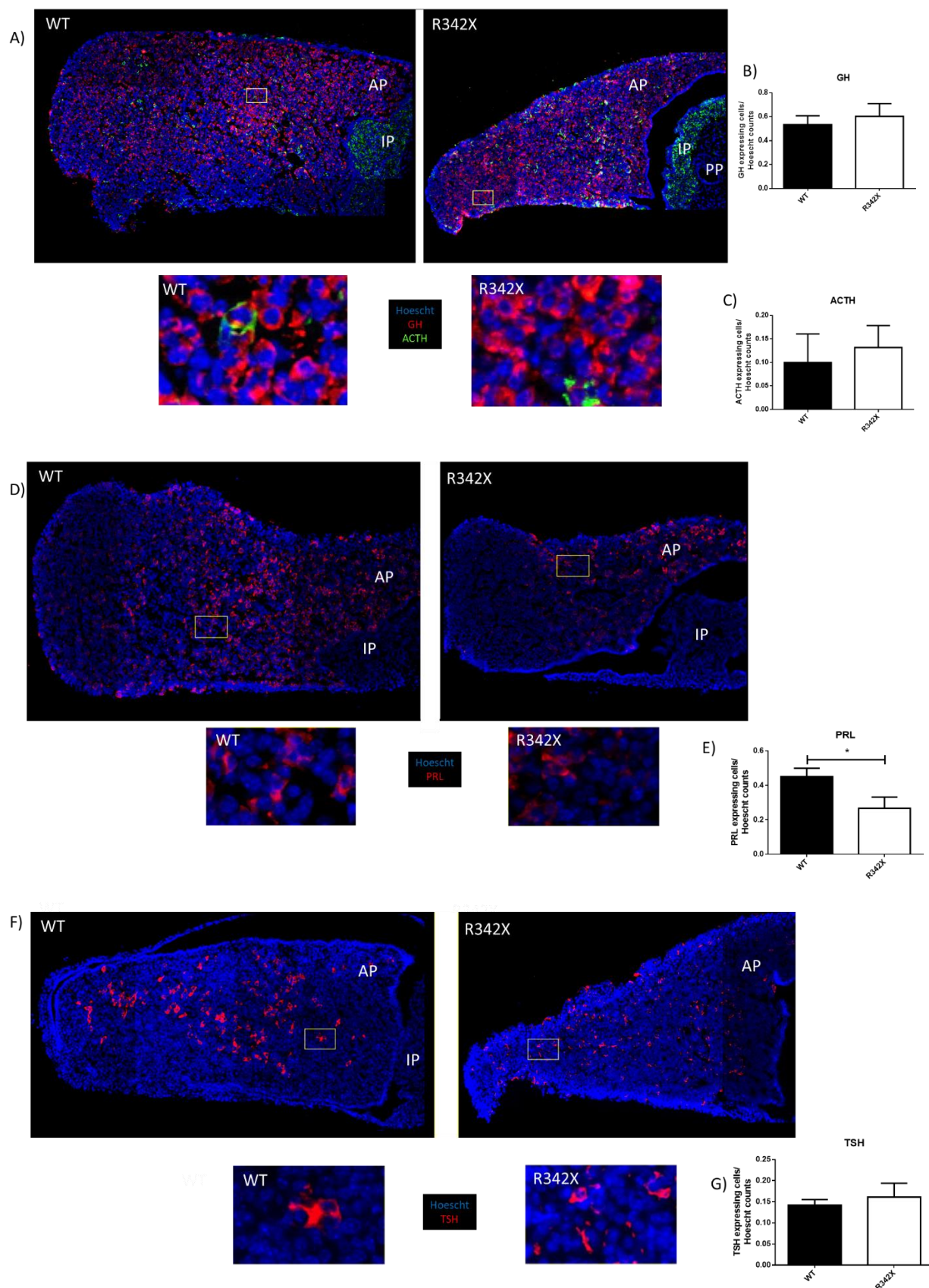




**Figure 3-10. Immunofluorescent stains of hormone produce cells in the pituitary gland.** 21-day old pituitary gland was stained with Hoechst stained in blue, (A) GH stained in red and ACTH stained in green, (D) PRL stained in red and (F) TSH stained in red. Images were taken at 20X magnification and magnified pictures presented under the sections. Cells in the anterior pituitary gland were counted and presented in graphs (B), (C), (E) and (G). There appeared to fewer PRL expressing cells in the R342X AP in comparison to WT AP. AP denotes the anterior pituitary, IP the intermediate pituitary and PP the posterior pituitary gland. n=3, p<0.05.

### **3.5. Structural analysis of brain development in the R342X mice**

Given the high expression pattern of PHF6 present in the developing mouse brain, we thought it would be important to perform a structural analysis of the brain in the R342X mice (Voss et al. 2007). Furthermore, ID is one of main phenotypes of BFLS and it would be interesting to find a link between a structural defect which could perhaps drive this ID phenotype in BFLS patients (Turner et al. 2004). Additionally, brain structural abnormalities like microcephaly, macrocephaly, coarse gyri, widened ventricular system and cortical abnormalities were reported in BFLS patients, and it would be interesting to observe if and how these phenotypes manifest in the brain of the R342X mice (Brun et al. 1974; Gecz et al. 2006; Jahani-Asl et al. 2016; Kasper et al. 2017).

As an initial test to determine whether the R342X mice had any brain abnormalities, we performed Nissl staining of brain tissue sections. As shown in Figure 3-11 we observed no gross differences in brain structures, although the brains were smaller. Given that the brain/body weight ratios between WT and R342X mice were the same, we concluded that the R342X brains were smaller but proportional in size. Next, we performed volumetric measurements to compare different regions of the brain using high-resolution MRI (Figure 3-12A, 3-12B and 3-12C). Volumetric analysis using the MRI data set confirmed that the overall volume of the R342X brain was smaller than WT littermates. This experiment also revealed further differences in the brains of the R342X mice (Figure 3-13). Volumes of 181 defined regions as a proportion of whole brain volume was calculated, and using an FDR approach, a cut-off of  $p < 0.01$  was chosen as significant. In this way, we identified 52 brain regions with significant volumetric changes. These changes are presented as a heat map superimposed onto a brain image, with red representing regions with increased volumes and blue representing areas of decreased volume

(Figure 3-13A). The altered regions are listed in Figure 3-13B, with a notable decrease in the volumes of cerebellar regions, like lobule 8: pyramis, simple lobule, crus 2: ansiform lobule, paraflocculus, lobule 8 white matter, simple lobule white matter, crus 1 white matter, crus 2 white matter, paramedian lobule and paraflocculus white matter. The change in volume of the cerebellum was also noticeable in Nissl stained sections and in MRI images (Figure 3-11C and Figure 3-12A, respectively). Other interesting changes from figure 3-13B included increased volume of the amygdala, the hypothalamus and the periaqueductal grey region, and decreased volume of the striatum and the CA1 layer of the hippocampus. Therefore, it seems that the R342X mutant protein inhibits the development of specific brain regions. We also noticed that once we reached  $\geq 5$ th generation, 1/3 of R342X mice developed hydrocephaly (Supplementary Table 6-3). Several R342X mice brains showed hydrocephaly from the MRI but these datasets were excluded from the volumetric analysis (Figure 3-12D).

In a complementary experiment, we performed RNA-seq using cortical tissue isolated from newborn mice to examine gene expression differences in the R342X mice. We used 2 WT samples and 3 R342X samples for the experiment. Unfortunately, the WT samples were not clustered closely on the principal component analysis (PCA) plot (Supplementary Figure 6-1). This led to more than 1000 genes being differentially expressed when the first WT sample, called WT1, was compared to the 3 R342X samples. However, when the second WT sample, called WT2 was included in the comparison, under 50 genes were differentially expressed. The differential gene expression analyses were performed by lab members, Dr. Farshad Niri and Laura Goodwin. The lists were generated using an adjusted p-value, otherwise known as a q-value, of  $< 0.1$ . The top 11 genes which appeared in the comparison of 2 WT vs 3 R342X samples generated by Niri and Goodwin are presented in Figure 3-14A. Out of these genes, we

validated the altered expression of the following genes by qRT-PCR (Figure 3-14): Folate receptor 1 (*Folr1*), a folate receptor that regulates metabolism and may contribute to the decreased weight of R342X mice; aquaporin 1 (*Aqp1*), a water channel that could explain the increased incidence of hydrocephaly, and high mobility group AT-hook 1b (*Hmgalb*), a gene involved in the regulation of chromatin and gene expression. To confirm these differences, we performed qRT-PCR on these targets of interest (Figure 3-14). RNA-seq analysis results for these genes can be found in the Appendix (Supplementary Table 6-1).

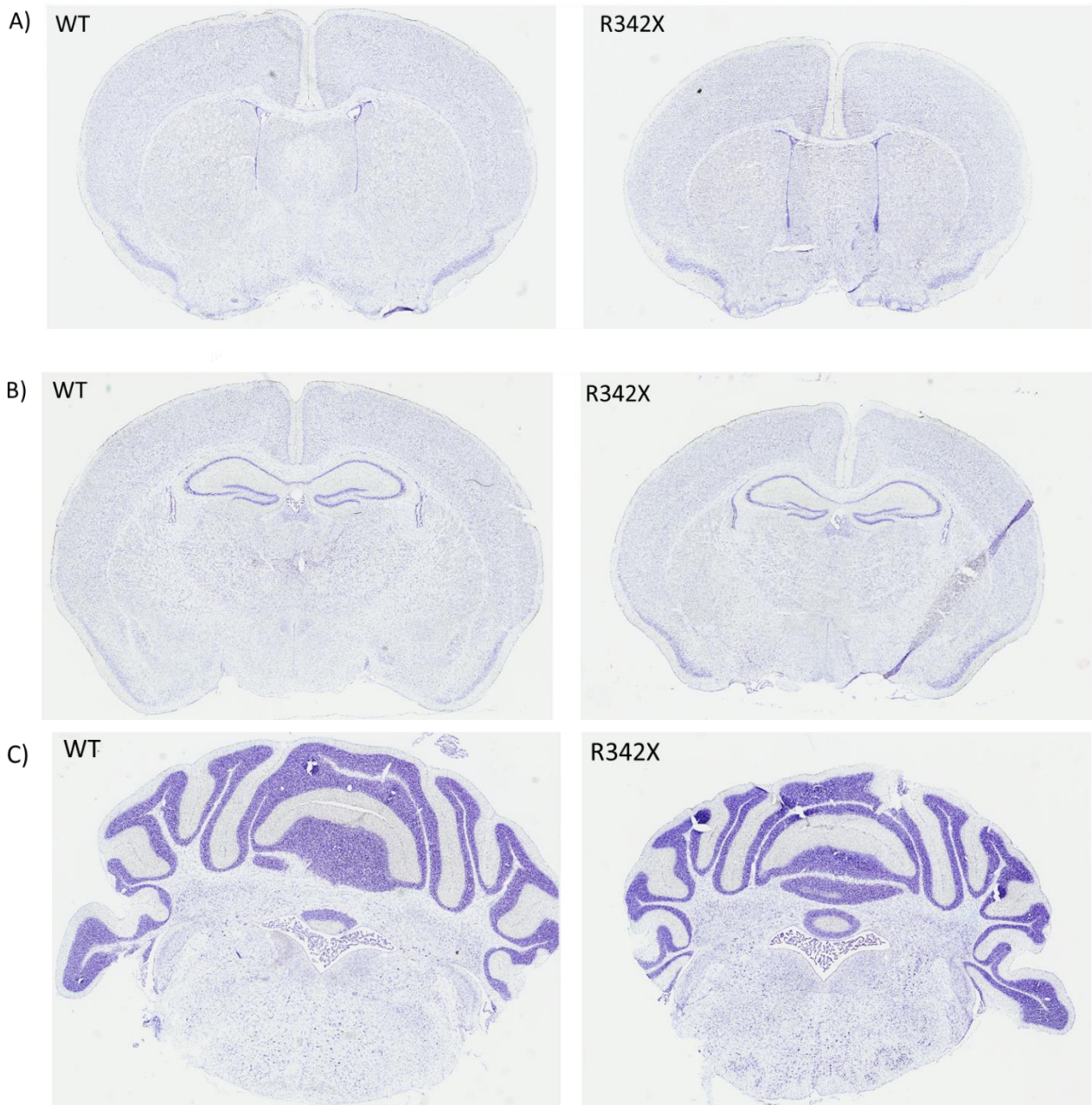


**Figure 3-11. Nissl stains comparing WT and R342X brain regions.** Nissl staining was performed on 24-day old mice brain coronal sections comparing (A) cortex, (B) hippocampus and (C) cerebellum. Magnification for (A) and (B) was 1.4X and 1.6X for (C). Figure was generated by Gerardo Zapata (Dr. David Picketts Lab).

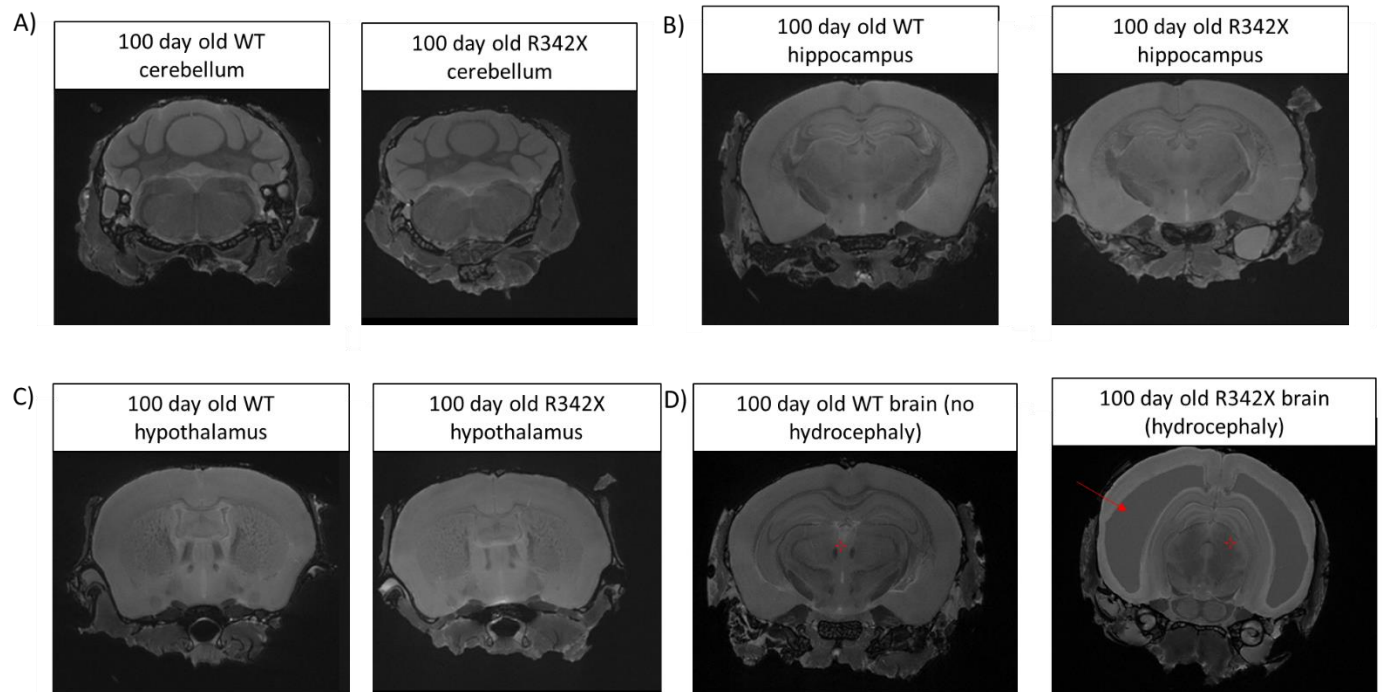


**Figure 3-12. MRI images comparing WT and R342X mouse brain structures.** MRI images of 100-day old WT and R342X (A) cerebellum, (B) hippocampus and (C) hypothalamus. Imaging was performed by Dr. Jason Lerch's lab (Hospital for Sick Children, Toronto). (D) We also observed that 1/3 of R342X mice on a pure C57BL/6J background ( $\geq 5$ th generation) developed hydrocephaly which was evident from the large ventricles in the MRI (arrows).

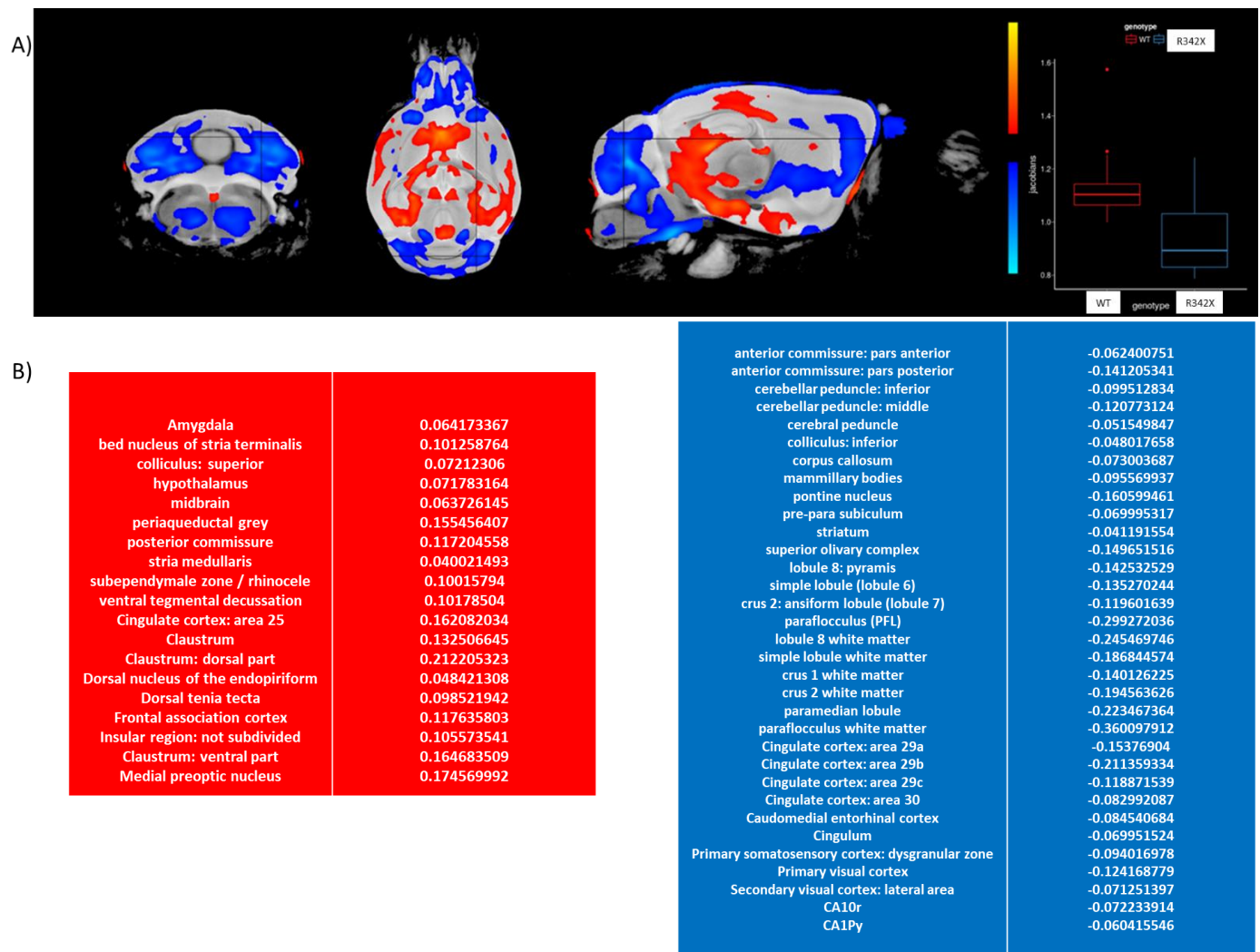


**Figure 3-13. Volumetric analysis of the MRI data comparing WT and R342X mice brains.**

(A) Heatmap images of the volumetric analysis with red denoting an increase in the size and blue denoting a decrease in the size of specific brain regions. Volumetric data was calculated following measurements in three planes. (B) Red and blue tables depict the brain regions with significantly increased and decreased changes in volume, respectively. The number corresponding to each region signifies the percent change from the total volume of the whole brain.  $n=8$ ,  $P<0.01$  with FDR approach.

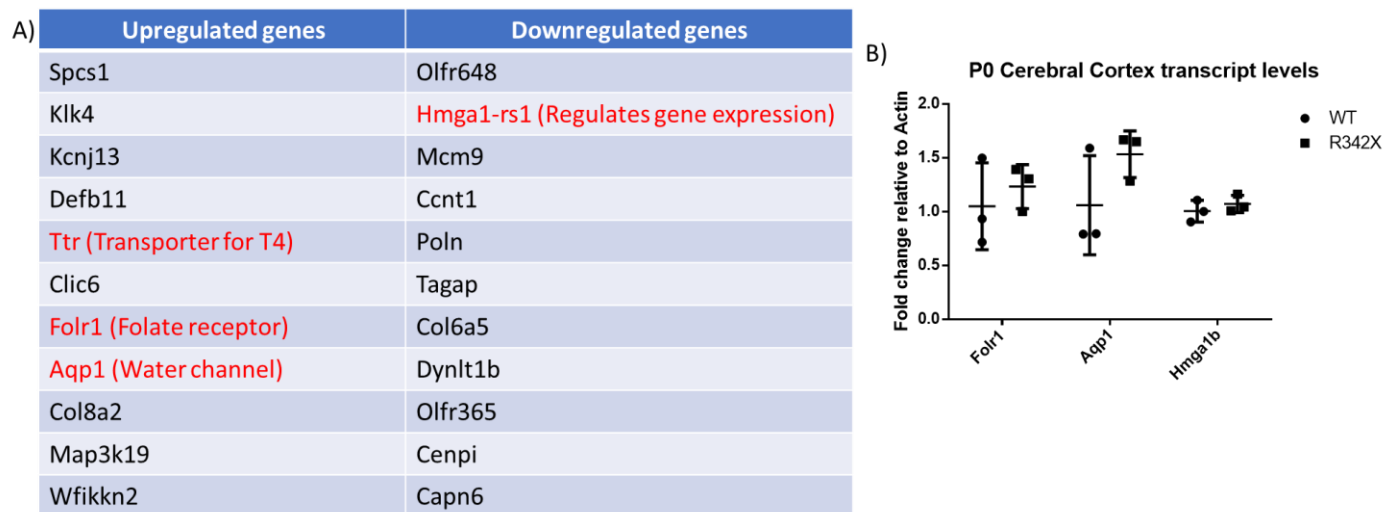


**Figure 3-14. RNA-seq differentially expressed genes and qRT-PCR validation.** (A) Table depicting the top upregulated and downregulated genes from the RNA-seq analysis of RNA isolated from P0 cerebral cortices from WT and R342X mice. (B) Log<sub>2</sub> fold change differences validated by qRT-PCR analysis of genes selected because of their functional interest.



### **3.6 Characterization of neuronal migration in the R342X mice**

In mice, high PHF6 expression was observed in the developing cortex during embryogenesis while lower levels of PHF6 were detected in the cerebral cortex postnatally and into adulthood (Voss et al. 2007). This is interesting considering the intellectual disability phenotype which arises in childhood or adolescence and the suggested role of PHF6 in cortical development (Turner et al. 2004; Zhang et al. 2013; Franzoni et al. 2015; Kasper et al. 2017). Therefore, to begin with, we confirmed a loss of PHF6 protein in the developing cortex, a time when PHF6 expression is supposed to be high (Figure 3-15). Note that we recognize that there may be a very low level of PHF6 present in R342X samples as we demonstrated in cortical lysates, but we were unable to detect it via immunofluorescence.

To study cortical development in the R342X mice, we stained the developing cortex at different times (E13.5, E15.5, E18.5 and P5) for markers of different cell types: PAX6 which marks RGCs, TBR2 which marks IPs, TBR1 and CTIP2 which mark cells destined for the deep layers, VI and V, respectively; Forkhead box protein P1 (FOXP1) which marks cells destined for the layer IV; CUX1 which marks cells destined for the upper layers, II/III; and EdU which marks cells in the S-phase of the cell cycle. In this way, we expected to determine whether there were any differences in cortical development in the R342X mice. Importantly for these experiments, we analyzed the same region of the cortex when comparing WT and R342X samples.

The first question we asked was whether there were normal numbers of neural progenitors in the developing cortex. WT and R342X E13.5 sections were stained and counted to determine the percentage of PAX6<sup>+</sup> and TBR2<sup>+</sup> RGCs and IPs in the VZ and SVZ, respectively. We observed no differences in the proportion of RGCs or IPs compared to controls suggesting

that the progenitor pool was appropriately maintained in the R342X developing cortex at E13.5 (Figures 3-16 A, B and E, F). Next, we examined the percentage of cells in S-phase after a 1-hour pulse of EdU at E13.5. This experiment also showed no differences in the percentages of EdU+ cells (Figures 3-16 A, C and E, G). Moreover, no differences were observed for the percentage of double labelled (EdU+, PAX6+) cells, suggesting that RGC proliferation state was normal at E13.5 (Figures 3-16 A, D). However, we did observe an increased percentage of double labelled (EdU+, TBR2+) cells (Figures 3-16 E, H). Last, we counted the percentage of cells which were TBR1+ in layers V/VI. We observed no difference between WT and R342X TBR1+ counts suggesting that the lower layers were being formed normally at E13.5 (Figures 3-16 I, J).

At E15.5, we performed the PAX6, TBR2 and EdU counts as we had done at E13.5. However, we observed no difference in these counts suggesting that at E15.5, the progenitor pool was appropriately maintained, and the cell cycle kinetics of the progenitors was normal (Figures 3-17 D-K). Moreover, we counted the percentage of CTIP2 +cells in layers V/VI which appeared to be normal in the R342X cortices suggesting that at E15.5, the lower layers were being formed normally (Figures 3-17 A, C). We also quantified the percentage of CUX1+ cells in layers II/III. However, we observed no difference suggesting that the upper layers were being formed normally (Figures 3-17 A, B). At E18.5 and P5, we counted the percentage of cells which are TBR1+ and CTIP2+ in layers V/VI, FOXP1+ in layer IV and CUX1+ in layers II/III. There was no observable difference in these counts suggesting that upon the completion of the six-layer cortex, the lower layers, the intermediate layers and the upper layers were formed normally in the R342X mice.

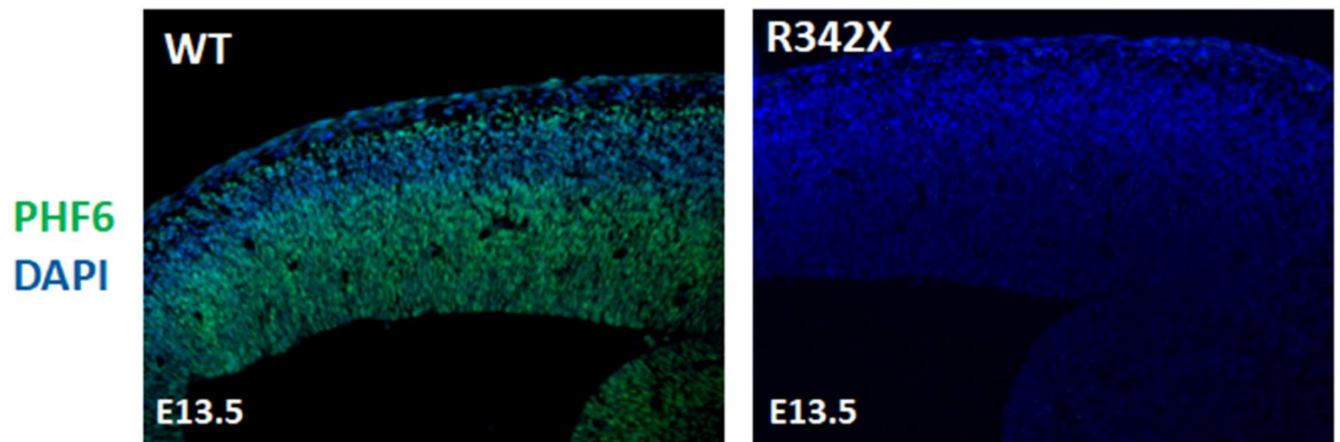


**Figure 3-15. PHF6 expression in E13.5 R342X cerebral cortex.** Immunofluorescently stained images of E13.5 cerebral cortex showing PHF6 expression present in WT mice but not R342X mice. PHF6 labeling (green) and Hoechst nuclear stain (blue) are shown. The magnification is at 5X.

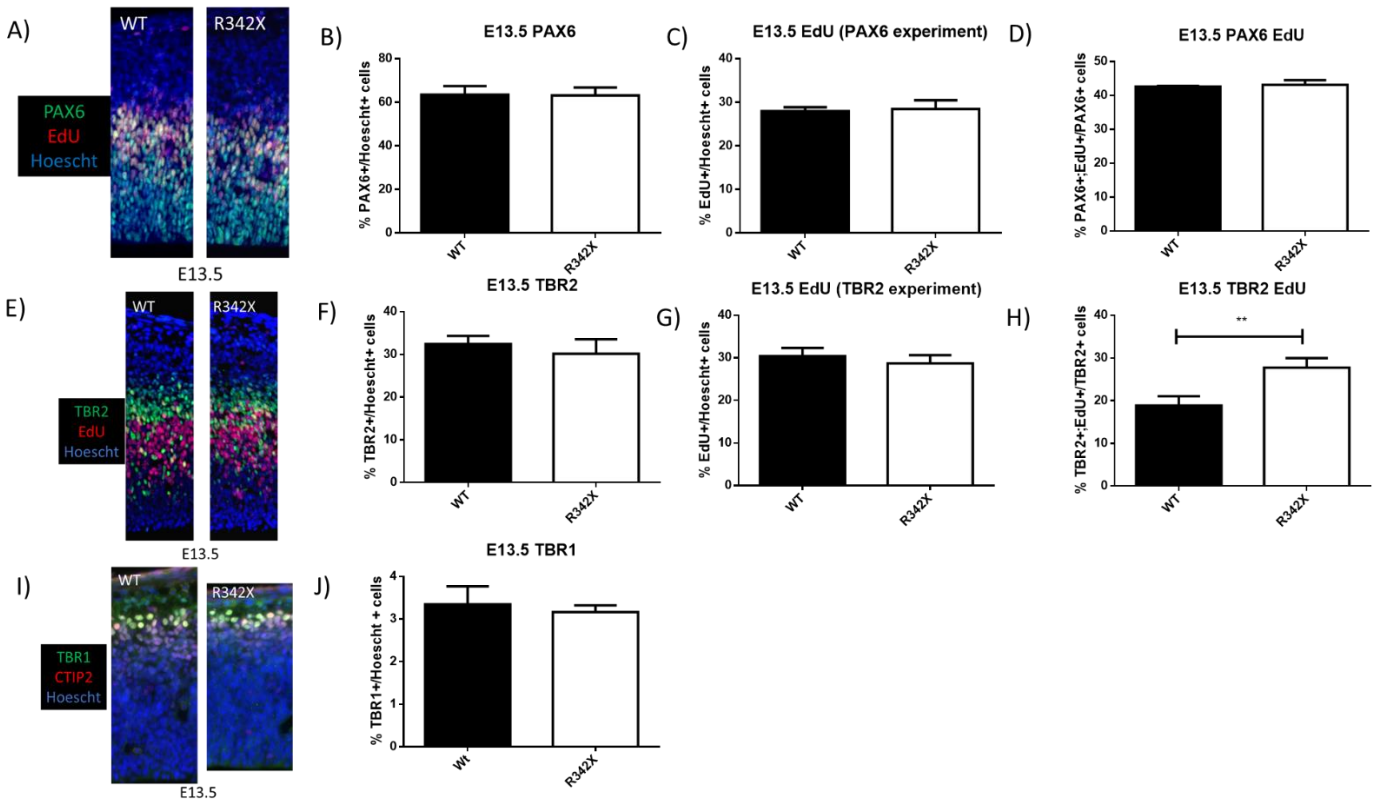


**Figure 3-16. Investigation of the process of cortical development in the E13.5 R342X cerebral cortex.** Immunofluorescence of E13.5 cerebral cortex with (A) PAX 6 stained in green, EdU in red, Hoechst in blue, (E) TBR2 stained in green, EdU in red, Hoechst in blue and (I) TBR1 stained in green, CTIP2 stained in red and Hoechst stained in blue. Counts from the stained images are presented in graphs (B), (C), (D), (F), (G), (H) and (J). Magnification for the images was 20X. n=3, \*\*=p<0.01. Keqin Yan assisted in data generation.

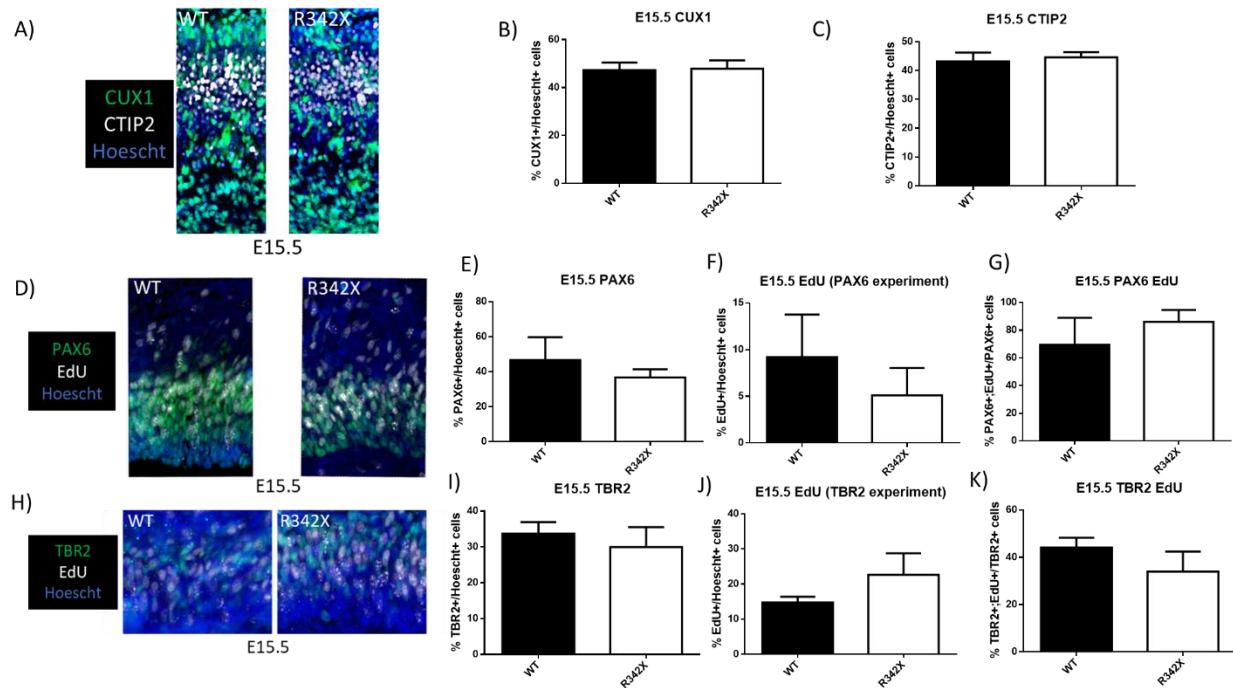


**Figure 3-17. Investigation of the process of cortical development in the E15.5 R342X cerebral cortex.** Immunofluorescence of E15.5 cerebral cortex with (A) CUX1 stained in green, CTIP2 in white, Hoechst in blue, (D) PAX6 stained in green, EdU in white, Hoechst in blue and (H) TBR2 stained in green, EdU stained in white and Hoechst stained in blue. Counts from the stained images are presented in graphs (B), (C), (E), (F), (G), (I), (J) and (K). Magnification for the images was 20X. n=3.

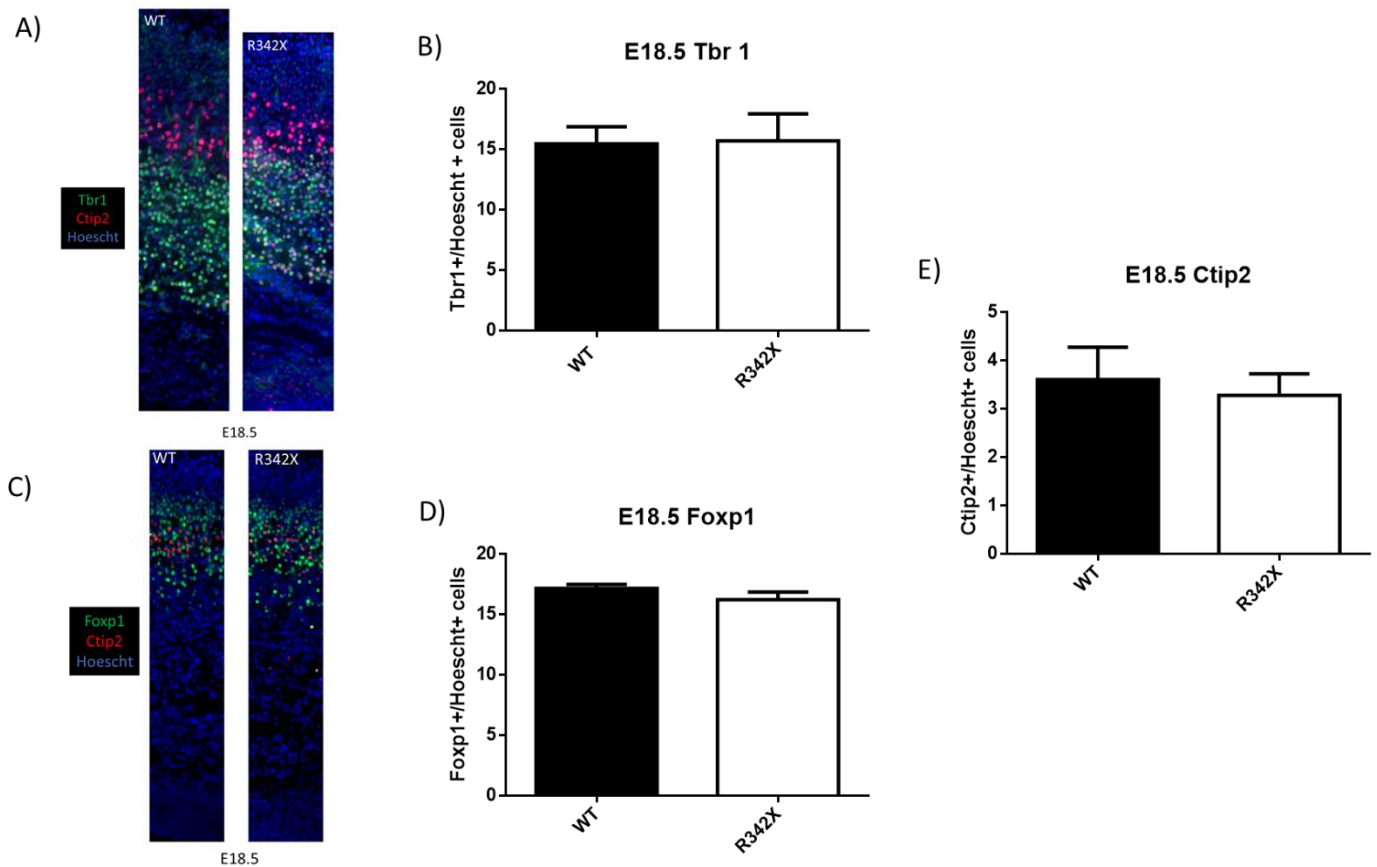


**Figure 3-18. Investigation of the process of cortical development in the E18.5 R342X cerebral cortex.** Immunofluorescence of E18.5 cerebral cortex with (A) TBR1 stained in green, CTIP2 stained in red and Hoechst stained in blue (C) FOXP1 stained in green, CTIP2 stained in red, Hoechst stained in blue. Counts from the stained images are presented in graphs (B), (D) and (E). The counts from (E) includes counts from both (A) and (C). TBR1 and FOXP1 counts n=3. Ctip2 counts n=6. Magnification for the images was 20X.

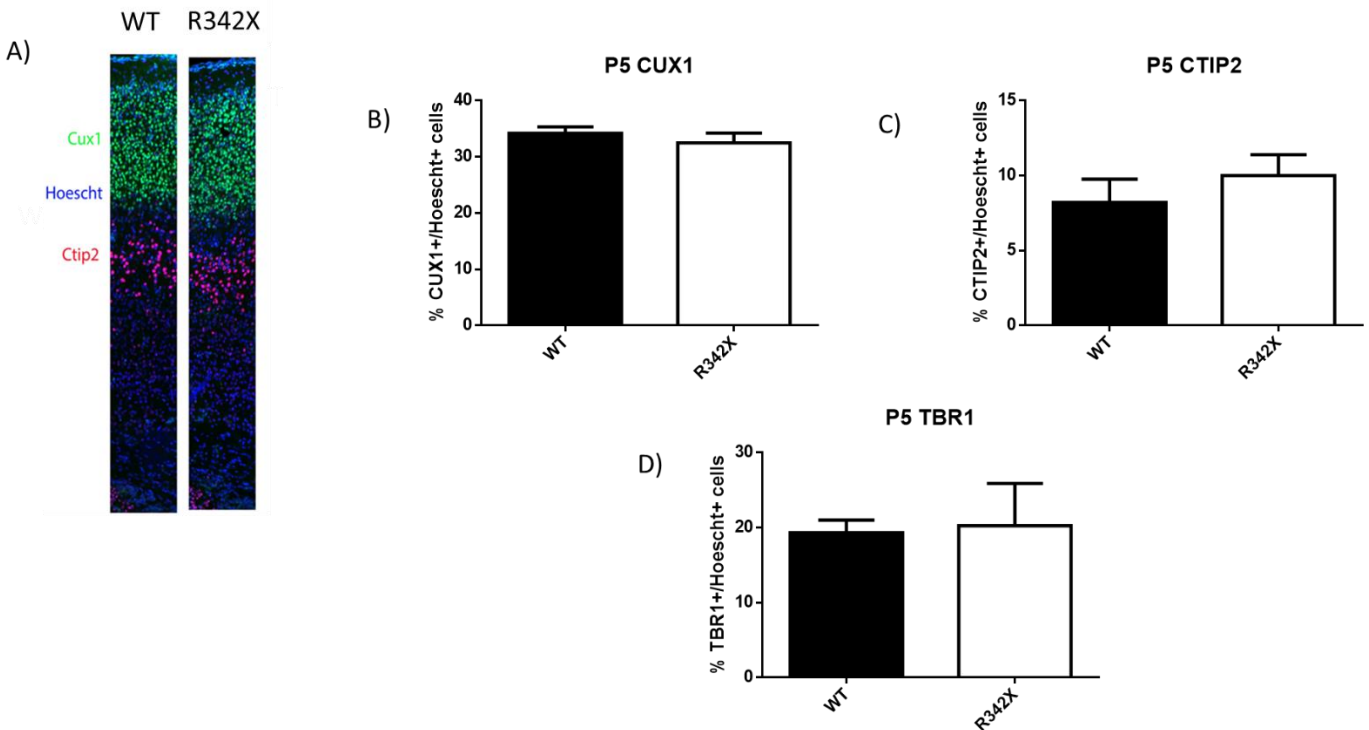


**Figure 3-19. Investigation of the process of cortical development in the P5 R342X cerebral cortex.** Immunofluorescence of P5 cerebral cortex with (A) CUX1 stained in green, CTIP2 stained in red and Hoest stained in blue. Counts from (A) are presented in graphs (B) and (C). Counts for P5 cerebral cortex TBR1 are presented in (D). Magnification for the image was 20X. n=3.

### **3.7 Behavioural assessment of the R342X mice**

To further characterize the R342X mice, we decided to perform behavioural tests on the R342X mice. This was important given that BFLS patients are affected by ID which inhibits cognitive function (Turner et al. 2004). Moreover, many BFLS patients exhibit behavioural traits like hyperactivity, rule-breaking and challenging behaviour, and sexual deviance while at the same time exhibiting a friendly behaviour and a happy-go-lucky attitude, scoring low on anxiety tests (Visootsak et al. 2004; Winter et al. 2009). It seems that the BFLS patients lack a sense of normal inhibitions. Therefore, to assess these phenotypes in the R342X mice, we decided to perform behavioral tests investigating learning, memory and anxiety. Furthermore, since human BFLS patients are affected by hypotonia, we wanted to test if there was any observable weakness in the R342X mice (Turner et al. 2004). Behavioral tests on the R342X mice were performed by Valerie Cardin (Dr. David Picketts Lab).

To investigate anxiety, two tests were performed. First, we used the elevated plus maze (EPM) test. Mice are placed in an elevated maze with open and closed arms. A normal response for the mice is to spend more time in the closed arms than in the open arms. The R342X mice spent more time in the open arms than WT mice (Supplementary Figure 6-2A). Second, the open field test was conducted. Mice are placed in a box with a centre region and 4 corners. The centre is illuminated with a light source while the corners are darker. A normal response for the mice is to spend more time in the dark corners than in the centre. The R342X mice spent less time in the corners than the WT mice, instead spending more time in the centre (Supplementary Figure 6-2B and 6-2C). Therefore, the phenotype of R342X mice is to be less anxious than control animals in these tests.



Given this inability to sense anxiety provoking situations, we hypothesized that the mice might be less depressed. To investigate depression, a forced swim test was conducted. Mice are placed in water for 6 minutes and the time they spend immobile is used as a measure of behavioral despair. The R342X mice spent less time immobile than WT mice, implying that they show less behavioral despair (Supplementary Figure 6-3).

To test learning and memory, we performed additional tests. First, to test learning and working memory we performed a Y-maze experiment. In this test, mice are placed in a maze with three arms and the frequency of unique entries into the different arms (alterations) is measured (Supplementary Figure 6-4A). A higher number of alterations represents better working memory. However, no significant difference was observed between R342X mice and WT mice. Next, the fear conditioning experiment was performed which examines associative learning and memory in the context of aversive stimuli. Mice are placed in a new cage on day 0 and an aversive stimuli (shock) is applied. They are then returned to their cages. On day 1, the mice are transferred to the cage where the shock was applied and the time the mice spend immobile is measured. This is repeated on day 3 and day 17. The time spent immobile is a measure of fear related memory. It appears that the R342X mice have a weaker memory response to aversive stimuli as they spent less time immobile when placed in the cage where the shock was applied on day 3 and day 17 (Supplementary Figure 6-4B).

To test strength in the R342X mice we performed the hanging wire experiment. Mice are forced to hang on a wire and the time spent until they fall off the wire is measured. The time spent is used as a measure of strength in the mice. We observed that the R342X mice performed similar to WT mice (Supplementary Figure 6-5).

## 4.0 Discussion

PHF6 is a chromatin adaptor protein which interacts with dsDNA, miRNA, the NuRD complex, UBF and the Paf1C complex (Todd and Picketts 2012; Wang et al. 2013; Zhang et al. 2013; Liu et al. 2014; Franzoni et al. 2015; Liu et al. 2015; Todd et al. 2015). Through these interactions, it is postulated that the PHF6 protein changes the chromatin landscape. We generated a transgenic mouse line with a common BFLS patient mutation to better our understanding of the disease and the function of the protein. Here we report changes to the genomic and expression profile of the *Phf6* R342X gene in the mouse and describe the pathological features in the R342X mice in the context of the BFLS disease.

### 4.1 Assessing the R342X mice as a model of BFLS

During our gross characterization of the R342X mice, we noticed that R342X pups ( $\geq$  6th generation; C57BL/6J background) experienced postnatal lethality. Moreover, the R342X mice on the pure C57BL/6J background were smaller and weaker than the R342X mice on the mixed background. Additionally, 1/3 of the  $\geq$ 5th generation R342X mice on the pure C57BL/6J background developed hydrocephaly by weaning age (Supplementary Table 6-3).

The postnatal lethality in the R342X mice might occur due to the early development of hydrocephaly in R342X pups. Hydrocephaly is a condition involving accumulation of cerebral spinal fluid (CSF) in the brain which occurs when CSF circulating in the brain is unable to drain out into the venous system or when CSF is overproduced by the choroid plexus (Kartal and Algin 2014). Hydrocephaly arises due to defects in genes involved in brain patterning and brain vasculature development and maintenance (Huh et al. 2009). From our RNA-seq data, we observed *Aqp1* to be upregulated. *Aqp1* is a water channel protein expressed in the epithelial

cells of the choroid plexus (Speake et al. 2003). Furthermore, the gene contributes to CSF production by maintaining the osmotic gradient at the choroid plexus (Oshio et al. 2004; Steffensen 2018). In the R342X mice, the upregulation of *Aqp1* at a transcriptional level due to the loss of PHF6 function might drive hydrocephaly. Using qRT-PCR, we were not able to replicate the increase of *Aqp1* expression. Reinvestigation of *Aqp1* using qRT-PCR and immunoblotting using a bigger sample size might provide a more accurate representation of the link between *Aqp1* and hydrocephaly in the R342X mice.

The postnatal lethality might also arise from a feeding defect in the R342X pups on the pure C57BL/6J background. Interestingly, during infancy, a few BFLS patients failed to thrive and experienced feeding difficulties, while two male BFLS patients died during childhood due to hindered developmental (Turner et al. 2004 and Carter et al. 2009). A postnatal lethality by feeding defect can be investigated by examining the milk pouch in dead pups as has been done by others (Turgeon and Meloche 2009).

The background of the mice seems to play an important role in the pathogenesis of BFLS in mice. The pure C57BL/6J R342X mice are difficult to study due to postnatal lethality and the frequent development of hydrocephaly. The background of the mice leads to a severe phenotype which is likely due to the effect of modifier genes that influence the function of the mutated gene being studied (Eshraghi et al. 2016). Therefore, in an effort to overcome the drawbacks of the C57BL/6J background, we have begun backcrossing the C57BL/6J background R342X mice on the FVB background, hoping for the absence of postnatal lethality and hydrocephaly, and the manifestation of the R342X phenotype associated with BFLS.

Next, we noticed that the R342X mice are smaller in size but have no difference in WAT accumulation in comparison to WT littermates. However, the variance in the fat weighing

experiment was higher prompting future re-investigation with a greater sample size and an older timepoint allowing further fat accumulation. Regardless, our data presents a contradictory feature of the R342X mice when compared to human BFLS patients who are affected by truncal obesity (Turner et al. 2004). This contradictory feature might result from compensation by another protein with overlapping functions to PHF6 that may be specific to the mouse species. Furthermore, the R342X mice might present itself as a limited mouse model for BFLS. We will further describe this concept later in this section.

BFLS patients are affected by hypogonadism and inhibition of sexual development (Turner et al. 2004). However, the testes in the R342X mice were proportionally the same size when compared to WT mice and the R342X mice were fertile. Nonetheless, additional studies are required to fully assess testicular development. Future studies should perform immunohistochemistry of the testes to examine testes structure and cell populations. Testosterone levels in the plasma could also be measured to further characterize the sexual development of the R342X mice.

Furthermore, BFLS patients are affected by digit abnormalities and facial dysmorphia, but no obvious defects of this nature were observed in the R342X mice, although future computed tomography (CT) studies may help evaluate digit abnormalities more thoroughly (Turner et al. 2004).

As part of the characterization of the expression profile of the *Phf6* gene in the R342X mice, we observed that the R342X mice produced a truncated PHF6 protein at very low levels. Moreover, the *Phf6* transcript levels in the R342X mice were 50% lower which suggests that the transcripts undergo NMD. Alternatively, the protein itself could be unstable but we have not investigated this possibility. To test whether the R342X transcript is undergoing NMD, the ratio

of the R342X *Phf6* transcript to the WT *Phf6* transcript could be compared by qRT-PCR in primary cortical cells following puromycin (NMD inhibitor) treatment. Next, we observed that a novel transcript isoform, the SKRTT transcript was being produced in the R342X mice. We were uncertain whether the shorter truncated PHF6 band in R342X immunoblots was a product of the R342X transcript being translated or the SKRTT transcript being translated. We performed an immunoblot experiment with a large gel to increase the separation of WT and R342X cortical sample proteins. We observed a single band in the R342X samples which suggests that only one of the transcripts was being translated (Figure 3-6B). Furthermore, we used a logSize vs distance travelled graph based on the distance travelled by protein bands of known molecular size to extrapolate the size of the shorter truncated PHF6 protein band. Although it seems that the truncated protein size is closer to the size of the predicted R342X protein than the hypothetical SKRTT protein, our molecular weight extrapolation procedure for determining the truncated band size is not very precise. To prove that SKRTT is not produced, the truncated PHF6 protein must be isolated from embryonic R342X brain samples using co-immunoprecipitation. Then the isolated protein can be subjected to mass spectrometry, allowing us to determine the amino acid sequence of the C-terminal end where the SKRTT protein would be different from the R342X protein.

In addition, there might be a possibility that the mutation introduced into the PHF6 gene affects an exon splicing enhancer (ESE) sequence in exon 10 or introduces an exon splicing silencer (ESS) sequence in exon 10 which leads to the exclusion of exon 10. To study the possibility that we have disrupted the recruitment of the spliceosome, future studies will scan the mutated sequence within exon 10 using ESE/ESS prediction software which are able to identify if mutations create or ablate binding sites for splicing factors. Furthermore, the spliceosome

recruitment process would be investigated using RNA-immunoprecipitation, to elucidate how the mutation affects binding to splicing factors. Last, using PCR, the splicing process around exon 10 in human R342X patient cell lines would be examined to determine if the SKRTT transcripts are present in human R342X patients.

#### **4.2 Elucidating the pituitary gland postnatal growth defect in the R342X mice**

The development process of the pituitary gland is controlled by a tightly regulated genetic network. Based on our finding that at E18.5, WT and R342X mice have similar size APs, but by P25, the R342X AP is considerably smaller than the WT AP, we concluded that the R342X mice experience a postnatal growth defect in the anterior pituitary gland. By birth, pituitary gland development is complete, and all the endocrine cell populations are present (Rizzoti 2015). We decided to narrow down a genetic regulatory network involved in the differentiation of progenitor cells in the pituitary into somatotropes (produce GH), lactotropes (produce PRL) and thyrotropes (produce TSH). These cell types were chosen based on our finding that the levels of *Gh* and *Prl* transcripts were lower in the R342X mouse pituitary gland, the percentage of PRL+ cells in the AP were lower in the R342X mice, the levels of T4 were lower in the R342X mouse plasma and the levels of *Ttr* RNA were lower in R342X mouse cerebral cortex. Interestingly, POU class 1 homeobox 1 (PIT1) positive cells represent the progenitors which eventually give rise to thyrotropes, lactotropes and somatotropes (Ward et al. 2006; Zhu et al. 2006). AT Motif-Binding Factor 1 (*Atbf1*) is another gene which maintains the PIT1 lineage and PIT1 expression (Qi et al. 2008; Prince et al. 2011). Furthermore, postnatal and adult pituitary glands contain SRY-Box 2 (SOX2) positive stem cells which can give rise to the PIT1 lineage, contributing to postnatal expansion (Mollard et al. 2012). From the experiments involving qRT-PCR of P21 pituitary glands, we can see that the downregulation of *Gh* RNA and

*Prl* RNA in R342X mice occurs at a similar rate (~4-fold decrease). Cells expressing more than one hormone type is not uncommon, present from the embryonic stages into adulthood (Seuntjens et al. 2002). Somatolactotrophs seem to be the most highly upregulated two-hormone expressing cell type in adulthood, compared to the embryonic and P1 timepoints, suggesting that somatotrophs and lactotrophs are closely regulated during the postnatal expansion phase (Seuntjens et al. 2002). However, we were only able to see a corresponding decrease in the fraction of PRL producing cells in the AP of R342X mice via immunofluorescent staining but there was no significant difference for GH producing cells. Interestingly, neuronal differentiation 4 (*Neurod4*) knockout leads to an appropriate number of GH+ cells in the anterior pituitary gland but the cells are functionally irrelevant as they do not express the growth hormone-releasing hormone (GHRH) receptor (Rizzoti 2015). Therefore, in R342X mice, there might be a lack of functional GH+ cells. Moreover, ELISA of IGF-1 revealed no differences between R342X and WT mice. However, only an n of 3 was used in the experiment and a larger sample size might help reduce the variability between animals and provide a more accurate representation of IGF-1 levels in the plasma of R342X mice. Therefore, it might be interesting to investigate *Pit1*, *Atbf1* and *Sox2* in the pituitary gland, and *Ghrh* in the hypothalamus, via qRT-PCR and immunoblotting during the postnatal expansion phase.

*Tsh* RNA levels in the pituitary gland and the population dynamics of thyrotropes in the AP were unaffected in the R342X mice but T4 values were low in the plasma. This suggests that there might be a thyroid defect in the R342X mice. Moreover, *Ttr*, a gene encoding a transporter for T4, was upregulated in the cerebral cortex perhaps to compensate for the decrease in T4 levels. However, if hypothyroidism was a condition in the mice, we would expect to see an obese phenotype. The decrease in T4 levels was small and there was no change in T3, and therefore the

thyroid defect might not be severe enough to manifest as hypothyroidism. To determine if there is a thyroid defect in the mice, future studies should investigate the thyroid structure in the R342X mice using immunohistochemistry and investigate the functional capability of the thyroid using qRT-PCR, immunofluorescence and immunoblotting for the TSH receptor in the thyroid gland.

The hypothalamus also contributes to the development and function of the pituitary gland. Genes from the hypothalamus are upstream regulators of the genetic network involved in pituitary gland development (Lechan and Toni 2016). The hypothalamus produces GHRH which stimulates somatotropes, thyrotropin-releasing hormone (TRH) which stimulates thyrotropes and dopamine which stimulates lactotropes (Lechan and Toni 2016). Interestingly, the hypothalamus volume is increased in R342X mice compared to WT mice. Perhaps cell types producing the proteins which affect thyrotropes, somatotropes and lactotropes are in a hyperactive state, trying to compensate for the GH, PRL, and TSH defect, resulting in the enlargement of the hypothalamus. This can be investigated by staining the hypothalamus with antibodies against the proteins produced in the hypothalamus which are upstream regulators of *Gh*, *Prl* and *Tsh* in the AP.

#### **4.3 Characterizing the brain development phenotype in the R342X mice**

We performed structural analysis of the R342X brains using immunohistochemistry and MRI in an effort to study brain development. Interestingly, the MRI volumetric analysis yielded significant change in regions involved in anxiety and depression. There was an increase in volume of the amygdala and the periaqueductal grey, and there was a decrease in volume of the striatum and the CA1 pyramidal layer of the hippocampus. Additionally, Voss et al. in 2017 reported postnatal PHF6 expression in the hippocampal formation and adult PHF6 expression in



the dentate gyrus. It has been shown that the amygdala, periaqueductal grey, striatum and the hippocampus are involved in regulating anxiety and depression (Berton et al. 2007; Etkin et al. 2009; Russo and Nestler 2013; Felmingham et al. 2014; Engin et al. 2016; Watson et al. 2016; Liu et al. 2017). It is possible that the loss of inhibition phenotype observed in the R342X mice could involve one or more of these brain regions involved in an anxiety and depression circuitry. RNA-seq analysis of the amygdala, periaqueductal grey, striatum and hippocampus could be performed, followed by qRT-PCR to confirm RNA-seq results, in an effort to determine a regulatory pathway.

The most notable change in brain structure involved the decrease in size of the cerebellum which was evident both from the immunohistochemistry experiments and the volumetric analysis via MRI. Interestingly, Voss et al. in 2007, reported PHF6 expression in the internal granular layer of the cerebellum following birth, and PHF6 expression in the adult cerebellar Purkinje cells of the cerebellum. Moreover, SWI/SNF Related, Matrix Associated, Actin Dependent Regulator Of Chromatin, Subfamily A, Member 5 (*Smarca5*), an ATP-dependent nucleosome-remodeller, was shown to be ~60% downregulated from the microarray analyses of primary rat cortical neurons in which *Phf6* was knocked down (Zhang et al. 2011). *Smarca5* has been shown to be involved in cerebellar development (Saavedra et al. 2014). Additionally, from our RNA-seq analysis, we found *Smarca5* to be ~50% downregulated in cortical samples (Supplementary Table 6-2). Therefore, *Phf6* might control *Smarca5* expression or interact with the SNF2H protein encoded by the gene to mediate cerebellar development. Future studies must first confirm this decrease in *Smarca5* in the cerebellum by qRT-PCR. Next, it will be interesting to establish if PHF6 interacts with SNF2H in the cerebellum by co-immunoprecipitation. Furthermore, it will be interesting to study the cerebellar developmental

process using immunohistochemistry, investigating the cell population distribution in the components of the cerebellum. Although one would expect motor skill dysfunction and learning disabilities from a cerebellar defect, no such phenotype is observed in the R342X mice. However, additional behavioural tests investigating motor defects like staircase or paw reaching tests, which investigates fine motor skills, and the rotarod test which measures motor function in the context of balance could also help elucidate any cerebellar dysfunction. Moreover, the novel object recognition test investigating recognition memory, the Morris water maze test investigating spatial and long-term memory, and the Intellicage used to investigate cognitive ability of mice in a social environment will provide further insight into the cognitive phenotype of the R342X mice.

In the study of the cortical development process, we found a higher percentage of TBR2+EdU+/TBR2+ cells in R342X mice at E13.5 (Figure 3-16H). However, this defect does not appear to have a significant impact on cortical development as the other counts at later timepoints showed no change. This suggests that at E13.5 IPs are in S-phase for a longer time in R342X mice than in WT mice but after E13.5 certain events take place which lead to a normal cortical layer formation. Immunofluorescence studies at E14.5 and further investigation of the cell cycle kinetics could reveal more about the R342X neuronal migration phenotype.

Nonetheless, this was a surprising finding since Zhang et al. in 2013 and Franzoni et al. 2015 have shown that knockdown of *Phf6* results in neuronal migration defects. However, we observe no such phenotype in the R342X mice as the cortex forms normally. Why is this the case? For one, in the studies by Zhang et al. 2013 and Franzoni et al. 2015, *Phf6* was knocked down from E14-E15.5. Meanwhile, the R342X mice essentially have a reduced version of PHF6 from conception. The process of neuronal migration begins at E10, Layer VI formation begins at

E12.5 and is complete by E13.5, and Layer V formation begins at E13.5 and is complete by E14.5 (Rodriguez et al. 2012 and Sakayori et al. 2013). Disrupting a potentially involved gene at a timepoint after the migration process has already begun, might not provide any room for adjustment in the regulation network to rescue cortical development. Interestingly, by RNA-seq, we noticed the differential regulation of 27 protocadherin genes, 25 of which were upregulated and 2 of which were downregulated (Supplementary Table 6-2). Protocadherins have been shown to be important in the process of neuronal migration (Garett et al. 2012; Suo et al. 2012; Fan et al. 2018). Upregulation of these protocadherins might rescue the cortical development defect from the loss of PHF6. To test the role of protocadherins in the R342X mice, one must first confirm the upregulation of the protocadherin RNA-seq targets by qRT-PCR in embryonic cortical samples. Next, knockdown of protocadherin gene clusters would be performed at embryonic timepoints to elucidate whether the overexpression is responsible for the predicted rescue of the cortical development defect in the R342X mice. Last, WT mice would be co-transfected with shRNA against *Phf6* and protocadherin gene cluster overexpression vectors to identify if protocadherins can reverse the cortical development defect from acute *Phf6* knockdown.

#### **4.4 Exploring the PHF6 R342X protein as a functional hypomorphic protein**

We had initially mentioned that the R342X mice might be a functionally limited model. Here I delve into this argument. Unlike *PHF6* cancer mutations that result in complete ablation of the PHF6 protein, male BFLS *PHF6* mutations do not lead to misfolding of the protein or complete ablation of PHF6 expression (Liu et al. 2014). It seems that *PHF6* mutations which involve severe mutations like frameshift mutations, deletions and point mutations in residues involved in maintaining PHF6 structure, severely disrupts PHF6 and is likely to be incompatible

with life in the developing fetus. In 2016, Dickinson et al. conducted a high-throughput analysis of genes in mice involved in viability and development. A *Phf6* knockout mouse line missing exon 2 was generated on the C57BL/6N background. Of 71 pups weaned, ~31% were WT males, 38% were WT females and ~31% were heterozygous females. No hemizygous males were born suggesting that *Phf6* knockout mice are hemizygous lethal. Female BFLS carriers can possess more severe forms of mutations like frameshift mutations and deletions. However, the effect of X-inactivation probably dilutes the overall effect of the severe mutations. Furthermore, in the 2014 study by Liu et al., the authors investigated the dsDNA binding ability of the C-terminal end of the PHF6 protein which included the second ZaP domain, using electrophoretic mobility shift assay (EMSA) and fluorescence polarization anisotropy. It was shown that a PHF6 peptide consisting of amino acids 208-365 had a higher dsDNA binding ability than a PHF6 peptide consisting of amino acids 208-333. Therefore, in the case of the R342X mice, we could assume that the dsDNA binding ability of the protein is less than that of the full-length WT protein, suggesting that PHF6 protein function is not completely lost but is hampered. Another study, using co-immunoprecipitation experiments, was able to show that introducing *PHF6* male BFLS patient mutations into the PHF6 protein inhibited its ability to bind to UBF (Wang et al. 2013). Therefore, in the R342X mouse chromatin landscape, PHF6 is still expressed at low levels, but is able to conduct some of its function albeit at a lower efficiency. The location of the male BFLS *PHF6* mutation might dictate which function(s) of PHF6 are compromised. To test whether the R342X PHF6 protein is a functional hypomorph, mass spectroscopy would be used to compare the binding partners of the WT and mutant protein, and Ch-IP experiments would be necessary to compare the differential binding of the protein to target DNA sequences. In conclusion, the PHF6 R342X protein might exist as a functional hypomorph which leads to the manifestation of

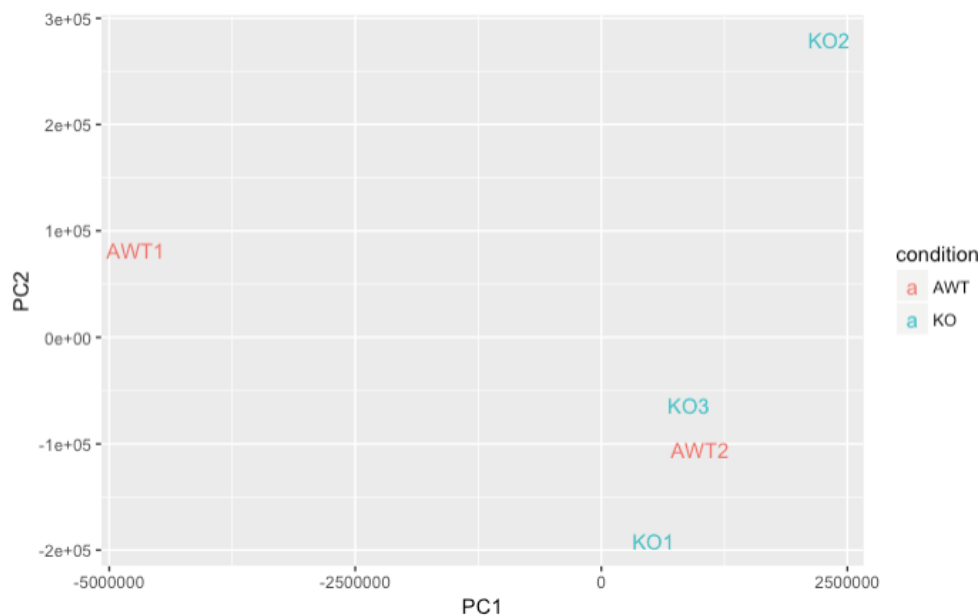
certain features in the R342X mice, primarily the decrease in weight, the postnatal pituitary gland growth defect, the brain development defect as observed from the variation in the regions of the R342X brains, and the loss of inhibitions in behavioral tests.

## 5.0 Collaborations

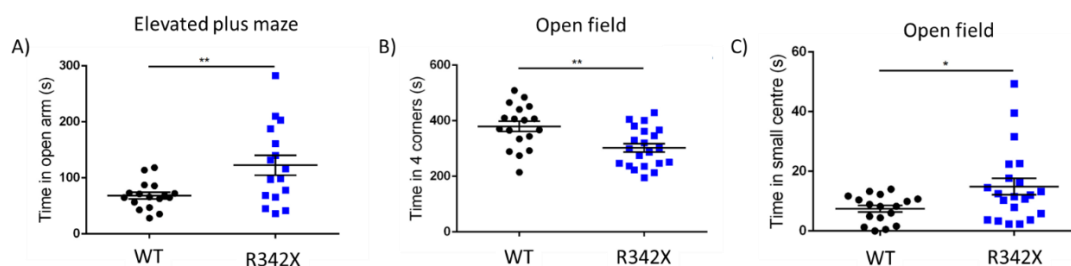
With respects to the project, I would like to acknowledge Shihab Sarwar for generating the R342X mice, Keqin Yan for helping with the immunofluorescence experiments used to study the cortical development process (Figure 3-16, 3-18, 3-19), Dr. Farshad Niri and Laura Goodwin for performing the RNA-seq analysis (Supplementary Figure 6-1; Supplementary Table 6-1, Supplementary Table 6-2), Valerie Cardin for conducting the behavioural tests (Supplementary Figure 6-2, 6-3, 6-4, 6-5), Dr. Gregory Cron for helping with the initial MRI studies, Dr. Jason Lerch and Lily Qiu for the volumetric MRI analysis (Figure 3-12, 3-13), Gerardo Zapata for helping with nissl staining used to study brain structure (Figure 3-11), Eve Technologies (Canada) for performing the ELISA experiments (Figure 3-9) and the uOttawa Histology core for helping with pituitary gland immunofluorescent staining (Figure 3-7).

## 6.0 Appendix

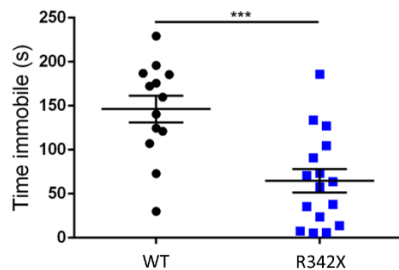
### 6.1 Supplementary Figures



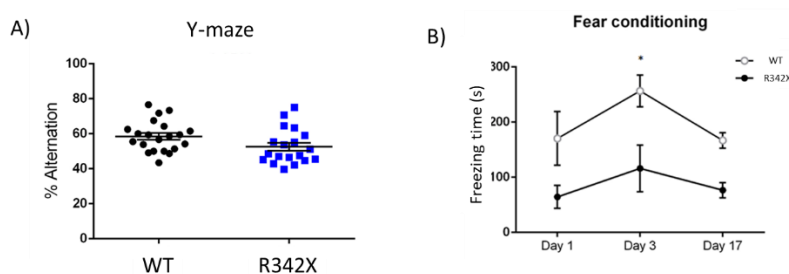
**Supplementary Figure 6-1. PCA plot comparing the variation in the data between samples.** AWT1 and AWT2 are the WT1 and WT2 samples, respectively. KO1, KO2 and KO3 are the R342X1, R342X2 and R342X3 samples, respectively. As evident from the graph, the WT2 sample is clustered with the R342X samples.



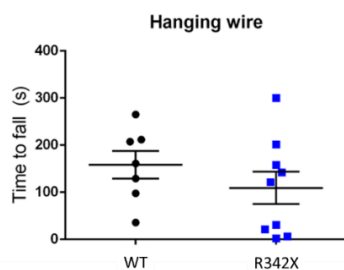
**Supplementary Figure 6-2. Behavioral tests measuring anxiety in the R342X mice.** (A) Elevated plus maze experiment investigating anxiety. The mice were 60 days old. WT n=17, R342X n=16. \* =  $p < 0.05$ , \*\* =  $p < 0.01$ . (B and C) Open field experiment investigating anxiety. The mice were 60 days old. WT n=18, R342X n=21. \* =  $p < 0.05$ , \*\* =  $p < 0.01$ .



**Supplementary Figure 6-3. Behavioural test measuring behavioral despair.** Forced swim test measuring depression. The mice were 60 days old. WT n=13, R342X n=16. \*\*\*=p<0.001



**Supplementary Figure 6-4. Behavioral tests measuring learning and memory.** (A) Y-maze measuring working memory. The mice were 60 days old. WT n=21, R342X n=19. Student's t-test. (B) Fear conditioning measuring memory in response to aversive stimuli. The mice were 60 days old. WT n=6, R342X n=5. \* = p<0.05. Two-way ANOVA.



**Supplementary Figure 6-5. Behavioral test measuring strength.** Hanging wire test measuring strength. The mice were 60 days old. WT n=7, R342X n=9.



**6.2 Supplementary Tables**

Gene ID	Gene name	Base mean	log2fold change	lfcSE	stat	pvalue	padj
ENSMU SG00000 061808	<i>Ttr</i>	25539 .3502 7	4.535269198	0.250600356	18.097 6	3.33E-73	6.71E-69
ENSMU SG00000 078249	<i>Hmgal b</i>	408.0 70181 4	-3.5521866	0.272685769	-13.027	8.63E-39	5.80E-35
ENSMU SG00000 001827	<i>Folr1</i>	308.4 53595 8	2.86342086	0.291932504	9.8085	1.03E-22	5.22E-19
ENSMU SG00000 004655	<i>Aqp1</i>	579.0 19795 7	2.24960492	0.249260915	9.0251	1.80E-19	7.24E-16

**Supplementary Table 6-1. RNA-seq analysis results for genes of interest selected for qRT-PCR.** These genes appeared in the 2 WTs vs 3 R342X samples comparisons performed by Dr. Farshad Niri and Laura Goodwin. An adjusted p-value cutoff of  $q < 0.1$  was used.

Gene ID	Gene name	Base mean	log2fold change	lfcSE	stat	pvalue	padj
ENSMU SG00000 023036	<i>Pcdhgc 4</i>	4205. 05721 2	2.080559552	0.2704086 43	7.6941 31101	1.42E-14	1.79E-11
ENSMU SG00000 103585	<i>Pcdhgb 4</i>	310.8 83523 7	1.982133412	0.3960108 94	5.0052 49714	5.58E-07	0.000105 9
ENSMU SG00000 103793	<i>Pcdhga 6</i>	926.9 77655 5	1.930490538	0.3110862 02	6.2056 4501	5.45E-10	2.68E-07
ENSMU SG00000 104346	<i>Pcdhga 3</i>	1336. 02651 9	1.789780968	0.3319210 28	5.3921 89161	6.96E-08	1.84E-05

ENSMU SG00000 102543	Pcdhgc 5	485.4 76854 9	1.786343334	0.3569611 54	5.0043 07373	5.61E-07	0.000105 9
ENSMU SG00000 103897	Pcdhga 8	758.9 90528 7	1.772957874	0.3112080 03	5.6970 18902	1.22E-08	4.20E-06
ENSMU SG00000 103677	Pcdhga 4	987.5 99474 9	1.770724949	0.3253192 79	5.4430 37231	5.24E-08	1.50E-05
ENSMU SG00000 102918	Pcdhgc 3	4891. 22060 9	1.744672457	0.2617151 74	6.6663 02263	2.62E-11	1.72E-08
ENSMU SG00000 102440	Pcdhga 9	548.7 43791 8	1.728457442	0.3468643 35	4.9830 93577	6.26E-07	0.000115
ENSMU SG00000 103037	Pcdhgb 1	718.0 56810 6	1.727286467	0.3622443 04	4.7682 91589	1.86E-06	0.000246 2
ENSMU SG00000 103749	Pcdhgb 5	334.8 78155	1.66774599	0.3952814 81	4.2191 35144	2.45E-05	0.001482 5
ENSMU SG00000 102428	Pcdhga 12	1510. 70946 2	1.658800962	0.3002072 41	5.5255 1949	3.29E-08	9.92E-06
ENSMU SG00000 103088	Pcdhgb 6	1257. 86453	1.629800737	0.3668390 02	4.4428 22952	8.88E-06	0.000794 6
ENSMU SG00000 103332	Pcdhga 2	1117. 16857 6	1.596177616	0.3292744 28	4.8475 60219	1.25E-06	0.000189 3
ENSMU SG00000 103310	Pcdha1 2	445.7 23263	1.54788443	0.3580690 59	4.3228 65639	1.54E-05	0.001108
ENSMU SG00000 103707	Pcdha6	293.5 78200 3	1.543180514	0.3833064 08	4.0259 71079	5.67E-05	0.002581
ENSMU SG00000 103567	Pcdhga 5	612.9 87585	1.539519725	0.3338438 42	4.6114 96545	4.00E-06	0.000451 7
ENSMU SG00000 102748	Pcdhgb 2	469.2 87758 9	1.463908263	0.3472838 94	4.2153 071	2.49E-05	0.001494 8
ENSMU SG00000 102697	Pcdhac 2	1389. 44222 1	1.459840144	0.2763204 8	5.2831 41306	1.27E-07	3.07E-05

ENSMU SG00000 103144	Pcdhga 1	814.3 98730 4	1.417202442	0.3542489 45	4.0005 83381	6.32E-05	0.002793 4
ENSMU SG00000 102742	Pcdhga 11	1392. 74498 5	1.379671834	0.3581688 77	3.8520 14852	0.000117 15	0.004119 1
ENSMU SG00000 104063	Pcdhgb 7	719.7 92323 9	1.249894242	0.3402629 83	3.6733 18301	0.000239 421	0.006547 5
ENSMU SG00000 051375	Pcdh1	6438. 67794 8	1.239822228	0.2531236 08	4.8980 9006	9.68E-07	0.000156 5
ENSMU SG00000 103472	Pcdhga 7	979.8 41088 7	1.17815554	0.3002442 64	3.9239 90173	8.71E-05	0.003381 5
ENSMU SG00000 104148	Pcdha2	355.2 94155 3	0.951123276	0.3822748 46	2.4880 6137	0.012844 157	0.071759 6
ENSMU SG00000 029108	Pcdh7	3413. 05914 3	-0.624220757	0.2700596 52	- 2.3114 1806	0.020809 774	0.097624 6
ENSMU SG00000 046387	Pcdhb1 7	1021. 75571 3	-0.709998319	0.2932736 36	- 2.4209 4151	0.015480 368	0.080728 7
ENSMU SG00000 031715	Smarca 5	3616. 95592	-0.997777339	0.3224778 92	- 3.0940 9533	0.001974 14	0.023260 8

**Supplementary Table 6-2. RNA-seq analysis results for protocadherins and *Smarca5*.** These genes appeared in the WT 1 vs 3 R342X samples comparison as performed by Dr. Farshad Niri, using an adjusted p-value of <0.1 cut-off.

WT (42)		R342X (20)	
Non-hydrocephalic	Hydrocephalic	Non-hydrocephalic	Hydrocephalic
42 (100%)	0 (0%)	13 (65%)	7 (35%)

**Supplementary Table 6-3. Percentage of hydrocephalic brains at P21 when comparing WT and R342X mice.** Upon brain dissection, brain morphology was examined. Hydrocephalic brains are easily differentiated based on their tendency to deflate upon removal from the skull. These hydrocephalic samples were excluded from the pituitary gland qRT-PCR analysis, ELISA analysis and IHC analysis.

### 6.3 Antibodies and Primers

<b>Antibody</b>	<b>Source</b>	<b>Application</b>
PHF6 (rabbit)	Sigma HPA001023-100UL	W 1:2500 1:20000 Anti-Rabbit  W (Increased R342X protein loading) 1:500 for 1 hour 1:5000 Anti-Rabbit  W (Big gel) 1:750 for 2 days 1:2500 Anti- Rabbit 1hour 30mins  E18.5 Pituitary IF 1:50 1:500 Anti-Rabbit E13.5 Cortex IF 1:150 1:1000 Anti-Rabbit
Vinculin (rabbit)	Abcam ab129002	W 1:2500 1:20000 Anti-Rabbit
GH (rabbit)	Parlow (NIDDK) AFP5672099	IF 1:1000 (Antigen Retrieval) 1:750 Anti-Rabbit
ACTH (guinea pig)	Parlow (NIDDK) AFP- 71111591	IF 1:1000 (Antigen Retrieval) 1:750 Anti-Rabbit
PRL (rabbit)	Parlow (NIDDK) AFP107120402	IF 1:1000 (Antigen Retrieval) 1:750 Anti-Rabbit
TSH (rabbit)	Parlow (NIDDK) AFP- 1274789	IF 1:1000 (Antigen Retrieval) 1:750 Anti-Rabbit
PAX6 (rabbit)	Cedarlane PRB-278P-100	IF 1:400 (Antigen Retrieval) 1:500 Anti-Rabbit
TBR2 (rabbit)	Abcam ab23345	IF 1:300 (Antigen Retrieval) 1:500 Anti-Rabbit
TBR1 (rabbit)	Abcam ab31940	IF 1:100 (Antigen Retrieval) 1:500 Anti-Rabbit
FOXP1 (rabbit)	Abcam ab16645	IF 1:300 (Antigen Retrieval) 1:500 Anti-Rabbit
CUX1 (rabbit)	Santa Cruz sc-13024	IF 1:50 (Antigen Retrieval) 1:500 Anti-Rabbit
CTIP2 (rat)	Abcam ab18465	IF 1:250 (Antigen Retrieval) 1:1000 Anti-Rat

<b>Chemical</b>	<b>Source</b>	<b>Application</b>
Hoechst	Sigma B2261-25MG	IF 1:4000

Primer name	Sequence	Annealing temperature (°C)	Application
Phf6 RNA F Phf6 RNA R	GCAGTGCCGGAGAACCGAC GTGGCAGGTTTTTCACATCAC	55	qRT-PCR qRT-PCR
Phf6 a/b F Phf6 a/b R	ATGAAATGTACACTTTGCAGTCAGCC GACTGCTTCCCAGAAACTGC	55	Sequencing Sequencing
Gh F Gh R	CTTCTCGCTGCTGCTCATC TTGGCGTCAAACCTTGTCATA	55	qRT-PCR qRT-PCR
Gapdh F Gapdh R	CGGCAAATTCAACGGCACAG TCACAAACATGGGGGCATCG	50-60	qRT-PCR qRT-PCR
Actin F Actin R	AGATCAAGATCATTGCTCCTCCTG AGGGTGTAACGCAGCTCAG	50-60	qRT-PCR qRT-PCR
Prl F Prl R	CTCACTACATCCATACCCTG TTGAATACCACCTACTCCA	50	qRT-PCR qRT-PCR
Pomc F Pomc R	AGCAACCCGCCAAGG GCGTCTGGCTCTTCTCGG	60	qRT-PCR qRT-PCR
Fshb F Fshb R	TGCCCGCCACTCAGACTCC GTGGGCGAACGGCAATGT	60	qRT-PCR qRT-PCR
Lhb F Lhb R	TGGCCGCAGAGAATGAGTT CCAGGGAGGCGGACAGA	55	qRT-PCR qRT-PCR
Tshb F Tshb R	GTAGTGGGTGGAGAAGAGT CAGATGGTGGTGTGATG	50	qRT-PCR qRT-PCR
Ttr F Ttr R	CTGCTGTAGACGTGGCTGTAA CTTCCAGTACGATTTGGTGTCC	55	qRT-PCR qRT-PCR
Folr1 F Folr1 R	TGATGTGGATGGCCGAATGTG GTCGTGTAAATTGTCCTCAGGG	55	qRT-PCR qRT-PCR
Aqp1 F Aqp1 R	AGGCTTCAATTACCCACTGGA GTGAGCACCGCTGATGTGA	55	qRT-PCR qRT-PCR
Hmga1b F Hmga1b R	GCCCCACACATAGAGAAGGA TCTCTTCGGAGTTGGCACTT	55	qRT-PCR qRT-PCR
Phf6 R342X F Phf6 R342X R	GTGGCATGGTGTACAAGTGG TTTAGTGTGCACGGTGTTC	Refer to Methods 2.1D	Genotyping Genotyping

## **7.0 References**

Alvarez-Saavedra, M., De Repentigny, Y., Lagali, P. S., Raghu Ram, E. V., Yan, K., Hashem, E., Ivanochko, D., Huh, M. S., Yang, D., Mears, A. J., Todd, M. A., Corcoran, C. P., Bassett, E. A., Tokarew, N. J., Kokavec, J., Majumder, R., Ioshikhes, I., Wallace, V. A., Kothary, R., Meshorer, E., Stopka, T., Skoultchi, A. I., ... Picketts, D. J. (2014). Snf2h-mediated chromatin organization and histone H1 dynamics govern cerebellar morphogenesis and neural maturation. *Nature communications*, 5, 4181. doi:10.1038/ncomms5181

Antony, J. M., Paquin, A., Nutt, S. L., Kaplan, D. R., & Miller, F. D. (2011). Endogenous microglia regulate development of embryonic cortical precursor cells. *Journal of Neuroscience Research*, 89(3), 286–298. <https://doi.org/10.1002/jnr.22533>

Asami, M., Pilz, G. A., Ninkovic, J., Godinho, L., Schroeder, T., Huttner, W. B., & Gotz, M. (2011). The role of Pax6 in regulating the orientation and mode of cell division of progenitors in the mouse cerebral cortex. *Development*, 138(23), 5067–5078. <https://doi.org/10.1242/dev.074591>

Badenhorst, P., Voas, M., Rebay, I., & Wu, C. (2002). Biological functions of the ISWI chromatin remodeling complex NURF. *Genes & Development*, 16(24), 3186–3198. <http://doi.org/10.1101/gad.1032202>

Bao, Y., Liu, Z., Zhang, J., Wu, J., & Shi, Y. (2015). <sup>1</sup>H, <sup>13</sup>C and <sup>15</sup>N resonance assignments and secondary structure of the human PHF6-ePHD1 domain. *Biomolecular NMR Assignments*, 10(1), 1–4. <https://doi.org/10.1007/s12104-015-9627-x>

Basta, J., & Rauchman, M. (2015). The Nucleosome Remodeling and Deacetylase (NuRD) Complex in Development and Disease. *Translational Research: The Journal of Laboratory and Clinical Medicine*, 165(1), 36–47. <http://doi.org/10.1016/j.trsl.2014.05.003>

Berton, O., Covington, H. E., III, Ebner, K., Tsankova, N. M., Carle, T. L., Ulery, P., ... Nestler, E. J. (2007). Induction of  $\Delta$ FosB in the Periaqueductal Gray by Stress Promotes Active Coping Responses. *Neuron*, 55(2), 289–300. <https://doi.org/10.1016/j.neuron.2007.06.033>

Birrell, G., Lampe, A., Richmond, S., Bruce, S. N., Gecz, J., Lower, K., ... Checham, T. D. (2003). Borjeson-Forssman-Lehmann Syndrome and Multiple Pituitary Hormone Deficiency. *Journal of Pediatric Endocrinology and Metabolism*, 16(9). <https://doi.org/10.1515/jpem.2003.16.9.1295>

Börjeson, M., Forssman, H., & Lehmann, O. (1962). An X-linked, Recessively Inherited Syndrome Characterized by Grave Mental Deficiency, Epilepsy, and Endocrine Disorder. *Acta Medica Scandinavica*, 171, 13–21.

- Bowman, G. D., & Poirier, M. G. (2015). Post-Translational Modifications of Histones That Influence Nucleosome Dynamics. *Chemical Reviews*, 115(6), 2274–2295. <http://doi.org/10.1021/cr500350x>
- Bronfman, Z. Z., Ginsburg, S., & Jablonka, E. (2014). Shaping the learning curve: epigenetic dynamics in neural plasticity. *Frontiers in Integrative Neuroscience*, 8. <https://doi.org/10.3389/fnint.2014.00055>
- Brun, A., Borjeson, M., Forssman, H. (1974). An inherited syndrome with mental deficiency and endocrine disorder. A patho-anatomical study. *Journal of Intellectual Disability Research*, 18(4), 317–325. <https://doi.org/10.1111/j.1365-2788.1974.tb01243.x>
- Bultje, R. S., Castaneda-Castellanos, D. R., Jan, L. Y., Jan, Y.-N., Kriegstein, A. R., & Shi, S.-H. (2009). Mammalian Par3 regulates progenitor cell asymmetric division via Notch signaling in the developing neocortex. *Neuron*, 63(2), 189–202. <http://doi.org/10.1016/j.neuron.2009.07.004>
- Burgold, T., Spreafico, F., De Santa, F., Totaro, M. G., Prosperini, E., Natoli, G., & Testa, G. (2008). The Histone H3 Lysine 27-Specific Demethylase Jmjd3 Is Required for Neural Commitment. *PLoS ONE*, 3(8), e3034. <http://doi.org/10.1371/journal.pone.0003034>
- Campos, E. I., & Reinberg, D. (2009). Histones: Annotating Chromatin. *Annual Review of Genetics*, 43(1), 559–599. <https://doi.org/10.1146/annurev.genet.032608.103928>
- Capili, A. D., Schultz, D. C., Rauscher, F. J., & Borden, K. L. B. (2001). Solution structure of the PHD domain from the KAP-1 corepressor: structural determinants for PHD, RING and LIM zinc-binding domains. *The EMBO Journal*, 20(1-2), 165–177. <http://doi.org/10.1093/emboj/20.1.165>
- Carter, M. T., Picketts, D. J., Hunter, A. G., & Graham, G. E. (2009). Further clinical delineation of the Börjeson-Forssman-Lehmann syndrome in patients with PHF6 mutations. *American Journal of Medical Genetics Part A*, 149A(2), 246–250. <https://doi.org/10.1002/ajmg.a.32624>
- Chao, M. M., Todd, M. A., Kontny, U., Neas, K., Sullivan, M. J., Hunter, A. G., ... Kratz, C. P. (2010). T-cell Acute Lymphoblastic Leukemia in Association with Börjeson-Forssman-Lehmann Syndrome Due to a Mutation in PHF6. *Pediatric Blood & Cancer*, 55(4), 722–724. <http://doi.org/10.1002/pbc.22574>
- Crawford, J., Lower, K. M., Hennekam, R. C. M., Van Esch, H., Mégarbané, A., Lynch, S. A., ... Gécz, J. (2006). Mutation screening in Börjeson-Forssman-Lehmann syndrome: identification of a novel de novo PHF6 mutation in a female patient. *Journal of Medical Genetics*, 43(3), 238–243. <http://doi.org.proxy.bib.uottawa.ca/10.1136/jmg.2005.033084>
- Cunningham, C. L., Martínez-Cerdeño, V., & Noctor, S. C. (2013). Microglia regulate the number of neural precursor cells in the developing cerebral cortex. *The Journal of Neuroscience* :

The Official Journal of the Society for Neuroscience, 33(10), 4216–4233.  
<http://doi.org/10.1523/JNEUROSCI.3441-12.2013>

Darnell, D., & Gilbert, S. F. (2016). Neuroembryology. Wiley Interdisciplinary Reviews: Developmental Biology, 6(1), e215. <https://doi.org/10.1002/wdev.215>

de Rooij, J. D. E., van den Heuvel-Eibrink, M. M., van de Rijdt, N. K. A. M., Verboon, L. J., de Haas, V., Trka, J., ... Zwaan, C. M. (2015). PHF6 mutations in paediatric acute myeloid leukaemia. British Journal of Haematology, 175(5), 967–971. <https://doi.org/10.1111/bjh.13891>

Dickinson, M. E., Flenniken, A. M., Ji, X., Teboul, L., Wong, M. D., ... Murray, S. A. (2016). High-throughput discovery of novel developmental phenotypes. Nature, 537(7621), 508–514. <https://doi.org/10.1038/nature19356>

Dobyns, W. B., Reiner, O., Carrozzo, R., Ledbetter, D. H. (1993). Lissencephaly. A human brain malformation associated with deletion of the LIS1 gene located at chromosome 17p13. JAMA, 270(23), 2838-2842.

Dong, Z., Yang, N., Yeo, S.-Y., Chitnis, A., & Guo, S. (2012). Intra-lineage Directional Notch Signaling Regulates Self-renewal and Differentiation of Asymmetrically Dividing Radial Glia. Neuron, 74(1), 65–78. <http://doi.org/10.1016/j.neuron.2012.01.031>

Engin, E., Smith, K. S., Gao, Y., Nagy, D., Foster, R. A., Tsvetkov, E., Keist, R., Crestani, F., Fritschy, J. M., Bolshakov, V. Y., Hajos, M., Heldt, S. A., ... Rudolph, U. (2016). Modulation of anxiety and fear via distinct intrahippocampal circuits. eLife, 5, e14120. doi:10.7554/eLife.14120

Eshraghi, M., McFall, E., Gibeault, S., & Kothary, R. (2016). Effect of genetic background on the phenotype of the Smn2B<sup>-</sup> mouse model of spinal muscular atrophy. Human Molecular Genetics, ddw278. <https://doi.org/10.1093/hmg/ddw278>

Etkin, A., Prater, K. E., Schatzberg, A. F., Menon, V., & Greicius, M. D. (2009). Disrupted Amygdalar Subregion Functional Connectivity and Evidence of a Compensatory Network in Generalized Anxiety Disorder. Archives of General Psychiatry, 66(12), 1361. <https://doi.org/10.1001/archgenpsychiatry.2009.104>

Fan, L., Lu, Y., Shen, X., Shao, H., Suo, L., & Wu, Q. (2018). Alpha protocadherins and Pyk2 kinase regulate cortical neuron migration and cytoskeletal dynamics via Rac1 GTPase and WAVE complex in mice. eLife, 7, e35242. doi:10.7554/eLife.35242

Franzoni, E., Booker, S. A., Parthasarathy, S., Rehfeld, F., Grosser, S., Srivatsa, S., ... Wulczyn, F. G. (2015). miR-128 regulates neuronal migration, outgrowth and intrinsic excitability via the intellectual disability gene Phf6. eLife, 4. <https://doi.org/10.7554/elife.04263>



Fagiolini, M., Jensen, C. L., & Champagne, F. A. (2009). Epigenetic Influences on Brain Development and Plasticity. *Current Opinion in Neurobiology*, 19(2), 207–212.

<http://doi.org/10.1016/j.conb.2009.05.009>

Felmingham, K. L., Falconer, E. M., Williams, L., Kemp, A. H., Allen, A., Peduto, A., & Bryant, R. A. (2014). Reduced amygdala and ventral striatal activity to happy faces in PTSD is associated with emotional numbing. *PloS one*, 9(9), e103653. doi:10.1371/journal.pone.0103653

Feng, J., Zhou, Y., Campbell, S. L., Le, T., Li, E., Sweatt, J. D., ... Fan, G. (2010). Dnmt1 and Dnmt3a maintain DNA methylation and regulate synaptic function in adult forebrain neurons. *Nature Neuroscience*, 13(4), 423–430. <https://doi.org/10.1038/nn.2514>

Fischer, A., Sananbenesi, F., Wang, X., Dobbin, M., & Tsai, L.-H. (2007). Recovery of learning and memory is associated with chromatin remodelling. *Nature*, 447(7141), 178–182.

<https://doi.org/10.1038/nature05772>

Franzoni, E., Booker, S. A., Parthasarathy, S., Rehfeld, F., Grosser, S., Srivatsa, S., ... Wulczyn, F. G. (2015). miR-128 regulates neuronal migration, outgrowth and intrinsic excitability via the intellectual disability gene Phf6. *eLife*, 4. <https://doi.org/10.7554/elife.04263>

Garrett, A. M., Schreiner, D., Lobas, M. A., & Weiner, J. A. (2012).  $\gamma$ -protocadherins control cortical dendrite arborization by regulating the activity of a FAK/PKC/MARCKS signaling pathway. *Neuron*, 74(2), 269-76.

Gécz, J., Turner, G., Nelson, J., & Partington, M. (2006). The Börjeson–Forssman–Lehman syndrome (BFLS, MIM #301900). *European Journal of Human Genetics*, 14(12), 1233–1237. <https://doi.org/10.1038/sj.ejhg.5201639>

Gedeon, A. K., Kozman, H. M., Robinson, H., Pilia, G., Schlessinger, D., Turner, G., & Mulley, J. C. (1996). Refinement of the background genetic map of Xq26-q27 and gene localisation for Börjeson-Forssman-Lehmann syndrome. *American Journal of Medical Genetics*, 64(1), 63–68. [https://doi.org/10.1002/\(sici\)1096-8628\(19960712\)64:1<63::aid-ajmg9>3.0.co;2-s](https://doi.org/10.1002/(sici)1096-8628(19960712)64:1<63::aid-ajmg9>3.0.co;2-s)

Gibbons, R. J., Bachoo, S., Picketts, D. J., Aftimos, S., Asenbauer, B., Bergoffen, J., ... Higgs, D. R. (1997). Mutations in transcriptional regulator ATRX establish the functional significance of a PHD-like domain. *Nature Genetics*, 17(2), 146–148. <https://doi.org/10.1038/ng1097-146>

Goodfellow, S. J., & Zomerdijk, J. C. B. M. (2012). Basic Mechanisms in RNA Polymerase I Transcription of the Ribosomal RNA Genes. *Sub-Cellular Biochemistry*, 61, 10.1007/978-94-007-4525-4\_10. [http://doi.org/10.1007/978-94-007-4525-4\\_10](http://doi.org/10.1007/978-94-007-4525-4_10)

Greer, E. L., & Shi, Y. (2012). Histone methylation: a dynamic mark in health, disease and

inheritance. *Nature Reviews. Genetics*, 13(5), 343–357. <http://doi.org/10.1038/nrg3173>

Gupta, A., Tsai, L.-H., & Wynshaw-Boris, A. (2002). Life is a journey: a genetic look at neocortical development. *Nature Reviews Genetics*, 3(5), 342–355. <https://doi.org/10.1038/nrg799>

Hajjari, M., Salavaty, A., Crea, F., & Kee Shin, Y. (2015). The potential role of PHF6 as an oncogene: a genotranscriptomic/proteomic meta-analysis. *Tumor Biology*, 37(4), 5317–5325. <https://doi.org/10.1007/s13277-015-4250-0>

Hargreaves, D. C., & Crabtree, G. R. (2011). ATP-dependent chromatin remodeling: genetics, genomics and mechanisms. *Cell Research*, 21(3), 396–420. <http://doi.org/10.1038/cr.2011.32>

Hevner, R. F., & Haydar, T. F. (2011). The (Not Necessarily) Convolved Role of Basal Radial Glia in Cortical Neurogenesis. *Cerebral Cortex*, 22(2), 465–468. <https://doi.org/10.1093/cercor/bhr336>

Hu, G., & Wade, P. A. (2012). NuRD and Pluripotency: A Complex Balancing Act. *Cell Stem Cell*, 10(5), 497–503. <http://doi.org/10.1016/j.stem.2012.04.011>

Hu, N., Strobl-Mazzulla, P. H., & Bronner, M. E. (2014). Epigenetic regulation in neural crest development. *Developmental Biology*, 396(2), 159–168. <https://doi.org/10.1016/j.ydbio.2014.09.034>

Huh, M. S., Todd, M. A. M., & Picketts, D. J. (2009). SCO-ping Out the Mechanisms Underlying the Etiology of Hydrocephalus. *Physiology*, 24(2), 117–126. <https://doi.org/10.1152/physiol.00039.2008>

Hyun, K., Jeon, J., Park, K., & Kim, J. (2017). Writing, erasing and reading histone lysine methylations. *Experimental & Molecular Medicine*, 49(4), e324. <http://doi.org/10.1038/emm.2017.11>

Itoh, Y., Moriyama, Y., Hasegawa, T., Endo, T. A., Toyoda, T., & Gotoh, Y. (2013). Scratch regulates neuronal migration onset via an epithelial-mesenchymal transition-like mechanism. *Nature Neuroscience*, 16(4), 416–425. <https://doi.org/10.1038/nn.3336>

Jahani-Asl, A., Cheng, C., Zhang, C., & Bonni, A. (2016). Pathogenesis of Börjeson-Forssman-Lehmann Syndrome: Insights from PHF6 Function. *Neurobiology of Disease*, 96, 227–235. <http://doi.org/10.1016/j.nbd.2016.09.011>

Jobe, E. M., Gao, Y., Eisinger, B. E., Mladucky, J. K., Giuliani, C. C., Kelnhofer, L. E., & Zhao, X. (2016). Methyl-CpG-Binding Protein MBD1 Regulates Neuronal Lineage Commitment through Maintaining Adult Neural Stem Cell Identity. *The Journal of Neuroscience*, 37(3), 523–

536. <https://doi.org/10.1523/jneurosci.1075-16.2016>

Juliandi, B., Abematsu, M., & Nakashima, K. (2010). Chromatin remodeling in neural stem cell differentiation. *Current Opinion in Neurobiology*, 20(4), 408–415. <https://doi.org/10.1016/j.conb.2010.04.001>

Kartal, M. G., & Algin, O. (2014). Evaluation of hydrocephalus and other cerebrospinal fluid disorders with MRI: An update. *Insights into Imaging*, 5(4), 531–541. <https://doi.org/10.1007/s13244-014-0333-5>

Kasper, B. S., Dörfler, A., Di Donato, N., Kasper, E. M., Wiczorek, D., Hoyer, J., & Zweier, C. (2017). Central nervous system anomalies in two females with Borjeson-Forssman-Lehmann syndrome. *Epilepsy & Behavior*, 69, 104–109. <https://doi.org/10.1016/j.yebeh.2017.01.022>

Katsura, Y. (2002). Redefinition of lymphoid progenitors. *Nature Reviews Immunology*, 2(2), 127–132. <https://doi.org/10.1038/nri721>

Katz, G., & Lazcano-Ponce, E. (2008). Intellectual disability: definition, etiological factors, classification, diagnosis, treatment and prognosis. *Salud Pública de México*, 50. <https://doi.org/10.1590/s0036-36342008000800005>

Kawaguchi, D., Furutachi, S., Kawai, H., Hozumi, K., & Gotoh, Y. (2013). Dll1 maintains quiescence of adult neural stem cells and segregates asymmetrically during mitosis. *Nature Communications*, 4, 1880–. <http://doi.org/10.1038/ncomms2895>

Kleefstra, T., Schenck, A., Kramer, J. M., & van Bokhoven, H. (2014). The genetics of cognitive epigenetics. *Neuropharmacology*, 80, 83–94. <https://doi.org/10.1016/j.neuropharm.2013.12.025>

Klose, R. J., & Bird, A. P. (2006). Genomic DNA methylation: the mark and its mediators. *Trends in Biochemical Sciences*, 31(2), 89–97. <https://doi.org/10.1016/j.tibs.2005.12.008>

Knock, E., Pereira, J., Lombard, P. D., Dimond, A., Leaford, D., Livesey, F. J., & Hendrich, B. (2015). The methyl binding domain 3/nucleosome remodeling and deacetylase complex regulates neural cell fate determination and terminal differentiation in the cerebral cortex. *Neural Development*, 10(1). <https://doi.org/10.1186/s13064-015-0040-z>

Kochinke, K., Zweier, C., Nijhof, B., Fenckova, M., Cizek, P., Honti, F., ... Schenck, A. (2016). Systematic Phenomics Analysis Deconvolutes Genes Mutated in Intellectual Disability into Biologically Coherent Modules. *American Journal of Human Genetics*, 98(1), 149–164. <http://doi.org/10.1016/j.ajhg.2015.11.024>

Kriaucionis, S., & Bird, A. (2003). DNA methylation and Rett syndrome. *Human Molecular Genetics*, 12(suppl 2), R221–R227. <https://doi.org/10.1093/hmg/ddg286>

- Krogan, N. J., Dover, J., Wood, A., Schneider, J., Heidt, J., Boateng, M. A., ... Shilatifard, A. (2003). The Paf1 Complex Is Required for Histone H3 Methylation by COMPASS and Dot1p: Linking Transcriptional Elongation to Histone Methylation. *Molecular Cell*, 11(3), 721–729. [https://doi.org/10.1016/s1097-2765\(03\)00091-1](https://doi.org/10.1016/s1097-2765(03)00091-1)
- Kusek, G., Campbell, M., Doyle, F., Tenenbaum, S. A., Kiebler, M., & Temple, S. (2012). Asymmetric Segregation of the Double-Stranded RNA Binding Protein Stauf2 during Mammalian Neural Stem Cell Divisions Promotes Lineage Progression. *Cell Stem Cell*, 11(4), 505–516. <http://doi.org/10.1016/j.stem.2012.06.006>
- Lai, A. Y., & Wade, P. A. (2011). NuRD: A multi-faceted chromatin remodeling complex in regulating cancer biology. *Nature Reviews. Cancer*, 11(8), 588–596. <http://doi.org.proxy.bib.uottawa.ca/10.1038/nrc3091>
- Lechan, R. M, Toni R. (2016). Functional Anatomy of the Hypothalamus and Pituitary. In: De Groot LJ, Chrousos G, Dungan K, et al., editors. *Endotext* [Internet]. South Dartmouth (MA): MDText.com, Inc.; 2000-. Available from: <https://www.ncbi.nlm.nih.gov/books/NBK279126/>
- Lee, S., Lee, B., Lee, J. W., & Lee, S.-K. (2009). Retinoid signaling and Neurogenin2 function are coupled for the specification of spinal motor neurons through a chromatin modifier CBP. *Neuron*, 62(5), 641–654. <http://doi.org/10.1016/j.neuron.2009.04.025>
- Li, X., Yao, H., Chen, Z., Wang, Q., Zhao, Y., & Chen, S. (2012). Somatic mutations of PHF6 in patients with chronic myeloid leukemia in blast crisis. *Leukemia & Lymphoma*, 54(3), 671–672. <https://doi.org/10.3109/10428194.2012.725203>
- Liu, W., Ge, T., Leng, Y., Pan, Z., Fan, J., Yang, W., & Cui, R. (2017). The Role of Neural Plasticity in Depression: From Hippocampus to Prefrontal Cortex. *Neural plasticity*, 2017, 6871089.
- Liu, Z., Li, F., Ruan, K., Zhang, J., Mei, Y., Wu, J., & Shi, Y. (2014). Structural and Functional Insights into the Human Börjeson-Forssman-Lehmann Syndrome-associated Protein PHF6. *Journal of Biological Chemistry*, 289(14), 10069–10083. <https://doi.org/10.1074/jbc.m113.535351>
- Liu, Z., Li, F., Zhang, B., Li, S., Wu, J., & Shi, Y. (2015). Structural Basis of Plant Homeodomain Finger 6 (PHF6) Recognition by the Retinoblastoma Binding Protein 4 (RBBP4) Component of the Nucleosome Remodeling and Deacetylase (NuRD) Complex. *Journal of Biological Chemistry*, 290(10), 6630–6638. <https://doi.org/10.1074/jbc.m114.610196>
- Lower, K. M., Turner, G., Kerr, B. A., Mathews, K. D., Shaw, M. A., Gedeon, Á. K., ... Géczy, J. (2002). Mutations in PHF6 are associated with Börjeson–Forssman–Lehmann syndrome. *Nature*

Genetics, 32(4), 661–665. <https://doi.org/10.1038/ng1040>

Lower, K. M., Solders, G., Bondeson, M.-L., Nelson, J., Brun, A., Crawford, J., ... Gécz, J. (2004). 1024C>T (R342X) is a recurrent PHF6 mutation also found in the original Börjeson–Forssman–Lehmann syndrome family. *European Journal of Human Genetics*, 12(10), 787–789. <https://doi.org/10.1038/sj.ejhg.5201228>

Lupo, G., Harris, W. A., & Lewis, K. E. (2006). Mechanisms of ventral patterning in the vertebrate nervous system. *Nature Reviews Neuroscience*, 7(2), 103–114. <https://doi.org/10.1038/nrn1843>

Luger, K., Mäder, A. W., Richmond, R. K., Sargent, D. F., & Richmond, T. J. (1997). Crystal structure of the nucleosome core particle at 2.8 Å resolution. *Nature*, 389(6648), 251–260. <https://doi.org/10.1038/38444>

Mangelsdorf, M., Chevrier, E., Mustonen, A., & Picketts, D. J. (2009). Börjeson-Forssman-Lehmann Syndrome Due to a Novel Plant Homeodomain Zinc Finger Mutation in the PHF6 Gene. *Journal of Child Neurology*, 24(5), 610–614. <https://doi.org/10.1177/0883073808327830>

Maulik, P. K., Mascarenhas, M. N., Mathers, C. D., Dua, T., & Saxena, S. (2011). Prevalence of intellectual disability: A meta-analysis of population-based studies. *Research in Developmental Disabilities*, 32(2), 419–436. <https://doi.org/10.1016/j.ridd.2010.12.018>

Mollard, P., Hodson, D. J., Lafont, C., Rizzoti, K., & Drouin, J. (2012). A tridimensional view of pituitary development and function. *Trends in Endocrinology & Metabolism*, 23(6), 261–269. <https://doi.org/10.1016/j.tem.2012.02.004>

Molyneaux, B. J., Arlotta, P., Menezes, J. R. L., & Macklis, J. D. (2007). Neuronal subtype specification in the cerebral cortex. *Nature Reviews Neuroscience*, 8(6), 427–437. <https://doi.org/10.1038/nrn2151>

Murao, N., Noguchi, H., & Nakashima, K. (2016). Epigenetic regulation of neural stem cell property from embryo to adult. *Neuroepigenetics*, 5, 1–10. <https://doi.org/10.1016/j.nepig.2016.01.001>

Muzio, L., & Mallamaci, A. (2005). Foxg1 Confines Cajal-Retzius Neuronogenesis and Hippocampal Morphogenesis to the Dorsomedial Pallium. *Journal of Neuroscience*, 25(17), 4435–4441. <https://doi.org/10.1523/jneurosci.4804-04.2005>

Niederberger, E., Resch, E., Parnham, M. J., & Geisslinger, G. (2017). Drugging the pain epigenome. *Nature Reviews Neurology*, 13(7), 434–447. <https://doi.org/10.1038/nrneurol.2017.68>

- Nitarska, J., Smith, J. G., Sherlock, W. T., Hillege, M. M. G., Nott, A., Barshop, W. D., ... Riccio, A. (2016). A Functional Switch of NuRD Chromatin Remodeling Complex Subunits Regulates Mouse Cortical Development. *Cell Reports*, 17(6), 1683–1698. <http://doi.org/10.1016/j.celrep.2016.10.022>
- Okano, M., Bell, D. W., Haber, D. A., & Li, E. (1999). DNA Methyltransferases Dnmt3a and Dnmt3b Are Essential for De Novo Methylation and Mammalian Development. *Cell*, 99(3), 247–257. [https://doi.org/10.1016/s0092-8674\(00\)81656-6](https://doi.org/10.1016/s0092-8674(00)81656-6)
- Ooi, S. K. T., O'Donnell, A. H., & Bestor, T. H. (2009). Mammalian cytosine methylation at a glance. *Journal of Cell Science*, 122(16), 2787–2791. <http://doi.org/10.1242/jcs.015123>
- Oshio, K., Binder, D. ., Yang, B., Schecter, S., Verkman, A. ., & Manley, G. . (2004). Expression of aquaporin water channels in mouse spinal cord. *Neuroscience*, 127(3), 685–693. <https://doi.org/10.1016/j.neuroscience.2004.03.016>
- Paridaen, J. T. M. L., Wilsch-Bräuninger, M., & Huttner, W. B. (2013). Asymmetric Inheritance of Centrosome-Associated Primary Cilium Membrane Directs Ciliogenesis after Cell Division. *Cell*, 155(2), 333–344. <https://doi.org/10.1016/j.cell.2013.08.060>
- Paridaen, J. T., & Huttner, W. B. (2014). Neurogenesis during development of the vertebrate central nervous system. *EMBO Reports*, 15(4), 351–364. <http://doi.org/10.1002/embr.201438447>
- Peirs, S., Van der Meulen, J., Van de Walle, I., Taghon, T., Speleman, F., Poppe, B., & Van Vlierberghe, P. (2014). Epigenetics in T-cell acute lymphoblastic leukemia. *Immunological Reviews*, 263(1), 50–67. <https://doi.org/10.1111/imr.12237>
- Piton, A., Redin, C., & Mandel, J.-L. (2013). XLID-Causing Mutations and Associated Genes Challenged in Light of Data From Large-Scale Human Exome Sequencing. *American Journal of Human Genetics*, 93(2), 368–383. <http://doi.org/10.1016/j.ajhg.2013.06.013>
- Prince, K. L., Walvoord, E. C., & Rhodes, S. J. (2011). The role of homeodomain transcription factors in heritable pituitary disease. *Nature Reviews Endocrinology*, 7(12), 727–737. <https://doi.org/10.1038/nrendo.2011.119>
- Qi, Y., Ranish, J. A., Zhu, X., Kronen, A., Zhang, J., Aebersold, R., Rose, D. W., Rosenfeld, M. G., ... Carrière, C. (2008). Atbfl is required for the Pit1 gene early activation. *Proceedings of the National Academy of Sciences of the United States of America*, 105(7), 2481–6.
- Radtke, F., MacDonald, H. R., & Tacchini-Cottier, F. (2013). Regulation of innate and adaptive immunity by Notch. *Nature Reviews Immunology*, 13(6), 427–437. <https://doi.org/10.1038/nri3445>

- Ramírez, J., & Hagman, J. (2009). The Mi-2/NuRD complex: A critical epigenetic regulator of hematopoietic development, differentiation and cancer. *Epigenetics*, 4(8), 532–536. <https://doi.org/10.4161/epi.4.8.10108>
- Rasmussen, K. D., & Helin, K. (2016). Role of TET enzymes in DNA methylation, development, and cancer. *Genes & Development*, 30(7), 733–750. <http://doi.org/10.1101/gad.276568.115>
- Rizzoti, K. (2015). Genetic regulation of murine pituitary development. *Journal of Molecular Endocrinology*, 54(2), R55–R73. <http://doi.org/10.1530/JME-14-0237>
- Rodriguez, M., Choi, J., Park, S., & Sockanathan, S. (2012). Gde2 regulates cortical neuronal identity by controlling the timing of cortical progenitor differentiation. *Development*, 139(20), 3870–3879. <https://doi.org/10.1242/dev.081083>
- Rouso, D. L., Pearson, C. A., Gaber, Z. B., Miquelajauregui, A., Li, S., Portera-Cailliau, C., ... Novitsch, B. G. (2012). Foxp-Mediated Suppression of N-Cadherin Regulates Neuroepithelial Character and Progenitor Maintenance in the CNS. *Neuron*, 74(2), 314–330. <http://doi.org/10.1016/j.neuron.2012.02.024>
- Rowitch, D. H. (2004). Glial specification in the vertebrate neural tube. *Nature Reviews Neuroscience*, 5(5), 409–419. <https://doi.org/10.1038/nrn1389>
- Rowitch, D. H., & Kriegstein, A. R. (2010). Developmental genetics of vertebrate glial–cell specification. *Nature*, 468(7321), 214–222. <https://doi.org/10.1038/nature09611>
- Russo, S. J., & Nestler, E. J. (2013). The brain reward circuitry in mood disorders. *Nature reviews. Neuroscience*, 14(9), 609–25.
- Sakayori, N., Kimura, R., & Osumi, N. (2013). Impact of Lipid Nutrition on Neural Stem/Progenitor Cells. *Stem Cells International*, 2013, 1–12. <https://doi.org/10.1155/2013/973508>
- Sanchez, R., & Zhou, M.-M. (2011). The PHD Finger: A Versatile Epigenome Reader. *Trends in Biochemical Sciences*, 36(7), 364–372. <http://doi.org/10.1016/j.tibs.2011.03.005>
- Schindler, U., Beckmann, H., & Cashmore, A. (1993). HAT3.1, a novel Arabidopsis homeodomain protein containing a conserved cysteine-rich region. *The Plant Journal*, 4(1), 137–150. doi: 10.1046/j.1365-313x.1993.04010137.x
- Schwamborn, J. C., Berezikov, E., & Knoblich, J. A. (2009). The TRIM-NHL Protein TRIM32 Activates MicroRNAs and Prevents Self-Renewal in Mouse Neural Progenitors. *Cell*, 136(5), 913–925. <http://doi.org/10.1016/j.cell.2008.12.024>

- Seuntjens, E., Hauspie, A., Vankelecom, H., & Denef, C. (2002). Ontogeny of Plurihormonal Cells in the Anterior Pituitary of the Mouse, as Studied by Means of Hormone mRNA Detection in Single Cells. *Journal of Neuroendocrinology*, 14(8), 611–619. <https://doi.org/10.1046/j.1365-2826.2002.00808.x>
- Shahbazian, M. D., & Grunstein, M. (2007). Functions of Site-Specific Histone Acetylation and Deacetylation. *Annual Review of Biochemistry*, 76(1), 75–100. <https://doi.org/10.1146/annurev.biochem.76.052705.162114>
- Shen, S., Li, J., & Casaccia-Bonnel, P. (2005). Histone modifications affect timing of oligodendrocyte progenitor differentiation in the developing rat brain. *The Journal of Cell Biology*, 169(4), 577–589. <https://doi.org/10.1083/jcb.200412101>
- Shi, X., Hong, T., Walter, K. L., Ewalt, M., Michishita, E., Hung, T., ... Gozani, O. (2006). ING2 PHD domain links histone H3 lysine 4 methylation to active gene repression. *Nature*, 442(7098), 96–99. <http://doi.org/10.1038/nature04835>
- Smrt, R. D., Eaves-Egenes, J., Barkho, B. Z., Santistevan, N. J., Zhao, C., Aimone, J. B., ... Zhao, X. (2007). Mecp2 deficiency leads to delayed maturation and altered gene expression in hippocampal neurons. *Neurobiology of Disease*, 27(1), 77–89. <http://doi.org/10.1016/j.nbd.2007.04.005>
- Smrt, R. D., & Zhao, X. (2010). Epigenetic regulation of Neuronal dendrite and dendritic spine development. *Frontiers in Biology*, 5(4), 304–323. <http://doi.org/10.1007/s11515-010-0650-0>
- Sokpor, G., Xie, Y., Rosenbusch, J., & Tuoc, T. (2017). Chromatin Remodeling BAF (SWI/SNF) Complexes in Neural Development and Disorders. *Frontiers in Molecular Neuroscience*, 10. <https://doi.org/10.3389/fnmol.2017.00243>
- Speake, T., Freeman, L. J., & Brown, P. D. (2003). Expression of aquaporin 1 and aquaporin 4 water channels in rat choroid plexus. *Biochimica et Biophysica Acta (BBA) - Biomembranes*, 1609(1), 80–86. [https://doi.org/10.1016/s0005-2736\(02\)00658-2](https://doi.org/10.1016/s0005-2736(02)00658-2)
- Srinivasan, K., Leone, D. P., Bateson, R. K., Dobreva, G., Kohwi, Y., Kohwi-Shigematsu, T., ... McConnell, S. K. (2012). A network of genetic repression and derepression specifies projection fates in the developing neocortex. *Proceedings of the National Academy of Sciences of the United States of America*, 109(47), 19071–19078. <http://doi.org/10.1073/pnas.1216793109>
- Steffen, B., Müller-Tidow, C., Schwäble, J., Berdel, W. E., & Serve, H. (2005). The molecular pathogenesis of acute myeloid leukemia. *Critical Reviews in Oncology/Hematology*, 56(2), 195–221. <https://doi.org/10.1016/j.critrevonc.2004.10.012>



Steffensen, A. B., Oernbo, E. K., Stoica, A., Gerkau, N. J., Barbuskaite, D., Tritsarlis, K., ... MacAulay, N. (2018). Cotransporter-mediated water transport underlying cerebrospinal fluid formation. *Nature Communications*, 9(1). <https://doi.org/10.1038/s41467-018-04677-9>

Stoykova, A., Treichel, D., Hallonet, M., & Gruss, P. (2000). Pax6 Modulates the Dorsoventral Patterning of the Mammalian Telencephalon. *The Journal of Neuroscience*, 20(21), 8042–8050. <https://doi.org/10.1523/jneurosci.20-21-08042.2000>

Stubbs, D., DeProto, J., Nie, K., Englund, C., Mahmud, I., Hevner, R., & Molnár, Z. (2009). Neurovascular Congruence during Cerebral Cortical Development. *Cerebral Cortex (New York, NY)*, 19(Suppl 1), i32–i41. <http://doi.org/10.1093/cercor/bhp040>

Suganuma, T., & Workman, J. L. (2008). Crosstalk among Histone Modifications. *Cell*, 135(4), 604–607. <https://doi.org/10.1016/j.cell.2008.10.036>

Sultan, F. A., & Day, J. J. (2011). Epigenetic mechanisms in memory and synaptic function. *Epigenomics*, 3(2), 157–181. <https://doi.org/10.2217/epi.11.6>

Suo, L., Lu, H., Ying, G., Capecchi, M. R., & Wu, Q. (2012). Protocadherin clusters and cell adhesion kinase regulate dendrite complexity through Rho GTPase. *Journal of Molecular Cell Biology*, 4(6), 362–376. <https://doi.org/10.1093/jmcb/mjs034>

Tabata, T. (2001). Genetics of morphogen gradients. *Nature Reviews Genetics*, 2(8), 620–630. <https://doi.org/10.1038/35084577>

Todd, M. A. M., & Picketts, D. J. (2012). PHF6 Interacts with the Nucleosome Remodeling and Deacetylation (NuRD) Complex. *Journal of Proteome Research*, 11(8), 4326–4337. <https://doi.org/10.1021/pr3004369>

Todd, M. A. M., Ivanochko, D., & Picketts, D. J. (2015). PHF6 Degrees of Separation: The Multifaceted Roles of a Chromatin Adaptor Protein. *Genes*, 6(2), 325–352. <http://doi.org/10.3390/genes6020325>

Tomson, B. N., & Arndt, K. M. (2013). The many roles of the conserved eukaryotic Paf1 complex in regulating transcription, histone modifications, and disease states. *Biochimica et Biophysica Acta*, 1829(1), 116–126. <http://doi.org/10.1016/j.bbagr.2012.08.011>

Turner, G., Lower, K., White, S., Delatycki, M., Lampe, A., Wright, M., ... Partington, M. (2004). The clinical picture of the Börjeson-Forssman-Lehmann syndrome in males and heterozygous females with PHF6 mutations. *Clinical Genetics*, 65(3), 226–232. <https://doi.org/10.1111/j.0009-9163.2004.00215.x>

Turgeon, B., & Meloche, S. (2009). Interpreting Neonatal Lethal Phenotypes in Mouse Mutants:

- Insights Into Gene Function and Human Diseases. *Physiological Reviews*, 89(1), 1–26.  
<https://doi.org/10.1152/physrev.00040.2007>
- Tuoc, T. C., Narayanan, R., & Stoykova, A. (2013). BAF chromatin remodeling complex: Cortical size regulation and beyond. *Cell Cycle*, 12(18), 2953–2959.  
<http://doi.org/10.4161/cc.25999>
- van Bokhoven, H. (2011). Genetic and Epigenetic Networks in Intellectual Disabilities. *Annual Review of Genetics*, 45(1), 81–104. <https://doi.org/10.1146/annurev-genet-110410-132512>
- Vessey, J. P., Amadei, G., Burns, S. E., Kiebler, M. A., Kaplan, D. R., & Miller, F. D. (2012). An Asymmetrically Localized Staufen2-Dependent RNA Complex Regulates Maintenance of Mammalian Neural Stem Cells. *Cell Stem Cell*, 11(4), 517–528.  
<https://doi.org/10.1016/j.stem.2012.06.010>
- Visootsak, J., Rosner, B., Dykens, E., Schwartz, C., Hahn, K., White, S. M., ... Graham, J. M., Jr. (2004). Clinical and behavioral features of patients with Borjeson-Forssman-Lehmann syndrome with mutations in PHF6. *The Journal of Pediatrics*, 145(6), 819–825.  
<https://doi.org/10.1016/j.jpeds.2004.07.041>
- Vissers, L. E. L. M., Gilissen, C., & Veltman, J. A. (2015). Genetic studies in intellectual disability and related disorders. *Nature Reviews Genetics*, 17(1), 9–18.  
<https://doi.org/10.1038/nrg3999>
- Vlierberghe, P., Palomero, T., Khiabani, H., Van der Meulen, J., Castillo, M., Van Roy, N., ... Ferrando, A. (2010). PHF6 mutations in T-cell acute lymphoblastic leukemia. *Nature Genetics*, 42(4), 338–342. <http://doi.org/10.1038/ng.542>
- Vlierberghe, P., Patel, J., Abdel-Wahab, O., Lobry, C., Hedvat, C. V., Balbin, M., ... Ferrando, A. (2011). PHF6 mutations in adult acute myeloid leukemia. *Leukemia*, 25(1), 10.1038/leu.2010.247. <http://doi.org/10.1038/leu.2010.247>
- Voss, A. K., Gamble, R., Collin, C., Shoubridge, C., Corbett, M., Gécz, J., & Thomas, T. (2007). Protein and gene expression analysis of Phf6, the gene mutated in the Börjeson–Forssman–Lehmann Syndrome of intellectual disability and obesity. *Gene Expression Patterns*, 7(8), 858–871. <https://doi.org/10.1016/j.modgep.2007.06.007>
- Wang, J., Weaver, I. C. G., Gauthier-Fisher, A., Wang, H., He, L., Yeomans, J., ... Miller, F. D. (2010). CBP Histone Acetyltransferase Activity Regulates Embryonic Neural Differentiation in the Normal and Rubinstein-Taybi Syndrome Brain. *Developmental Cell*, 18(1), 114–125.  
<https://doi.org/10.1016/j.devcel.2009.10.023>
- Wang, J., Leung, J. W., Gong, Z., Feng, L., Shi, X., & Chen, J. (2013). PHF6 Regulates Cell Cycle Progression by Suppressing Ribosomal RNA Synthesis. *The Journal of Biological*

Chemistry, 288(5), 3174–3183. <http://doi.org/10.1074/jbc.M112.414839>

Wang, Q., Qiu, H., Jiang, H., Wu, L., Dong, S., Pan, J., ... Chen, S. (2011). Mutations of PHF6 are associated with mutations of NOTCH1, JAK1 and rearrangement of SET-NUP214 in T-cell acute lymphoblastic leukemia. *Haematologica*, 96(12), 1808–1814. <http://doi.org/10.3324/haematol.2011.043083>

Wang, X., Tsai, J.-W., Imai, J. H., Lian, W.-N., Vallee, R. B., & Shi, S.-H. (2009). Asymmetric centrosome inheritance maintains neural progenitors in neocortex. *Nature*, 461(7266), 947–955. <http://doi.org/10.1038/nature08435>

Ward, R. D., Stone, B. M., Raetzman, L. T., & Camper, S. A. (2006). Cell Proliferation and Vascularization in Mouse Models of Pituitary Hormone Deficiency. *Molecular Endocrinology*, 20(6), 1378–1390. <https://doi.org/10.1210/me.2005-0409>

Watson, T. C., Cerminara, N. L., Lumb, B. M., & Apps, R. (2016). Neural Correlates of Fear in the Periaqueductal Gray. *The Journal of neuroscience : the official journal of the Society for Neuroscience*, 36(50), 12707-12719.

Wilkinson, G., Dennis, D., & Schuurmans, C. (2013). Proneural genes in neocortical development. *Neuroscience*, 253, 256–273. <https://doi.org/10.1016/j.neuroscience.2013.08.029>

Winter, C. F., van Dijk, F., Stolker, J. J., & Hennekam, R. C. M. (2009). Behavioural phenotype in Börjeson-Forssman-Lehmann syndrome. *Journal of Intellectual Disability Research*, 53(4), 319–328. <https://doi.org/10.1111/j.1365-2788.2009.01156.x>

Wu, H., Coskun, V., Tao, J., Xie, W., Ge, W., Yoshikawa, K., ... Sun, Y. E. (2010). Dnmt3a-Dependent Nonpromoter DNA Methylation Facilitates Transcription of Neurogenic Genes. *Science (New York, N.Y.)*, 329(5990), 444–448. <http://doi.org/10.1126/science.1190485>

Wysocka, J., Swigut, T., Xiao, H., Milne, T. A., Kwon, S. Y., Landry, J., ... Allis, C. D. (2006). A PHD finger of NURF couples histone H3 lysine 4 trimethylation with chromatin remodelling. *Nature*, 442(7098), 86–90. <https://doi.org/10.1038/nature04815>

Yao, B., & Jin, P. (2014). Unlocking epigenetic codes in neurogenesis. *Genes & Development*, 28(12), 1253–1271. <http://doi.org/10.1101/gad.241547.114>

Yoo, N. J., Kim, Y. R., & Lee, S. H. (2011). Somatic mutation of PHF6 gene in T-cell acute lymphoblastic leukemia, acute myelogenous leukemia and hepatocellular carcinoma. *Acta Oncologica*, 51(1), 107–111. <https://doi.org/10.3109/0284186x.2011.592148>

Zhang, C., Mejia, L. A., Huang, J., Valnegri, P., Bennett, E. J., Anckar, J., ... Bonni, A. (2013). The X-linked Intellectual Disability Protein PHF6 Associates with the PAF1 Complex and

Regulates Neuronal migration in the Mammalian Brain. *Neuron*, 78(6), 986–993.  
<http://doi.org/10.1016/j.neuron.2013.04.021>

Zhang, Y., Smith, A. D., Renfrow, M. B., & Schneider, D. A. (2010). The RNA Polymerase-associated Factor 1 Complex (Paf1C) Directly Increases the Elongation Rate of RNA Polymerase I and Is Required for Efficient Regulation of rRNA Synthesis. *The Journal of Biological Chemistry*, 285(19), 14152–14159.  
<http://doi.org.proxy.bib.uottawa.ca/10.1074/jbc.M110.115220>

Zhao, X., Ueba, T., Christie, B. R., Barkho, B., McConnell, M. J., Nakashima, K., ... Gage, F. H. (2003). Mice lacking methyl-CpG binding protein 1 have deficits in adult neurogenesis and hippocampal function. *Proceedings of the National Academy of Sciences*, 100(11), 6777–6782.  
<https://doi.org/10.1073/pnas.1131928100>

Zhu, X., Zhang, J., Tollkuhn, J., Ohsawa, R., Bresnick, E. H., Guillemot, F., ... Rosenfeld, M. G. (2006). Sustained Notch signaling in progenitors is required for sequential emergence of distinct cell lineages during organogenesis. *Genes & Development*, 20(19), 2739–2753.  
<https://doi.org/10.1101/gad.1444706>

Zweier, C., Kraus, C., Brueton, L., Cole, T., Degenhardt, F., Engels, H., ... Wieczorek, D. (2013). A new face of Borjeson–Forssman–Lehmann syndrome? De novo mutations in PHF6 in seven females with a distinct phenotype. *Journal of Medical Genetics*, 50(12), 838–847.  
<https://doi.org/10.1136/jmedgenet-2013-101918>

## 8.0 Copyright permissions

Permission to use the figure in Figure 1-2 from Mangelsdorf et al. in 2009



The screenshot shows the Copyright Clearance Center RightsLink interface. At the top left is the Copyright Clearance Center logo. To its right is the RightsLink logo. Further right are three navigation buttons: Home, Create Account, and Help. On the far right is a chat icon. Below the navigation is the SAGE logo. The main content area displays the following information:

**Title:** Börjeson-Forssman-Lehmann Syndrome Due to a Novel Plant Homeodomain Zinc Finger Mutation in the PHF6 Gene

**Author:** Marie Mangelsdorf, Evelyne Chevrier, Aki Mustonen, et al

**Publication:** JOURNAL OF CHILD NEUROLOGY

**Publisher:** SAGE Publications

**Date:** 05/01/2009

Copyright © 2009, © SAGE Publications

On the right side of the search result, there is a LOGIN button and a text box that reads: "If you're a copyright.com user, you can login to RightsLink using your copyright.com credentials. Already a RightsLink user or want to learn more?"

### Gratis Reuse

Permission is granted at no cost for use of content in a Master's Thesis and/or Doctoral Dissertation. If you intend to distribute or sell your Master's Thesis/Doctoral Dissertation to the general public through print or website publication, please return to the previous page and select 'Republish in a Book/Journal' or 'Post on intranet/password-protected website' to complete your request.

[BACK](#)

[CLOSE WINDOW](#)

Copyright © 2019 [Copyright Clearance Center, Inc.](#) All Rights Reserved. [Privacy statement](#). [Terms and Conditions](#).  
Comments? We would like to hear from you. E-mail us at [customercare@copyright.com](mailto:customercare@copyright.com)